Imperial College London
Department of Computing

Drone Localisation and Navigation Enhancement using Radio Wave Sensing

Heba Abdelnasser Muhammad Awad

Submitted in part fulfilment of the requirements for the degree of
Doctor of Philosophy in Computing of Imperial College London May 2024

Copyright

© The copyright of this thesis rests with the author. Unless otherwise indicated, its contents are licensed under a Creative Commons Attribution-Non Commercial 4.0 International Licence (CC BY-NC).

Under this licence, you may copy and redistribute the material in any medium or format. You may also create and distribute modified versions of the work. This is on the condition that: you credit the author and do not use it, or any derivative works, for a commercial purpose.

When reusing or sharing this work, ensure you make the licence terms clear to others by naming the licence and linking to the licence text. Where a work has been adapted, you should indicate that the work has been changed and describe those changes.

Please seek permission from the copyright holder for uses of this work that are not included in this licence or permitted under UK Copyright Law.

Statement of Originality

This is to certify that this thesis is the result of the author's original research, except where explicitly stated and referenced.

May 2024 **Heba A. Awad**

Acknowledgements

I would like to thank my supervisor, Prof. Julie McCann, for all the support and constant guidance during the whole PhD. Thanks to my colleagues who I have worked with. It has been a great pleasure to do the research work with you. I extend my thanks to the rest of the team and staff at AESE group for assistance and useful discussions. A special thanks goes to Dr. Amani El-Kholy for your support, particularly during challenging times.

I would like to extend my deepest gratitude to my husband, Mohamed, whose unwavering support and endless patience have been my anchor throughout this challenging journey. Your support has made this achievement possible, and I am eternally grateful to have you by my side. My heartfelt thanks also extend to my loving family, especially my late father and my mother. Their encouragement and belief in me have been a constant source of strength throughout my academic journey.

To my dear little ones, Hana and Zain, who came into my life during this PhD journey, thank you for filling my days with joy and purpose. Your presence has given me the resilience to see this journey through to the end.

Say (O Muhammad SAW to mankind). "If the sea were ink for (writing) the Words of my Lord, surely, the sea would be exhausted before the Words of my Lord would be finished, even if we brought (another sea) like it for its aid."

Al-Kahf - 109

Abstract

Drones have become essential in various applications, increasing the need for robust systems to ensure safe and efficient operation. This thesis investigates the use of radio wave sensing for drone detection, localisation, and state estimation, offering a cost-effective and resilient alternative to optical systems, which can be hampered by environmental factors like lighting and obstructions.

The thesis leverages radio wave technology to sense both the coarse- and fine-grained movements of drones, demonstrating their impact on drone localisation and navigation stability. First, the thesis investigates the problem of sensing fine-grained drone movements during various flight situations. Two radio wave sensing technologies (5GHz RF OAM and 77GHZ mmWave radar) are adopted and evaluated to capture drone propeller speeds based on the Doppler shift effect. Then, the thesis proposes a passive indoor drone detection and 3D tracking system using a single-chip mmWave radar. This system combines extracted drone propeller rotation signatures with other mmWave radar measurements including range and angle, to achieve precise drone detection and motion type recognition, thereby enhancing the effectiveness of drone localisation. Finally, the thesis employs the radio-wave-sensed propeller speeds to enhance the autopilot's state estimation and motion control of the drone. Extensive experiments are conducted in different flying arenas using different drone models and sizes to execute a range of aerial manoeuvres, while encountering various line-of-sight and non-line-of-sight scenarios within dynamic environments to demonstrate the effectiveness of developed approaches. The experimental results highlight the system's ability to precisely discern the drone's coarse- and fine-grained movements and its robustness in detecting drones even in complex environments with moving objects, resulting in a significant reduction in localisation error compared to the classical baseline approach. Moreover, the system achieves enhanced drone trajectory tracking and improved navigation stability, even in challenging scenarios such as motor faults.

Contents

Copyright **1**

Statement of Originality **2**

Acknowledgements **3**

Abstract **5**

1 Introduction **17**

1.1 Thesis Aims, Challenges and Research Questions 22

1.1.1 Challenge 1: The Radio Wave Technology of Choice 23

1.1.2 Challenge 2: Accurate Drone Detection in Dynamic Environments 24

1.1.3 Challenge 3: Reliable Localisation Range Extension 25

1.1.4 Challenge 4: Enhancing Drone State Estimation and Control Stability . . 26

1.2 Thesis Contributions 26

1.3 Thesis Structure 29

2 Background and Concepts **30**

2.1 Drone Dynamics and Control Stack 30

2.1.1 Drone Classes Overview 30

2.1.2 Quadcopter Dynamics 32

2.1.3 Attitude Representation 35

2.1.4 Motion Equations 37

2.1.5 Drone Control Stack 38

2.1.6 Drone Localisation and Control Techniques 41

2.2 5GHz RF Sensing: OAM Waves 47

2.2.1 OAM Overview 47

2.2.2 OAM Theory 48

2.2.3 Rotational Doppler Shift 49

2.2.4 RF OAM Sensing Applications 50

2.3 Fundamentals of mmWave FMCW Radar 52

2.3.1 mmWave FMCW Radar Overview 52

2.3.2 Range Measurement 55

2.3.3 Velocity Measurement 57

2.3.4 Angle of Arrival Measurement 59

2.3.5 Conventional Point Cloud Generation 63

2.3.6 mmWaves Sensing Applications 64

2.4 Summary 67

3 Drone Propeller Rotation Speed Measurement Using Radio Wave Sensing 69

3.1 Motivation and Objectives 70

3.2 Rotor Speed Measurement Techniques 72

3.3 Drone Propeller Speed Measurement using 5GHz RF OAM Waves 74

3.3.1 Methodology 74

3.3.2 Evaluation 75

3.4 Drone Propeller Speed Measurement using FMCW mmWave Radar 80

3.4.1 Preliminaries 80

3.4.2 Methodology 81

3.4.3 Evaluation 82

3.5 Summary 84

4 Drone Localisation and Tracking using mmWave Radar 86

4.1 Motivation and Objectives 87

4.1.1 Challenges 89

4.1.2 Contributions 91

4.2 mmWave Radar Passive Localisation and Tracking Solutions 92

4.3 mmWave Drone Interference 94

4.3.1 FMCW mmWave Features 94

4.3.2 Drone Motion 95

4.4 Tracking Pipeline 97

4.4.1 Drone Detection . . . 98
4.4.2 Motion Recognition . . . 101
4.4.3 Drone Tracking . . . 104
4.5 Evaluation . . . 107
4.5.1 Implementation and Settings . . . 108
4.5.2 Motion Identification Performance . . . 111
4.5.3 Rotational Speed Measuring Performance . . . 112
4.5.4 Drone Tracking . . . 114
4.6 Discussion and Outlook . . . 117
4.7 Summary . . . 118

5 Drone State Estimation and Control Enhancement using Radio Sensing 120

5.1 Motivation and Objectives . . . 121
5.2 System . . . 123
5.2.1 Propeller Feedback Pose Tracker . . . 124
5.2.2 State Estimation Design . . . 125
5.2.3 Drone Control Enhancement . . . 127
5.3 Evaluation . . . 129
5.3.1 RF Sensor Implementation in Simulator . . . 130
5.3.2 Trajectory Tracking Performance . . . 131
5.3.3 Rotor Failure Time Tolerance . . . 134

5.4 Summary 135

6 Conclusion **136**

6.1 Summary and Contribution 136

6.2 Discussion and Future Directions 138

6.2.1 Deployment Scalability 139

6.2.2 Reducing Complexity and Running Time 141

6.3 Reflections 141

List of Tables

2.1 Features summary of drone localisation technologies 45

2.2 A brief summary of recent works in mmWave FMCW radar sensing for different categories. 65

4.1 TI antenna configuration parameters 109

List of Figures

1.1 Example applications of drones 18

1.2 A minimum of three markers is typically required to track a rigid body in 3D space using VICON motion capture systems. However, for more complex objects or applications requiring higher accuracy, additional markers may be necessary. . 23

2.1 Drone classes 32

2.2 Multirotor drones 32

2.3 Diagram of the quadrotor model illustrating the world and body frames. 33

2.4 Newton-Euler approach 35

2.5 Quaternion approach: object rotation from frame B to I by angle α around vector $\vec{k}$. 37

2.6 Quadcopter control stack 39

2.7 Wavefront of SAM waves vs. OAM waves 49

2.8 Sawtooth modulation chirp signal 53

2.9 FMCW radar basic architecture 53

2.10 Single-chip mmWave FMCW radar 54

2.11 IF signal 56

2.12 IF frequency components of multiple objects 56

2.13 Doppler-FFT separates the two targets at the same range with different speeds 58

2.14 AoA can be estimated from the phase shift caused by the slight distance difference between the target and the Rx antennas 60

2.15 MIMO layout of TI AWR2243 62

2.16 Point cloud pipeline 63

3.1 Radio sensing-based drone propeller speed measurement system overview. 71

3.2 Layout of the flight arena. 75

3.3 Holybro S500 V2 quadcopter, the used drone in the experiments. 76

3.4 Experimental setup for RF sensing approach. 76

3.5 Commanded PWM versus actual RPM measured by Tachometer and 5GHz RF OAM approach. 78

3.6 RPM estimation error and the relative error rate of RF speed sensing for the different flight speeds. 78

3.7 RF sensing distance range 79

3.8 RPM extraction workflow. 81

3.9 Micro-Doppler spectrum of a flying drone. 82

3.10 Experimental setup for the mmWave sensing approach. 83

3.11 The impact of distance between mmWave radar and drone on speed sensing accuracy 84

3.12 Accuracy of propeller speed sensing using mmWave radar when the drone is flying 85

4.1 Drone tracking approaches: compared to the other tracking approaches, the RaDro system utilises only a single-chip mmWave radar array, without requiring to attach any additional hardware to the drone's body. 89

4.2 Quadcopter model 96

4.3 Relation between quadcopter different motion types and propellers spinning direction (line thickness denotes high/low propeller speed). 96

4.4 Structural overview of RaDro 98

4.5 The different effects of humans and drones on the frequency spectrum 100

4.6 Range pattern of the drone while performing different motions 100

4.7 Micro-Doppler spectrogram of the drone's different motions 101

4.8 Wavelet denoising impact on micro-Doppler spectrum 102

4.9 Yaw motion direction 104

4.10 Experiment setup of RaDro. 107

4.11 Motion recognition confusion matrix of the four coarse-grained motions. 110

4.12 Fine-grained motion parameters recognition. 111

4.13 RPM relative error rate at different distances from the mmWave antenna. Shadows represent the 95% confidence interval of the error distribution. 112

4.14 RPM relative error rate for the four motions of the quadcopter. 114

4.15 RPM relative error rate of propeller speeds during a flight. 114

4.16 Drone localisation errors in two different areas. 115

4.17 Localisation errors for different drone models. 116

4.18 Localisation error with interfering human at different distances from the LoS . . 117

4.19 Through-the-wall localisation performance. Shadows represent the 95% confidence interval of the error distribution. 117

5.1 The system overview 123

5.2 Quadcopter enhanced control with feedback of the sensed propeller speeds. . . . 128

5.3 Quadcopter hardware setup for RF sensor simulation. 129

5.4 Sample trajectories used to test the impact of integrating actual propeller rotation speed to the autopilot. Typical used inertial sensors in PX4 are labelled as 'Standard', while 'Standard+Prop' denotes the case when propeller speeds feedback is added. 130

5.5 The CDF of position and attitude error using typical quadcopter sensors with PX4 autopilot, and after fusing propeller speed feedback in the state estimation (Prop state estimation) and autopilot control stack (Prop control). The impact of adding the combination of two modules is labeled as Standard+Prop. 132

5.6 Roll and pitch angles estimation over time with standard quadcopter sensors and after combining the speeds feedback. 132

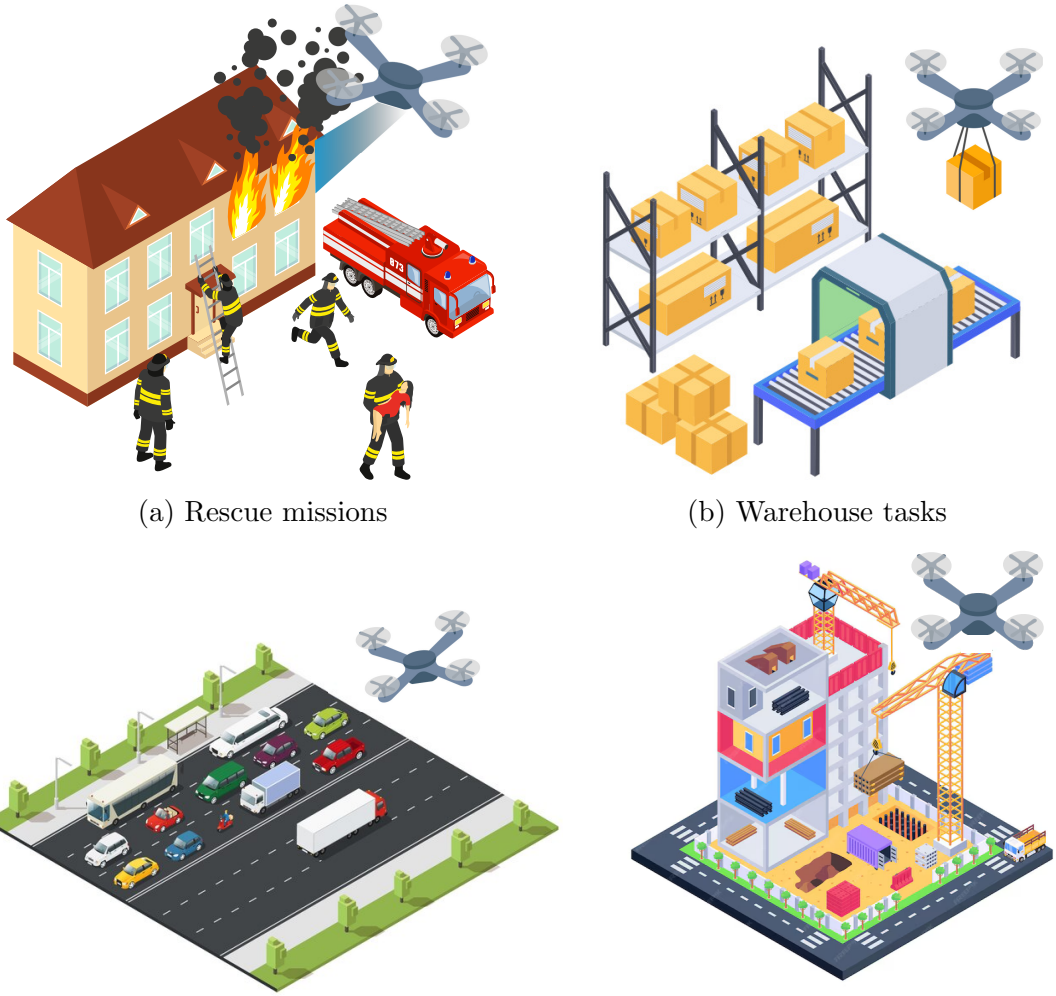
5.7 The impact of propeller speed feedback fusion on the quadcopter performance with two opposite rotors under failure. 133

Chapter 1

Introduction

In recent years, unmanned aerial vehicles (UAVs), commonly known as drones, have undergone a revolution as an emerging technology with diverse applications across military, civilian, and commercial sectors. These applications include search and rescue victims in disasters, industrial mining tasks, traffic surveillance, agricultural monitoring, infrastructure maintenance and warehouse operations [1], as exemplified in Figure 1.1. According to statistics from the United States Department of Transportation (DOT) [2], as a leading nation in UAV technology, the number of registered UAVs with DOT reached 1.37 million in 2020 with an average of around 10,300 registrations per month during 2021, thus emphasising the significant and widespread utilisation of drones.

While the widespread use of UAVs spans a massive number of applications, various safety and security concerns have been raised including collision risks, system failures, and potential misuse for malicious activities. These dangers increase when drones are deployed in urban areas or human-populated places like workplaces, posing a significant risk to public safety. To address these challenges, robust techniques for accurate detection and localisation, as well as resilient autopilot control systems are essential to mitigate the risks associated with drone utilisation,



(a) Rescue missions

(b) Warehouse tasks

(c) Traffic surveillance

(d) Construction and surveying

Figure 1.1: Example applications of drones

ensuring safe and responsible drone usage in various applications.

Localisation is crucial for the autonomous navigation of drones, as the autopilot relies on real-time tracking of its location during flight. Accurate localisation ensures drones can navigate effectively and reach their intended destinations without deviation, allowing for precise manoeuvring and obstacle avoidance. Drone detection serves as a prerequisite for localisation especially in dynamic environments where distinguishing flying drones from other moving objects is essential. Additionally, detection plays a pivotal role in intruder detection applications to identify unauthorised drones in security contexts. Resilient control systems enable drones to

maintain stable flight even in the presence of unexpected disturbances or failures. These control systems are informed by state estimation algorithms that provide up-to-date information about the drone's position, orientation, and velocity for autonomous navigation. These combined capabilities enable drones to operate autonomously and reliably across a diverse array of scenarios, ranging from hazardous or hard-to-reach areas to commercial deliveries.

Extensive research efforts have been dedicated to improving the accuracy and robustness of drone localisation and autonomous control. The primary technologies widely utilised for these purposes include global positioning systems (GPS) [3], vision-based [4, 5], and inertial measurement units (IMU)-based [6] systems. GPS receivers are standard components attached to most drones, providing information about the drone's latitude, longitude, and altitude which are used in the drone localisation to enhance drone navigation and autonomous control capabilities. However, GPS performance is weakened if obscured by an object and is virtually unusable in many indoor settings characterised by obstacles such as walls. Vision-based systems utilise cameras which are either mounted on the drone's body for visual navigation and obstacle detection for autonomous control, or installed within indoor environments to construct motion capture for indoor drone localisation applications. However, vision-based technology is a costly solution and sensitive to environmental illumination conditions. Additionally, camera-based motion capture systems, e.g., VICON system [1], require specialist multi-camera hardware to be preinstalled in indoor buildings, thereby increasing installation complexity, which is not suitable for several applications such as search and rescue missions. These systems also require attaching extra tags on the drone's body to help cameras track the drone. The effectiveness of detecting these tags is heavily reliant on environmental factors, such as well-lit surroundings and an unobstructed view which is not always guaranteed, particularly in scenarios where the drone is not within the line of sight (LoS) of the camera. IMUs are mounted on the drone's body and consist of sensors such as accelerometers and gyroscopes to measure the drone's acceleration

[1] www.vicon.com

and orientation. They are commonly used in combination with other localisation technologies to provide accurate positioning information. However, they experience error drifting which limits their localisation capabilities.

Researchers have been actively investigating advanced sensing approaches to improve drone localisation and autopilot control capabilities [7]. An optimal drone localisation sensor should fulfil three key properties: 1) **Reliability**: The sensor should be able to provide accurate information under different environmental conditions, such as changes in lighting. 2) **Cost-effectiveness**: Widespread adoption relies on the effectiveness of production and installation costs. 3) **Lightweight**: Weight is a critical consideration, particularly when incorporating sensors in a drone's body due to its weight limitations.

This thesis presents radio wave technology as a candidate sensing approach for drone detection and localisation, as well as for enhancing autopilot state estimation and control.

Radio wave sensing has been adopted as a proven technology in several research areas for diversified sensing applications, including localisation [8, 9], human health monitoring [10], and agricultural applications [11]. Compared to other alternatives, such as vision-based methods, radio sensing offers distinct advantages in certain scenarios, including enhanced performance in challenging environmental conditions and the ability to penetrate obstacles. It encompasses a range of technologies that utilise electromagnetic waves to sense and gather information about the surrounding environment. Examples for radio wave sensing technologies include frequency-modulated continuous wave (FMCW) millimeter-wave (mmWave) radar [12], radio frequency (RF) orbital angular momentum (OAM) sensing [13], and Wi-Fi channel state information (CSI) sensing [14, 15]. These technologies leverage the principles of electromagnetic wave propagation, modulation, and reception to perform various sensing tasks. The FMCW mmWave radar employs continuous-wave signals with modulated frequencies to measure range, velocity, and other characteristics of objects within its detection range, while OAM radio sensing depends on the spatial properties of radio waves to enable high-capacity communication and

sensing applications including detection and imaging. Wi-Fi CSI sensing utilises the phase and amplitude information of Wi-Fi signals to infer properties of the surrounding space, such as human presence or motion. Radio wave sensing has several attractive features which demonstrate great potential for widespread adoption in a diverse array of applications, including:

- **Resilience to varying illumination and non-line-of-sight conditions**: Radio wave sensing can effectively operate in challenging conditions, including varying illumination. It can also maintain reliable performance in non-line-of-sight (NLoS) scenarios due to the ability of radio waves to penetrate various obstacles such as interior walls, smoke, and fog. That is, radio sensing can work effectively in dark environments and through-the-wall applications, as well as in extreme environmental scenarios such as fire [16].

- **Ability to sense micro movements**: Radio waves have the ability to sense tiny movements especially with high-frequency waves. For instance, a 5GHz radio wave can detect small object motion within a range of a few centimetres (approximately 6cm), which makes it suitable for industrial purposes like monitoring rotation speeds of small wheels [17] and human sensing applications such as gesture recognition [15, 18]. As the radio wave frequency increases, the motion detection capability becomes more sensitive. For example, mmWave radar frequencies typically range between 30GHz to 300GHz which correspond to millimeter-level wavelengths between 1mm to 10mm. These frequencies enable precise detection and measurement of tiny movements and objects, making mmWave radar well-suited for wide micro-level sensing applications such as vibration detection [19] and detecting human heart rate [20].

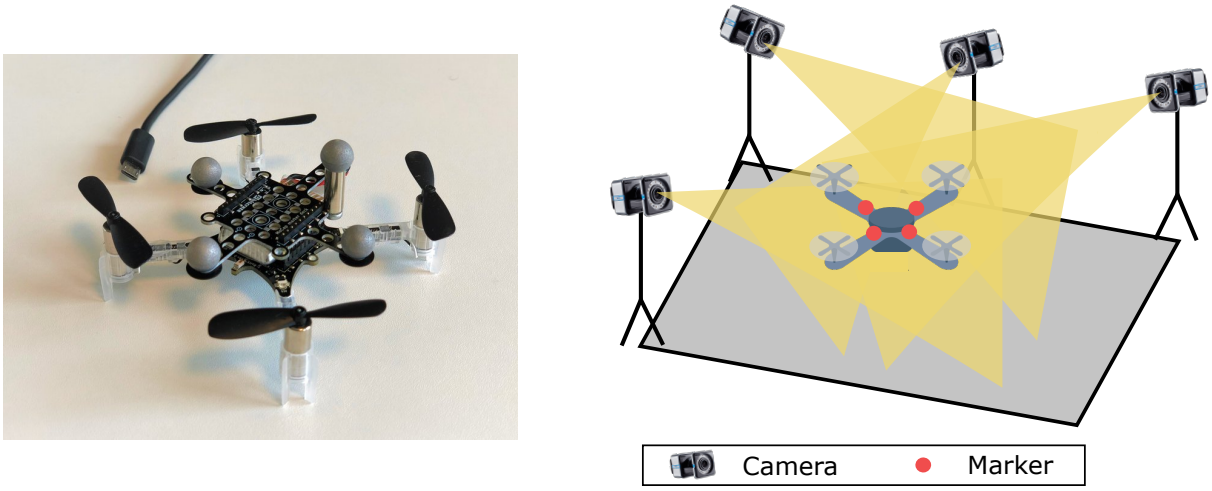
- **Ability to sense macro movements**: One of the key features of radio sensing is its ability to also recognise object macro movements, which is important for localisation and tracking applications. Various approaches are deployed for this aspect. Among them is the utilisation of FMCW mmWave radar to generate a 3D point cloud using range,

velocity, and angle measurement [21], enabling the estimation of target location which is fundamental in applications such as individual tracking, robot navigation and obstacle avoidance. Other radio sensing technologies, such as WiFi, leverage the attenuation effect on received signal strength caused by target objects to construct fingerprints, which are useful for indoor localisation and gesture recognition applications [15, 22].

- **Cost, weight, and power-consumption effectiveness**: Compared to other similar contenders, radio sensing is inexpensive, relatively light, and consumes low power. Radio sensing often utilises off-the-shelf components and relies on relatively simple hardware setups [16, 23], which can reduce manufacturing costs compared to more complex sensing technologies, such as optical or laser-based systems. Recent advancements in radio sensing technology have led to the development of compact and cost-effective integrated circuits and sensors, such as Texas Instruments single-chips mmWave radars [24]. Additionally, such radio sensing technology is known for its low power consumption characteristics. This is especially advantageous for battery-operated devices or applications where power efficiency is essential for prolonged operation time.

1.1 Thesis Aims, Challenges and Research Questions

This thesis aims to develop precise sensing approaches based on radio wave sensing technology to *passively* detect and localise drones in indoor settings and enhance autopilot state estimation and control for reliable navigation. These approaches leverage radio wave properties to overcome challenging sensing conditions such as varying environmental conditions and NLoS scenarios, to enable accurate and robust drone detection and localisation through sensing the coarse- and fine-grained movements of drones. By focusing on passive sensing techniques for detection and localisation, which dispenses the necessity of attaching extra sensors or reflectors to the drone's body, the developed approaches minimise the hardware complexity associated



(a) Reflective markers attached to a drone frame

(b) VICON system

Figure 1.2: A minimum of three markers is typically required to track a rigid body in 3D space using VICON motion capture systems. However, for more complex objects or applications requiring higher accuracy, additional markers may be necessary.

with traditional sensing methods, such as optical systems, further extending the system application to intruder detection scenarios. The rest of this section summarises the key challenges encountered with radio wave sensing for drone applications and outlines the research questions that have been formulated to address each challenge.

1.1.1 Challenge 1: The Radio Wave Technology of Choice

Various radio wave technologies, such as 5GHz RF OAM and 77GHz mmWave radar, can be used for drone detection and localisation depending on specific application requirements and the desired level of detection accuracy and coverage range. The 5GHz frequency band is commonly used for drone communication, potentially enabling the utilisation of existing drone radio communication modules to reduce hardware installation costs and simplify integration with existing drone systems. For example, in scenarios such as indoor drone surveillance in warehouses or industrial facilities where drones are already equipped with communication sys-

tems operating within the 5GHz band for remote control and data transmission, leveraging the 5GHz RF sensing for detection and localisation can offer a cost-effective solution without the need for additional specialised hardware. The mmWave radar which operates at higher frequencies, specifically at 77GHz, further extends the sensing capabilities by providing distance, velocity, and angle measurements of the target drone. Understanding the trade-offs between these technologies is essential to determine the best solution for specific operational needs, whether for fine-grained control or long-range detection.

Research Question 1: What are the trade-offs in performance and range between 5GHz RF OAM and 77GHz mmWave radar for drone detection, localisation, and control? Which technology is more suitable for specific applications?

1.1.2 Challenge 2: Accurate Drone Detection in Dynamic Environments

Several drone applications require navigation in dynamic environments that are mainly characterised by moving objects and variable weather and lighting conditions. As an example, drone applications in construction sites necessitate flying around moving machinery and potential hazards including scaffolding and construction materials. Drones' detection and recognition in such dynamic environments present a complex set of challenges, especially if no reflectors are attached to the drone body (Figure 1.2 illustrates an example of reflectors attached to the drone for simplified detection), which should be addressed for reliable and efficient drone functioning.

Research Question 2: How can radio wave sensing technology be used to reliably detect and distinguish drones from other moving objects passively in dynamic environments?

1.1.3 Challenge 3: Reliable Localisation Range Extension

Drone localisation is essential to accurately determine its position and orientation in space relative to its surroundings. Accurate localisation allows drones to navigate safely and autonomously, avoiding obstacles and complying with regulations. Localisation is also critical for intruder drone detection as it allows accurate determination of the intruding drone's position relative to a protected area or airspace. If precisely localised, security systems can effectively detect intruder drones and track their motions, enabling timely response measures to be taken. Conventional radio-based drone localisation typically employs low-frequency radar systems which are well-suited for long-range detection. However, such radar systems can be relatively expensive, bulky (measuring in metres), and consume large amounts of power which restrict their widespread adoption [25]. Recently, mmWave FMCW radar has gained popularity and expanded applications in smart environments, primarily due to advancements in single-chip mmWave radar technology which has reduced the cost to tens of dollars and the size to just a few centimetres. Point cloud approaches are commonly used as data representations in mmWave radar applications, which enable the estimation of target location through extracting range, speed, and angle measurements of the target. The principle of operation of point clouds-based localisation is straightforward where the centre of the target point cluster is used to extract the range-angle information corresponding to the target, which represents the location prediction. However, ensuring the precision of target tracking remains uncertain in practical applications. Conventional low-cost single-chip mmWave radar systems are limited to producing sparse point clouds due to hardware-based resolution constraints [26, 27]. Other factors such as noise, multipath effects, and limited resolution of certain information such as angle measurements [28] can lead to a performance decline when employing traditional signal processing methods, particularly at longer distances.

Research Question 3: How can mmWave radar technology be optimised to improve the precision and range of drone localisation?

1.1.4 Challenge 4: Enhancing Drone State Estimation and Control Stability

A robust and precise autopilot system for state estimation and control is essential for enabling reliable and autonomous drone navigation in the real world. The commonly used drone onboard sensing techniques for state estimation, including IMU- and vision-based techniques [29], sense the drone's surroundings to estimate the drone state relative to the environment without providing real-time feedback on the drone hardware status to the drone autopilot for immediate response to internal faults. Harsh working environments can lead to a range of problems, from deviation between actual and commanded drone propeller speeds to more complex situations such as motor faults and blade damage, which can ultimately result in drone failure [30]. When faults occur, they can significantly impact the drone dynamics leading to disruptions in its flying behaviour and stability. Such disruptions can result in positioning failures, where the drone may struggle to accurately maintain its reference position or trajectory. Since the rotation of drone propellers plays a key role in determining drone motion characteristics, precise knowledge of actual propeller speeds provides useful information that can enhance drone navigation and stability especially in such complex fault situations.

Research Question 4: How can real-time feedback from radio wave-sensed drone propeller speeds improve state estimation and enhance autopilot stability, particularly in the presence of faults such as motor failure or rotor blade damage?

1.2 Thesis Contributions

The contributions of this thesis primarily focus on two key directions: 1) enhancing drone detection and localisation in indoor environments and 2) promoting drone autopilot self-control and positioning for stable navigation.

Contribution 1: Chapter 3 introduces radio wave sensing techniques for measuring flying drone propeller speeds. Two radio wave sensors operating at frequency bands of 5GHz RF OAM and 77GHz mmWave radar are adopted and compared to sense the propeller rotation speed at various distances from the drone. To the best of our knowledge, this is the first work to sense the rotation speed of a dynamic object using radio waves. In the presented techniques, the rotating drone propellers introduce a unique phase change in the received radio wave signal, which is extracted and processed to calculate the propeller speeds. The experimental evaluation demonstrates that both 5GHz RF OAM and 77GHz mmWave radar approaches have highly accurate propeller speed measurements across the whole flying speed range, with mmWave radar exhibiting superior performance compared to RF OAM in terms of sensing distance. The longer sensing distance of the mmWave approach has the potential to extend the coverage area while preserving the high-resolution requirement for various drone applications. This work has been published in:

Heba Abdelnasser Awad and Julie A. McCann. "Drone Propeller Speed Measurement: Case Study using 5GHz RF and mmWave Radar" In 2024 IEEE 99th Vehicular Technology Conference (VTC2024-Spring).

Contribution 2: In Chapter 4, RaDro system is proposed; an indoor drone detection and localisation system using mmWave radar. The proposed system utilises a single-chip 77GHz mmWave radar array, eliminating the need for multiple point installations in the operational environment or any modifications to the drone hardware, which significantly reduces the setup and deployment effort required for new environments. Compared to other techniques used for indoor drone tracking, such as optical systems, RaDro is cost-effective and can penetrate obstacles which enhances its reliability for drone tracking in complex environments. In contrast to conventional mmWave radar localisation methods that rely on range and angle measurements, the developed drone localisation technique incorporates more robust mmWave measurements which expand the reliable localisation coverage area. Signal processing techniques are adopted

to capture reliable information from received mmWave signals. This includes extracting the distinctive micro-Doppler signature generated by drone propeller rotation, enabling differentiation between the flying drone and other moving objects, as well as identifying the drone's motion type. The recognised drone motions are further utilised to simplify the drone's dynamic model which is then integrated into the tracking module for further enhancement. The experimental evaluation demonstrates RaDro's precise drone localisation, achieving a significant reduction in localisation error compared to the conventional baseline. This localisation accuracy remains robust even when confronted with interference from other moving sources, such as humans. Additionally, it showcases the system's capability to accurately localise drones in NLoS scenarios where existing state-of-the-art optical technologies are unable to operate. The proposed system is presented in:

Heba Abdelnasser Awad, Mohammad Heggo, Oscar Pang, Mirko Kovac, and Julie A. McCann. "RaDro: Indoor Drone Tracking using Millimeter Wave Radar" Proceedings of the ACM on Interactive, Mobile, Wearable and Ubiquitous Technologies (IMWUT), 2024. Volume 8, Issue 3.

Contribution 3: Chapter 5 proposes a system that leverages direct feedback of drone propeller speeds sensed with the 5GHz RF OAM module to improve the drone motion stability and safety, especially in fault conditions such as rotor blade damage. This is achieved by incorporating the sensed propeller speeds into the drone's dynamic model to track its position and orientation which are then integrated into the state estimation module to further enhance the motion performance. Additionally, the sensed propeller speeds are incorporated into the autopilot's motion control to compensate for deviation errors from commanded speeds. The results demonstrate a significant reduction in the error of drone position while following a trajectory, as well as enhanced stability in scenarios involving motor faults. This work has been published in:

Heba Abdelnasser Awad, Mohammad Heggo, Oscar Pang, Mirko Kovac, and Julie A. Mc-

Cann. "Multirotor Motion Enhancement using Propeller Speed Measurements." In 2023 International Conference on Unmanned Aircraft Systems (ICUAS), IEEE, 2023.

1.3 Thesis Structure

The rest of this thesis is structured as follows: Chapter 2 provides a background review of this work, including drone dynamics and control fundamentals, a literature review of the drone localisation and autonomous control systems, principles of OAM radio waves and mmWave FMCW radar, and an overview of related topics in radio sensing. Chapter 3 presents two radio wave sensing approaches to sense the propeller speeds of flying drones and compares their performance. In Chapter 4, a novel drone localisation system is proposed, which tracks the micro and macro movements of drones indoors. Chapter 5 introduces state estimation and autopilot motion control approaches aimed at enhancing drone navigation stability. Finally, Chapter 6 concludes this thesis and discusses potential future directions.

Chapter 2

Background and Concepts

This chapter provides an overview of the background of the thesis. It discusses the various drone classes and the fundamental dynamics and control stack of quadcopters being the drone model type considered in this thesis. Furthermore, it presents recent advancements in techniques used to enhance drone localisation and autopilot motion control for stable navigation. The chapter also provides technical insights into the principles of radio sensing, particularly for 5GHz RF OAM wave and mmWave radar technologies, along with recent advancements in their sensing techniques.

2.1 Drone Dynamics and Control Stack

2.1.1 Drone Classes Overview

Drones are classified based on various factors, including weight, manoeuvrability, and their specific capabilities. In terms of weight, drones are categorised into several classes. Super Heavy Drones weigh over 2000 kg and are typically used for heavy industrial applications and mili-

tary operations. Heavy Drones, which weigh between 200 kg and 2000 kg, are often utilised in large-scale commercial activities, such as long-range delivery services and extensive surveillance operations. Medium drones, ranging from 50 kg to 200 kg, find their use in mid-sized commercial applications like agriculture monitoring and medium-scale delivery. Light/Mini Drones, weighing between 5 kg and 50 kg, are commonly used for recreational purposes, photography, and small-scale deliveries. Drones weighing less than 5 kg are classified as micro air vehicles (MAVs). These MAVs are frequently employed for indoor operations, research, hobbyist activities, and precise inspection tasks due to their small size and agility. In this thesis, the focus is on MAVs due to their versatility and suitability for various applications. Drones can also be classified based on their level of manoeuvrability into three categories [31]: Vertical Take-Off and Landing (VTOL), Horizontal Take-Off and Landing (HTOL), and hybrid models (Figure 2.1). VTOL models include helicopters, heliwings, and quadcopters. These models are typically capable of hovering and exhibit a high level of manoeuvrability, but they are limited in their cruise speed due to the stalling of retreating blades [32]. HTOL models are primarily fixed-wing aircraft, which generally have a higher cruise speed and can fly longer distances, but they offer limited manoeuvrability and usually require a runway for take-off and landing. Hybrid models have the capability to take-off and hover like a VTOL and fly like an HTOL drone; however, they are more complex in their design.

Multirotor MAVs (Figure 2.2) are a popular category of VTOL drones. Their small size and high manoeuvrability allow them to fly in various directions, not just forward. Consequently, they are ideal for surveying tasks, as they can access hard-to-reach places such as under bridges, inside buildings, and pipelines. Lift force in multirotor MAVs is generated by the continuous rotation of the propellers, which are essential for maintaining flight and manoeuvrability. The number of propellers can vary depending on the design and purpose of the drone. Among the various configurations, the quadcopter, featuring four propellers, is the most common and widely used. The propeller generated lift force can vary depending on the number of propeller



(a) VTOL [34] (b) HTOL [35] (c) Hybrid [36]

Figure 2.1: Drone classes



Figure 2.2: Multirotor drones [37]

blades [33]. The drone model used in this thesis is a quadcopter, however, all the approaches presented in the thesis are applicable to multirotor configurations.

2.1.2 Quadcopter Dynamics

Quadcopters have a simple structure that can be implemented using off-the-shelf, cheap, and lightweight components. A quadcopter is a cross-shaped rigid body that uses a minimum number of rotors to have four control inputs that are adequate to control its six degrees of freedom (position and orientation). Since the rotors are the only moving parts, the quadcopter's thrust can be controlled with the rotors' speed.

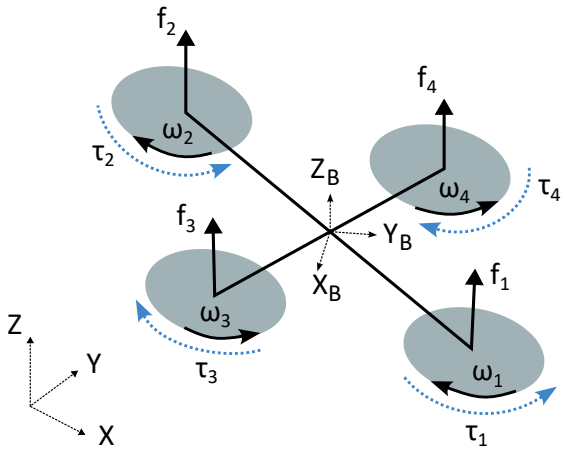


Figure 2.3: Diagram of the quadrotor model illustrating the world and body frames.

Two frames are commonly defined for the quadcopter structure model: inertial and body frames (Figure 2.3). The inertial frame is defined by the Earth's axes, where the negative direction of the z-axis is the direction of gravity. The body frame is defined by the quadcopter body orientation, where the z-axis is the rotors' thrust direction. The position of the quadcopter has a notation of $p_I = (x,\ y,\ z)$ in the inertial frame, while the attitude of the quadcopter can be identified with the three Euler angles $\eta = (\phi,\ \theta,\ \psi)$ in the body frame. The roll angle ϕ is the rotation around the x-axis, the pitch angle θ is the rotation around the y-axis, and the yaw angle ψ is the rotation around the z-axis.

The angular velocity ω_i of rotor i causes a force f_i in the rotor axis direction, and torque τ_i around the rotor axis as follows,

$$f_i = k\ \omega_i^2, \quad \tau_i = b\ \omega_i^2 \tag{2.1}$$

where k and b are constants which depend on various factors including the propeller motor specifications and aerodynamic properties. Torque refers to the rotational force applied to an object, causing it to rotate around an axis. The combined forces of the rotors generate a total

thrust F in the direction of the z-axis of the body frame as,

$$F = \sum_{i=1}^{4} f_i = k \sum_{i=1}^{4} w_i^2, \quad F_B = \begin{bmatrix} 0 \\ 0 \\ F \end{bmatrix} \tag{2.2}$$

where F_B is the total thrust in the body frame. The total torque M_B in the body frame can be expressed with its three components in the three angles directions τ_ϕ, τ_θ and τ_ψ, as

$$M_B = \begin{bmatrix} \tau_\phi \\ \tau_\theta \\ \tau_\psi \end{bmatrix} = \begin{bmatrix} L_{Roll}(-f_1 + f_2 + f_3 - f_4) \\ L_{Pitch}(f_1 - f_2 + f_3 - f_4) \\ \tau_1 + \tau_2 - \tau_3 - \tau_4 \end{bmatrix} \tag{2.3}$$

where L_{Roll} is the arm length generating the rolling moment, i.e. distance from the side motors to the center of mass of the quadcopter, and L_{Pitch} is the arm length generating the pitching moment, i.e. the distance from the front motors to the center of mass.

The angular velocity of the quadcopter ω_B is the angular velocity of the quadcopter body frame with respect to the inertial frame, which can be represented as follows,

$$\omega_B = \begin{bmatrix} \omega_x \\ \omega_y \\ \omega_z \end{bmatrix} = \begin{bmatrix} 1 & 0 & -\sin(\theta) \\ 0 & \cos(\phi) & \sin(\phi)\cos(\theta) \\ 0 & -\sin(\phi) & \cos(\phi)\cos(\theta) \end{bmatrix} \dot{\eta} \tag{2.4}$$

Because of the symmetry of the quadcopter, where the four arms are lined up with the body x- and y-axes, the body frame is assumed to be a principal axis frame, allowing for the following form of the inertia matrix to be used [38],

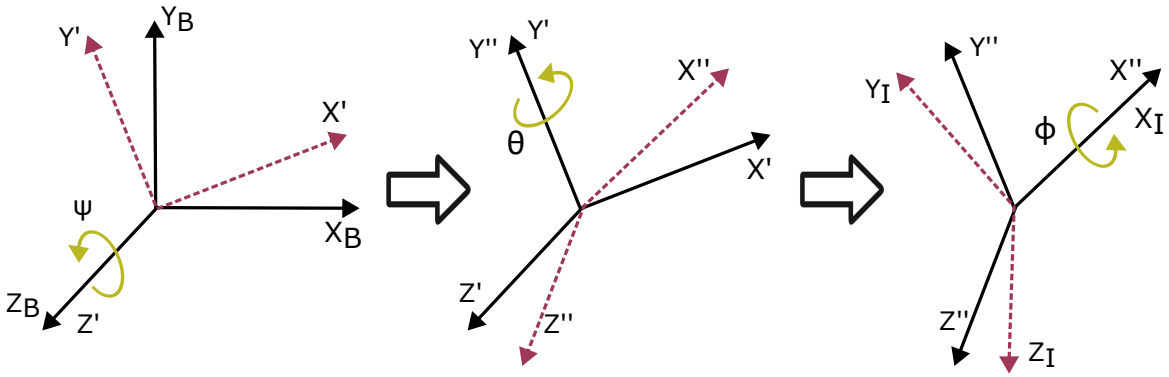


Figure 2.4: Newton-Euler approach: the rotations are applied successively about the object's axes: first about the z-axis (yaw), then about the y-axis (pitch), and finally about the x-axis (roll).

$$I = \begin{bmatrix} I_{xx} & 0 & 0 \\ 0 & I_{yy} & 0 \\ 0 & 0 & I_{zz} \end{bmatrix} \tag{2.5}$$

2.1.3 Attitude Representation

In literature, the orientation of a rigid body, such as a quadcopter, is described using various representations for motion in three-dimensional space, including the Newton-Euler and Quaternion approaches [39, 40].

Newton-Euler Approach

The orientation of the rigid body can be identified by the three Euler angles $\eta = (\phi,\ \theta,\ \psi)$. The rotation matrix $R_{IB}(\psi,\ \theta,\ \phi) \in SO(3)$ is typically a 3×3 matrix and is used to transform vectors from the body frame (B) to the inertial frame (I). It represents the orientation of the body frame relative to the inertial frame and can be represented as follows,

$$R_{IB}(\psi,\theta,\phi) = \begin{bmatrix} C_\theta C_\psi & S_\psi S_\theta & -S_\theta \\ C_\psi S_\theta S_\phi - S_\psi C_\phi & S_\psi S_\theta S_\phi + C_\psi C_\phi & C_\theta S_\phi \\ C_\psi S_\theta C_\phi + S_\psi S_\phi & S_\psi S_\theta C_\phi - C_\psi S_\phi & C_\theta C_\phi \end{bmatrix} \tag{2.6}$$

where C_x and S_x are abbreviations for $\cos(x)$ and $\sin(x)$, respectively. Each column of the rotation matrix represents the direction of one of the body frame axes (x, y, z) expressed in the inertial frame coordinates. For a given vector a in the body frame, the corresponding vector in the inertial frame is $R_{IB} \times a$ (an example is shown in Figure 2.4).

Quaternion Approach

Quaternion, a mathematical concept, finds application across diverse fields such as robotics and aerospace engineering. It is an alternative representation used to model attitude dynamics, aimed at avoiding the singularities inherent in classic representations such as Euler angles [41]. Each rotation can be represented by a single rotation about a fixed axis, denoted by the unit vector $\vec{k}$, and a rotation angle α; an example is depicted in Figure 2.5. This approach is known as eigenaxis rotation, incorporating the shortest rotation between two orientations. Using this concept, a unit quaternion is defined as follows,

$$Q = \begin{bmatrix} q_0 & q_1 & q_2 & q_3 \end{bmatrix}^T = \begin{bmatrix} q_0 \\ q_{1:3} \end{bmatrix} = \begin{bmatrix} cos(\frac{\alpha}{2}) \\ \vec{k}\ sin(\frac{\alpha}{2}) \end{bmatrix} \tag{2.7}$$

where the four parameters of quaternion (q_0, q_1, q_2, q_3) are subject to the constraint $\sum_{i=0}^{3} q_i^2 = 1$. These parameters belong to a complex number, which can be represented as follows,

$$Q = q_0 + q_1\mathbf{i} + q_2\mathbf{j} + q_3\mathbf{k} \tag{2.8}$$

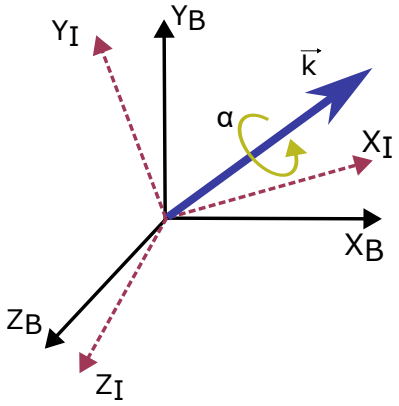


Figure 2.5: Quaternion approach: object rotation from frame B to I by angle α around vector $\vec{k}$.

In the context of dynamically representing an object's orientation in 3D space, all unit quaternions can be used to construct a matrix represented as follows [40, 42],

$$R(Q) = \begin{bmatrix} 1 - 2q_2^2 - 2q_3^2 & 2q_1q_2 - 2q_0q_3 & 2q_1q_3 + 2q_0q_2 \\ 2q_1q_2 + 2q_0q_3 & 1 - 2q_1^2 - 2q_3^2 & 2q_2q_3 - 2q_0q_1 \\ 2q_1q_3 - 2q_0q_2 & 2q_2q_3 + 2q_0q_1 & 1 - 2q_1^2 - 2q_2^2 \end{bmatrix} \tag{2.9}$$

$R(Q)$ satisfies $R(Q)R^T(Q) = I_{id}$ and $det(R(Q)) = 1$ which represents the rotation matrix. The mapping from Euler angles to unit quaternions can be as follows [39],

$$Q(\phi,\ \theta,\ \psi) = \begin{bmatrix} C_{\frac{\phi}{2}}\ C_{\frac{\theta}{2}}\ C_{\frac{\psi}{2}} + S_{\frac{\phi}{2}}\ S_{\frac{\theta}{2}}\ S_{\frac{\psi}{2}} \\ -C_{\frac{\phi}{2}}\ S_{\frac{\theta}{2}}\ S_{\frac{\psi}{2}} + C_{\frac{\theta}{2}}\ C_{\frac{\psi}{2}}\ S_{\frac{\phi}{2}} \\ C_{\frac{\phi}{2}}\ C_{\frac{\psi}{2}}\ S_{\frac{\theta}{2}} + S_{\frac{\phi}{2}}\ C_{\frac{\psi}{2}}\ S_{\frac{\psi}{2}} \\ C_{\frac{\phi}{2}}\ C_{\frac{\theta}{2}}\ S_{\frac{\psi}{2}} - S_{\frac{\phi}{2}}\ C_{\frac{\psi}{2}}\ S_{\frac{\theta}{2}} \end{bmatrix} \tag{2.10}$$

2.1.4 Motion Equations

The motion equations for a quadcopter typically include equations for translational motion and rotational motion [43, 44]. The quadcopter's dynamic transition can be represented by the

following equation,

$$m\ddot{p}_I = mg + R_{IB}F_B + F_{a,I} \tag{2.11}$$

where $g = [0, 0, g_e]^T$ represents the gravity vector, with g_e denoting the gravitational constant. $F_B = [0, 0, F]^T$ is the external force vector in the body frame. R_{IB} is the rotation matrix that allows transformation from body to inertial frame to represent the quadcopter attitude. $F_{a,I}$ is the aerodynamic force modelled in order to stop the vehicle in the absence of horizontal thrust. Thus, the required force to move a quadcopter of mass m with acceleration $\ddot{p}_I$ in the inertial frame is equal to the gravity force mg added to the inertial frame total thrust of the rotors $R_{IB}F_B$ and the aerodynamic force $F_{a,I}$. The dynamic equation denoting quadcopter rotation can be described with the external torque on the vehicle in the body frame as follows,

$$I\dot{\omega}_B + \omega_B \times I\omega_B = M_B + M_{a,B} \tag{2.12}$$

Where $M_{a,B}$ denotes aerodynamic drag moments, designed to counteract vehicle rotation in the absence of thruster moments.

The total thrust F and torques $M_B = [\tau_\phi, \tau_\theta, \tau_\psi]$ are generated by the control model via control inputs to the four rotors.

$$[F, \tau_\phi, \tau_\theta, \tau_\psi] = Hu \tag{2.13}$$

where $u \in \mathbb{R}^4$ represents thrust generated by each spinning rotor. $H \in \mathbb{R}^{4\times4}$ is a projection matrix that maps total thrust and moment forces to thrust generated by each rotor.

2.1.5 Drone Control Stack

The control stack consists of software and control systems that are used to manage and operate the drone. It encompasses the various layers or components involved in controlling a

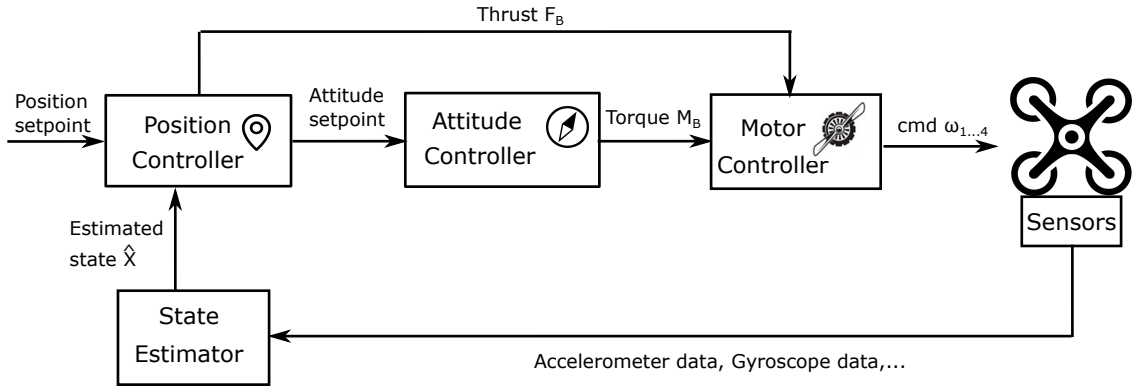


Figure 2.6: Quadcopter control stack: The estimated state $\hat{X}$ at a time instant t is fed to the position and attitude controllers to calculate the required total force F_B and total torque M_B that should be applied on the quadcopter to move to the desired position. The total force and torque are then fed to the motor controller to determine the commanded angular speeds of the four propellers. The quadcopter sensors then send their feedback measurements to the state estimator module to estimate the quadcopter state at a time instant $t + 1$.

drone's behaviour, from low-level flight control algorithms to high-level mission planning and decision-making processes. The stack typically includes hardware interfaces, flight controllers, communication protocols, navigation systems, and higher-level software for mission-specific tasks. The goal is to provide a systematic and organised framework for efficiently controlling and coordinating the different aspects of drone operations. The following highlights the control stake components that are related to this thesis.

Autopilot Controller

An autopilot in drones is a system that automates the control of the drone's flight path, allowing it to navigate, maintain stability, and perform complex manoeuvres without constant human intervention. This system integrates various components, including sensors and control algorithms to manage the drone's position, orientation, and velocity. For example, if the drone is supposed to hover at a specific altitude and orientation but starts drifting due to wind or other disturbances, the autopilot controller detects this deviation by comparing the actual state

against the setpoint. It then issues commands to the appropriate motors to increase or decrease thrust, thereby bringing the drone back to the intended position and orientation. This process happens continuously and rapidly, ensuring that the drone maintains stability and follows the planned flight path accurately. The typical design of the quadcopter autopilot control model is a hierarchical controller with two loops (Figure 2.6): an outer loop to control the position and an inner loop to control the attitude of the quadcopter body [45, 46].

- **Position Controller**: The outer loop typically has two inputs: position setpoints and the estimated position. The difference between these two inputs is the position error which is fed into a proportional-integral-derivative (PID) controller to compensate for the thrust based on the desired trajectory. The output of this loop is the desired attitude and the commanded thrust which direct the drone toward the desired position.
- **Attitude Controller**: The inner loop controls the attitude using another PID controller. It takes the desired attitude from the position controller in addition to the estimated attitude. The output is the commanded torques that achieve the desired attitude.

Motor Controller

The motor controller receives the commanded thrust and torques from the autopilot controller and accordingly generate commanded speeds of individual motors (propeller speeds) while ensuring that motor speed limits are not exceeded. These propeller rotation speeds generate the necessary lift and drag forces, which enable the drone to perform various flight manoeuvres. For instance, changing the drone's direction during flying involves altering the speeds of the drone's propellers. This adjustment modifies the lift thrust output of each motor, causing the drone to tilt and change its angle in the desired flight direction. By precisely controlling the propeller speeds, the drone can execute complex movements and maintain stability. This highlights the critical role of propeller speeds in the overall motion control of quadcopters and

multirotors in general. The ability to finely tune these speeds allows for precise navigation, responsive direction changes, and smooth operation in various flight conditions.

State Estimator

The state estimator is responsible for providing real-time information about the drone's current state, including position, attitude, velocity, and other relevant parameters. This information is essential for various tasks such as navigation, obstacle avoidance, path planning, and stabilisation. Without accurate state estimations, drones would struggle to maintain stable flight and navigate safely. Different sensor measurements such as accelerometers, gyroscopes, and GPS readings are utilised to provide real-time estimation of the dynamic drone state. This estimation is then used by the autopilot controller to provide control decisions for stable flight.

2.1.6 Drone Localisation and Control Techniques

This section presents a literature review on key aspects of drone localisation and stable autonomous navigation relevant to this thesis.

Drone Localisation and Tracking Methods

As previously discussed in Chapter 1, drone localisation methods involve determining the exact position of a drone within a specified environment. Precise drone localisation is crucial for enabling autonomous navigation and achieving accurate control, as well as being critical for intruder drone tracking applications. Various methods have been proposed in the literature to enhance drone localisation. GPS is a commonly used technique for drone localisation, which can provide meter-level accuracy. However, its application indoors presents significant

challenges due to the attenuation effects caused by structures and obstacles, leading to unreliable positioning data [47]. Several alternative techniques have been proposed to address these challenges, which are summarised in this section.

- **Vision Sensing Techniques**: Cameras can be mounted either within flying environments for applications related to drone localisation, or on the drone itself for tasks such as visual navigation and obstacle detection. The first category of techniques that mount cameras within the flying area [48, 49, 50] can provide precise estimations for localisation indoors, particularly with motion capture systems like VICON which are widely used in indoor environments, enabling the drone to determine its own position relative to its surroundings for effective navigation. However, this solution is costly and requires pre-installation within the deployment area, making it impractical for certain drone applications such as search and rescue missions. Additionally, most camera-based systems necessitate specialized marker attachments on the drone frame for detection. The camera's ability to identify these markers is heavily dependent on illumination levels and LoS conditions, which is not assured in various situations.

  The second category of vision-based techniques involves attaching cameras to the drone body to improve navigation stability through state estimation and map construction techniques. This approach enhances drone capabilities and increases navigation accuracy in uncontrolled environments. A fundamental method in this category is visual-inertial navigation systems (VINS) [51, 52]. The VINS technology combines camera and inertial IMU measurements in real-time to determine the six degrees of freedom pose of the drone and create a 3D map of surroundings by fusing the precise intermittent information obtained from the camera with the high-rate IMU readings. VINS has been proposed for visual-inertial simultaneous localisation and mapping (SLAM) [53, 54, 55] and for visual-inertial odometry [56, 57], which is the process of estimating the position and orientation of a moving object using data from motion sensors. However, the limitations posed by the

camera, such as motion blur, scale ambiguity, and limited dynamic range, as well as challenges inherent in IMU sensors, like error drifting, present hurdles for visual-inertial fusion systems across various manoeuvring scenarios.

- **Acoustics Sensing Techniques**: Acoustic-based techniques have been proposed for indoor drone localisation. Several systems [58, 59, 60] require careful attachment of anchors to the drone's body and placing acoustic modules in the flying environment, thereby increasing the installation complexity. For instance, a proposed system in [58] involves attaching two speakers to the drone to emit FMCW acoustic signals, which are then used to estimate the distance between the drone and a mobile phone. Other acoustic-based localisation systems [61, 62] can passively track drones without requiring any additional equipment to the drone's body, treating the drone as a mobile sound source. However, these systems exhibit errors in the meter range and can be easily interfered with by complex environmental sound noise, which is not suitable for many precise indoor applications [61].

- **Radio Sensing Techniques**: Various radio wave sensing technologies have been used for drone localisation and tracking methods. Ultra-wideband (UWB)-based ranging methods are widely used in indoor environments, achieving decimeter-level accuracy in drone tracking [63, 64]. UWB can be incorporated with other approaches including visual SLAM [65] and RGB-D cameras [66]. However, UWB-based techniques rely on integrating UWB transceivers onto the drone's frame. Additionally, they necessitate careful placement of spatially dispersed UWB transceivers, typically a minimum of three, throughout the tracking zone for calculating pairwise distances using time-of-flight (ToF) information. These requirements introduce considerable complexity to installation and calibration procedures. Another system, Wi-Drone [67] uses WiFi to track the position and orientation of a drone based on the angle-of-arrival (AoA), ToF and CSI phase information, however, it requires attaching up to 12 antennas to the drone body to achieve precise pose estimation which

increases the installation complexity and the drone battery power consumption due to the added weight. Alternatively, there are RF-based approaches that rely on the construction of an aerial mobile sensor network for indoor monitoring [68, 69]. Such approaches necessitate careful equipment placement and a large number of nodes/drones to ensure reliable navigation, which increases deployment costs and complexity. Additionally, these systems may experience a reduction in navigation accuracy over time due to error drifting.

Table 2.1 summarises the capabilities and limitations of various drone localisation techniques.

The drone localisation approach proposed in this thesis leverages the recent advancement in radio sensing technologies to *passively* detect and localise drones indoors. Additionally, it opens up opportunities to utilise existing radio sensors installed on drones to enhance navigation stability. By integrating these sensors, the drone control and state estimation modules can be improved, leading to more accurate and reliable assessments of the drone's position and movement. The proposed radio sensing approaches demonstrate their effectiveness even in complex environmental conditions, such as NLoS scenarios and varying illumination conditions. One significant advantage of the developed detection and localisation approaches is that they eliminate the need for attaching extra hardware to the drone's body, thereby reducing hardware installation complexity. Additionally, radio sensing technology has the capability to detect both macro and micro movements of tracked objects, making it highly suitable for a broad range of precise localisation applications.

Drone Motion Control Methods

Different methods have been proposed in the literature to enhance the autonomous motion control of drones. This subsection focuses on reviewing the proposed control techniques designed for quadcopters, the chosen drone model for this thesis. As previously noted, the quadcopter, characterized by its rigid body in a cross shape, employs the minimum number of rotors required

Localisation technique	Deployment cost	Resolution	Reliability
Vision motion capturing	High	Millimeters	Light sensitivity / requires LoS
UWB	High	Decimeter	LoS/NLoS
Acoustic	High	Centimeters	LoS/NLoS
Passive acoustic	Low	Meters	Audio noise sensitivity / LoS/NLoS

Table 2.1: Features summary of drone localisation technologies

to supply four control inputs, effectively managing its six degrees of freedom encompassing both position and orientation. Since the rotors are the only moving components, the quadcopter's thrust can be regulated through adjustments in rotor speed, thereby controlling the quadcopter dynamics [40, 70, 71].

Accurately modelling a flying quadcopter poses significant challenges, primarily because it requires capturing the complex interactions between motor dynamics and aerodynamic forces, which deeply influence drone performance and stability. These interactions cause rotor interference (e.g., when the airflow from one rotor interacts with the airflow from another rotor) that can affect propeller speeds [72, 73], particularly during high-speed flight. Conventional methods for quadrotor modelling typically incorporate simplistic representations that limit the captured effects to linear drag forces approximations and quadratic thrust curves that relate the commanded and actual propeller speeds in different conditions (e.g., under different battery voltage levels) [74, 75, 76]. Such approximations are more suitable when the quadcopter is moving at low speeds. At higher speeds, these approximations exhibit increasing bias as they neglect the influence of the inflow velocity on the generated thrust. Another approach, parametric gray-box models [77], seeks to address these limitations by expressing forces and torques as combinations of predefined mathematical functions. Although these models can exhibit strong performance, their effectiveness relies on selecting suitable basis functions, a task that demands expertise from human designers. Recent research models aerodynamic effects based on fluid dynamics

[78]. Despite their high accuracy, such approaches incur high computational costs and require hours of processing. Others use deep neural network modelling to estimate the forces applied on the flying quadcopters [79, 80, 81]. However, such solutions require large volumes of data, and are prone to over-fitting [81]. Another modelling challenge is that the quadcopter is an under-actuated system [82], where there are fewer control inputs (four motors) than the number of degrees of freedom (six) the vehicle possesses. This can result in instability when the system approaches its physical limits and escalate the complexity of control in the event of a motor failure. Several systems have proposed solutions aimed at stabilising quadcopters in the event of motor failure or saturation [83, 84, 85]. The proposed technique in this thesis incorporates sensed actual propeller speeds with radio waves to compensate for the quadcopter's desired forces and torques during flight, demonstrating noticeable improvements in motion accuracy and drone stability.

2.2 5GHz RF Sensing: OAM Waves

RF sensing enables non-contact sensing and detection solutions across a wide range of applications in aerospace, industries, and smart cities. By transmitting and receiving radio waves, RF sensing gathers crucial information about the surrounding environment or objects within the RF field. This information includes properties like distance, velocity, direction, and composition of objects or materials.

Operating within the 5GHz frequency band, 5GHz RF waves are widely utilised in diverse wireless communication systems, including Wi-Fi networks and Bluetooth devices. Recent advancements in wireless communication systems have led to the exploration of various techniques aimed at enhancing capacity and performance. Among these, emerging spatial multiplexing methods such as OAM, have garnered attention due to their potential advantages over traditional frequency-based multiplexing techniques like orthogonal frequency division multiplexing (OFDM), commonly employed in Wi-Fi standards and other communication protocols. For sensing applications in particular, 5GHz OAM radio wave has the potential to improve the performance of several sensing applications including object detection [86, 87]. The rest of this section discusses the OAM radio waves background and the rotational Doppler shift phenomenon which are used in drone sensing in Chapters 3 and 5.

2.2.1 OAM Overview

The advancement of wireless devices necessitates increased communication capacity. This can be achieved through various methods including transitioning to higher frequencies to access higher bandwidths or leveraging spatial properties of electromagnetic waves. OAM is a promising method that exploits electromagnetic waves spatial properties to enhance capacity. It involves twisting the phase of the wavefront along its propagation axis, creating multiple or-

thogonal channels within the same frequency band. By assigning different OAM mode values to electromagnetic waves, these channels can carry independent streams of data simultaneously, effectively increasing the overall data transmission capacity. OAM waves were initially observed in 1992 by Allen et al. in optical beams [88]. In 2007, Thidé et al. generated OAM in RF [89], which was then applied to wireless communication as an alternative multiplexing mode [90, 91].

OAM waves have been used in sensing applications and demonstrated superior performance in target detection and imaging [86, 87] with their increased capacity and robustness to interference. They have been also used in orbital movement detection applications [17, 92, 93, 94] which leverage rotational Doppler shift phenomenon to measure the rotation speed.

2.2.2 OAM Theory

Electromagnetic waves, as fundamental carriers of energy and information in the universe, possess dual characteristics of energy and momentum. This momentum encompasses both linear momentum, associated with the wave's propagation direction, and angular momentum, denoting the rotational motion of the wave's electric and magnetic fields [95]. The momentum carried by the electromagnetic field is directly proportional to the energy content of the wave and associated with the radiation pressure created by waves when interacting with an object [96]. Angular momentum is categorised based on polarisation into two main types: spin angular momentum (SAM) and OAM. SAM describes the polarisation state of the electromagnetic waves, and OAM characterises the spatial structure and rotational motion of a vortex of the wavefront [13, 97]. The primary distinction between SAM waves and OAM waves lies in their wavefront structures. SAM waves typically display parallel and separated rings in space, indicative of their circular polarisation. In contrast, OAM waves exhibit a distinctive helical wavefront, characterised by its continuous spatial spiral pattern. Figure 2.7 illustrates the

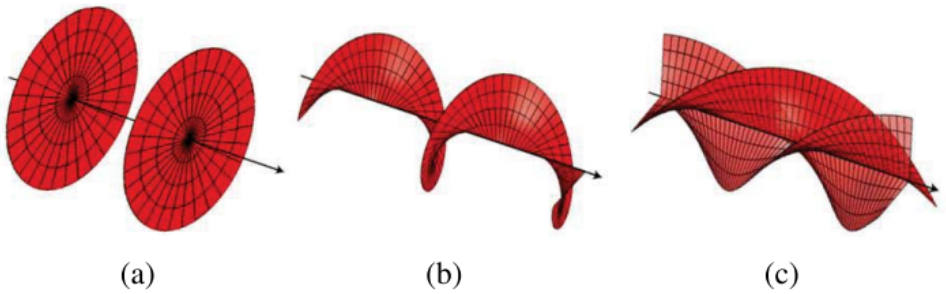


Figure 2.7: Wavefront of SAM waves vs. OAM waves [13] (a) SAM wave (b) OAM wave with topological charge $l = 1$ (c) OAM wave with topological charge $l = 3$.

contrast between these two wavefront structures.

OAM can be used to increase spectral efficiency and data transmission capacity by multiplexing multiple data streams on different OAM modes (also referred to as topological charges) [98]. Each OAM mode is an element of a complete orthogonal basis that can be employed for multiplexing different signals. Theoretically, the number of orthogonal OAM modes in a single beam is infinite, which significantly enhances spectrum efficiency. Compared to conventionally used frequency multiplexing such as OFDM which transmits and receives the data over multiple orthogonal subcarriers with different frequency spacing, OAM offers unique benefits for RF sensing applications, including higher spectral efficiency, improved spatial resolution, and enhanced interference robustness [86, 99]. OAM RF sensing is capable of detecting the orbital movement based on the rotational Doppler phenomenon.

2.2.3 Rotational Doppler Shift

Translational motion between an object and a source emitting electromagnetic waves leads to a linear Doppler shift. Conversely, rotational movement between an object and the wave source can induce a rotational Doppler shift, a concept initially introduced in optics [100]. The frequency of an optical beam carrying OAM changes when it interacts with a rotating object.

This frequency change is a consequence of the object rotational motion and is known as the rotational Doppler shift. The measurement of rotational Doppler shift was then introduced for RF waves as follows [101]: when an OAM RF wave interacts with a spinning object, the resulting rotational Doppler frequency shift Δf along the axis of the scattered wave can be represented in the frequency domain as follows,

$$\Delta f = \frac{\omega\ l}{2\pi} \tag{2.14}$$

where ω is the rotation speed of the spinning object in radians per second, l represents the topological charge (OAM mode), which is a numerical value denoting the phase front variation over a period of 2π [102]. Since $l\ >\ 0$ for OAM [103], the revolutions per minute (RPM) of the rotating object can be expressed as,

$$\omega_{rpm} = \frac{60 \times \Delta f}{l} \tag{2.15}$$

The rotational Doppler shift phenomenon has been widely used to measure rotational movement speeds using optical OAM beams for objects in the macroscopic scale [104], and using RF OAM wave for industrial purposes [17, 92, 93, 94].

2.2.4 RF OAM Sensing Applications

As previously discussed, OAM-carrying electromagnetic waves are recognised for their potential to enhance radio sensing techniques, offering advantages such as improved resolution, and enhanced robustness to interference. Additionally, OAM has the potential to enhance the performance of conventional object detection and imaging systems in sensing applications [86].

In recent years, enormous efforts have been made to improve imaging resolution using vortex

electromagnetic waves [105, 106, 107]. In 2013, Hu et al. [108] introduced the concept of electromagnetic vortex imaging, suggesting it can be used to create detailed images of targets. In RF OAM imaging, the azimuthal profiles of the objects are obtained where different azimuthal angles correspond to different spatial OAM modes, each carrying a unique amount of angular momentum and contributing to the overall spatial structure of the wave.

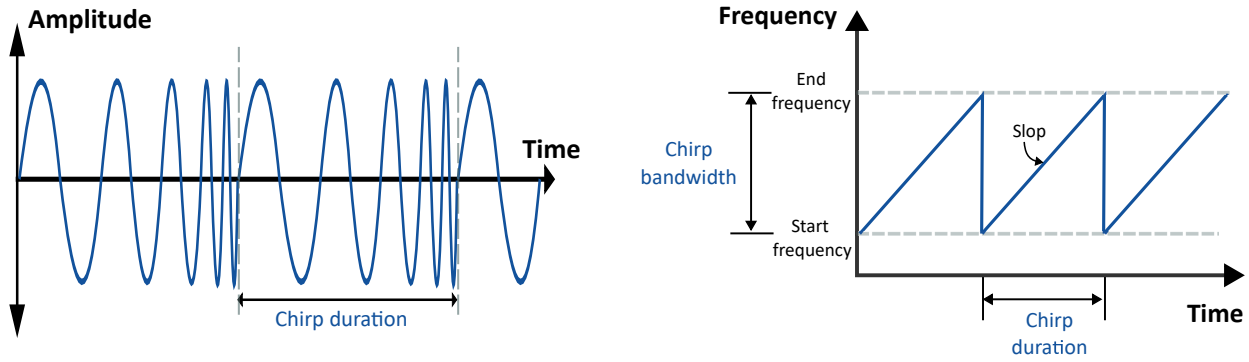
RF OAM is also capable of detecting and measuring the rotational velocity of a spinning object leveraging the rotational Doppler shift which is directly proportional to the rotational velocity of the object. This RF OAM property is used in this thesis to measure the rotation speed of drone propellers as introduced in Chapter 3.

2.3 Fundamentals of mmWave FMCW Radar

This section provides an overview of the fundamentals of mmWave FMCW radar, followed by discussions on range, Doppler, and angle measurements, as well as the primary data representations and techniques. Additionally, a review of recent advancement in mmWave sensing is provided.

2.3.1 mmWave FMCW Radar Overview

mmWave is a special class of radar technology that operates in the millimeter-wave frequency band, typically between 30GHz and 300GHz. The radar emits electromagnetic waves, which propagate through space and interact with objects within their path. These objects then reflect a portion of the electromagnetic waves back to the radar system. By capturing and analysing these reflected waves, the system can determine the distance, speed, and angle of the detected objects. mmWave radar transmits signals in millimeter-level wavelengths, which allows the detection of minute movements with high precision. This capability is achieved by using compact antennas due to the short wavelengths involved. mmWave radar can transmit different types of waveforms, such as pulsed, Frequency Shift Keying (FSK), Continuous Wave (CW), and FMCW [12]. This thesis uses FMCW radar waveform as a commonly employed type in mmWave radar systems. Unlike traditional CW radar systems, which emit waves at a fixed frequency, FMCW radar modulates the transmitting frequency. This frequency modulation enables the detection of target distance as well as Doppler effects. There are several modulation patterns for FMCW with different proprieties, such as sawtooth, triangular, rectangular, and staircase [109] where the sawtooth pattern is the most commonly used pattern with FMCW mmWave radar systems [28, 110] which is considered in this thesis. With the sawtooth pattern, the FMCW radar transmitter emits frequency-modulated chirps whose carrier frequency increases linearly with time. Figure 2.8 shows a representation of a chirp in time and frequency



(a) Chirp with amplitude as a function of time (b) Chirp with frequency as a function of time

Figure 2.8: Sawtooth modulation chirp signal

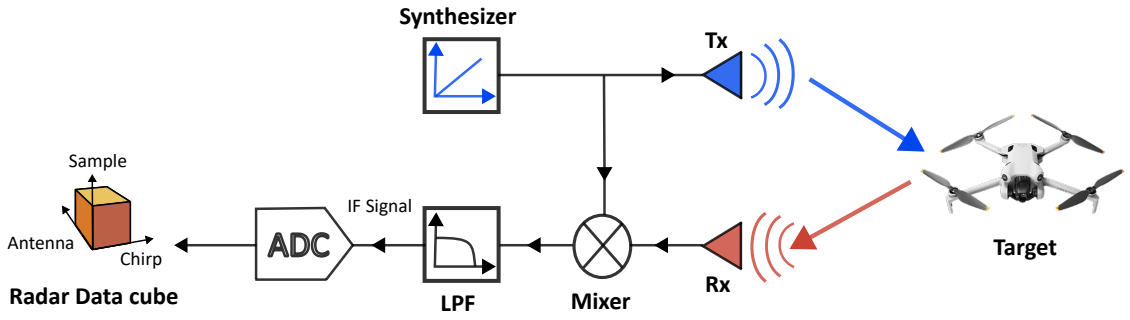
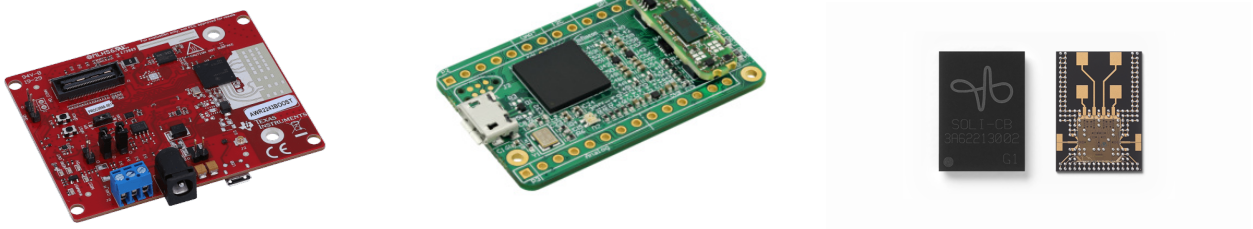


Figure 2.9: FMCW radar basic architecture

domains.

A simplified block diagram of FMCW radar is shown in Figure 2.9. The reflected waves from the target are received by the radar system and mixed with the original transmitted signal with a mixer which basically calculates the frequency difference between the transmitted and received signal. The low pass filter (LPF) filters out unrelated frequencies to produce the intermediate frequency (IF) signal, which contains information about the frequency shift caused by the target object's distance and velocity. The IF chirp signals are sampled using the analog-to-digital converter (ADC) and then processed to extract the raw radar data.

mmWave radar systems typically employ a multiple-input multiple-output (MIMO) antenna array, which is important for the target object's angle estimation by capturing the spatial



(a) TI AWR2243 (b) Infineon DE-MOBGT60LTR11AIP (c) Google Soli

Figure 2.10: Single-chip mmWave FMCW radar

diversity of reflected signals (further details are provided next). This involves a configuration of mixers, LPFs, and ADCs for each receiver (Figure 2.9 shows only one Tx-Rx pair). The received data from all receivers can be arranged into a 3D tensor of complex numbers, known as a radar data cube, that contains all the information provided by the radar device for a given time frame. For one frame that contains M chirps where each chirp contains N samples and transmitted-received by K antenna pairs, the radar data cube dimensions is represented as chirp data sample $1..N$ (denoted as fast time samples), chirp number $1..M$ (denoted as slow time samples), and Tx-Rx antenna pair $1..K$ (denoted as spatial dimension).

In order to address the requirements of diverse sensing tasks, a variety of commercial hardware devices have been deployed (examples are shown in Figure 2.10). Texas Instruments introduces the world's first single-chip mmWave radar, significantly reducing costs to tens of dollars, thereby making it affordable for vehicles and smart devices [111, 112]. Infineon developed tiny radar of size 3.3×6.7 mm which is a cost-effective sensor even in low power or battery-powered products. The tiny mmWave FMCW radar known as 'Soli' [113] was developed by Google's Advanced Technology and Projects (ATAP) group. Soli is smaller than a coin and has already been integrated on Google Pixel 4 smart phones for mid-air gesture interactions [114].

The rest of this section discusses range, velocity and AoA measurement details and estimation methods.

2.3.2 Range Measurement

The object's distance is estimated by extracting the peak frequency component of the IF signal, which corresponds to the frequency change caused by the round-trip time taken by the signal for back-and-forth traveling to the object. Figure 2.11 shows Tx and Rx chirps as a function of time for an individual detected object. Rx chirp is a time-delayed version of Tx chirp where the distance between the two chirp lines is fixed, which results in a constant frequency component f_0 in the IF signal and can be represented as follows,

$$\begin{aligned} f_0 &= S\ \tau \\ &= S\ \frac{2d}{c} \end{aligned} \tag{2.16}$$

where S is the chirp slop and τ is the time delay between the Tx and Rx chirps. τ can be further derived in terms of the distance between the radar and the detected object d, and the speed of light c. Therefore, the distance of the detected object is,

$$d = \frac{f_0\ c}{2\ S} \tag{2.17}$$

The distance is estimated by applying a Fast Fourier Transform (FFT) to the IF signal to extract frequency components corresponding to different target objects, which is known as Range-FFT.

The initial phase of the IF signal Φ_0 is the difference between the Tx and Rx chirp phases at the start time of the IF signal, that can be expressed as follows,

$$\Phi_0 = 2\pi f_c \tau \tag{2.18}$$

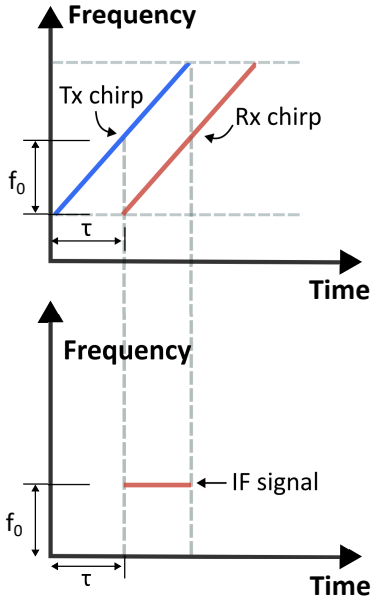


Figure 2.11: IF signal

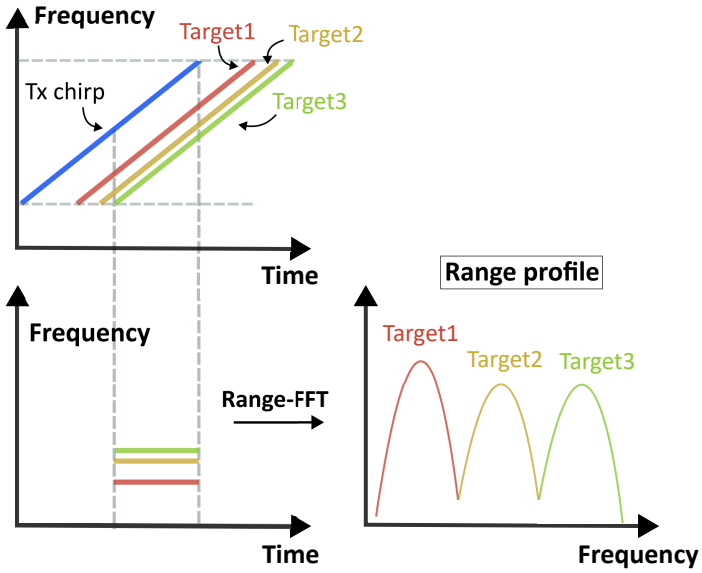


Figure 2.12: IF frequency components of multiple objects

where f_c is the chirp start frequency. Mathematically, Φ_0 can be further derived as follows,

$$\Phi_0 = \frac{4\pi d}{\lambda} \tag{2.19}$$

where λ is the wavelength (corresponds to the start frequency for simplicity). Thus, the IF signal of a single detected object at a distance d from the radar can be represented as follows,

$$A\sin\left(2\pi\ f_0\ t + \ \Phi_0\right) = A\sin\left(2\pi\ \frac{s2d}{c}\ t + \ \frac{4\pi d}{\lambda}\right) \tag{2.20}$$

Range Resolution: For multiple target objects at different distances from the radar, each reflected chirp from an object is received with a different amount of time delay proportional to the distance to the object. This variance in the arrival time translates into distinct frequency components in the IF signal, as shown in Figure 2.12. Based on Fourier transform theory [115], two frequency components need to be separated by more than $\frac{1}{T}$ Hz, where T is the observation interval, to be resolved in the frequency domain. Thus to distinguish between two different objects with the radar system, the difference between the corresponding frequencies

in the IF signal (Δf) needs to satisfy the following,

$$\Delta f > \frac{1}{T_c} \tag{2.21}$$

supposing T equals to the chirp time T_c. Given $\Delta f = \frac{S\ 2\Delta d}{c}$, the condition can be represented as follows,

$$\frac{S\ 2\ \Delta d}{c} > \frac{1}{T_c} \tag{2.22}$$

Since $B = S\ T_c$ where B is the chirp bandwidth, the range resolution d_{res} can be represented as follows,

$$d_{res} = \frac{c}{2B} \tag{2.23}$$

Equation 2.23 shows that the range resolution d_{res} depends only on the chirp bandwidth. Therefore, an FMCW radar with a chirp bandwidth of a few GHz can achieve a range resolution in centimetres.

Maximum Range: The maximum frequency component that can be captured in a signal is limited by the value of the sampling rate F_s. Thus, from Equation 2.17, the maximum detectable range d_{max} with the FMCW radar system is,

$$d_{max} = \frac{F_s\ c}{2\ S} \tag{2.24}$$

2.3.3 Velocity Measurement

mmWave radar has the capability to detect minute movements at the millimeter level of the target. Even a slight change in the target's distance induces a phase change across chirps in the reflected signal. By analysing the rate of chirp phase change, the radar can track micro-movements and accurately estimate the velocity of the target. In order to detect a target

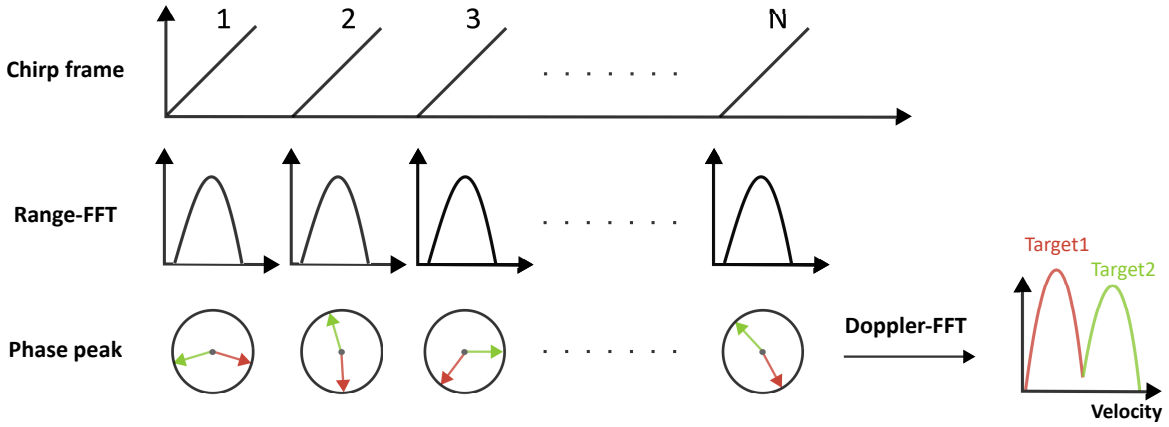


Figure 2.13: Doppler-FFT separates the two targets at the same range with different speeds

object velocity, the mmWave radar transmits two chirps separated by T_c. The range-FFT for each chirp will exhibit peaks at the same locations, but with different phases. The observed phase difference corresponds to an object motion of vT_c. The phase shift can be derived from Equation 2.19 as follows,

$$\begin{aligned} \Delta\Phi &= \frac{4\pi\Delta d}{\lambda} \\ &= \frac{4\pi v T_c}{\lambda} \end{aligned} \tag{2.25}$$

where Δd is the object's distance change. Thus, the object velocity can be derived as follows,

$$v = \frac{\lambda\ \Delta\Phi}{4\pi T_c} \tag{2.26}$$

FFT is used to estimate $\Delta\Phi$, known as Doppler-FFT, which is applied on the phase vector corresponding to the target range peak across all chirps.

For multiple objects, the radar system can distinguish between them if they move at different velocities even if they are equidistant from the radar. This is illustrated in Figure 2.13, where multiple targets moving at different speeds result in multiple peaks in the Doppler-FFT output. However, this distinction is subject to certain constraints, as elaborated next.

Velocity Resolution According to the theory of discrete Fourier transforms (DFT), the two frequencies can be resolved if their phase difference $\Delta\Phi$ is greater than $2\pi/N$, where N represents the total number of samples in the FFT or, in this context, the number of chirps in a frame. By substituting this phase difference condition in Equation 2.25,

$$\begin{aligned} \frac{2\pi}{N} &< \frac{4\pi\ \Delta v\ T_c}{\lambda} \\ \Delta v &> \frac{\lambda}{2NT_c} \end{aligned} \tag{2.27}$$

Since the frame time T_f equals NT_c,

$$v_{res} = \frac{\lambda}{2T_f} \tag{2.28}$$

Equation 2.28 shows that the radar's velocity resolution v_{res} is inversely proportional to the frame time T_f.

Maximum Velocity: Since the phase is periodic, $|\Delta\Phi|$ needs to be less than π to avoid ambiguity. This implies the following,

$$v_{max} = \frac{\lambda}{4T_c} \tag{2.29}$$

Equation 2.29 shows that shortening the transmission time between chirps results in a higher v_{max}.

The range-FFT and Doppler-FFT are often applied to the IF signal to generate a 'Range-Doppler Heatmap', where each peak represents a detected object at a specific range and speed.

2.3.4 Angle of Arrival Measurement

FMCW radar systems can estimate the angle of the reflected signal on the radar array if it has at least two receivers. The spatial position difference between the receivers results in variations

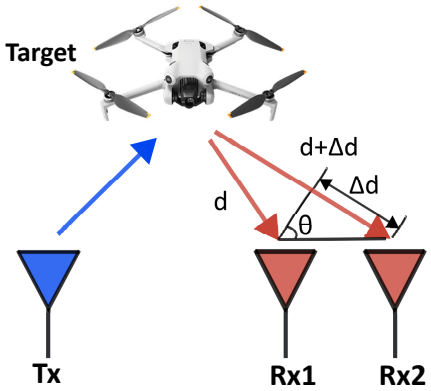


Figure 2.14: AoA can be estimated from the phase shift caused by the slight distance difference between the target and the Rx antennas

in the traveling distances (as shown in Figure 2.14), which leads to a phase shift in the FFT peak. The difference in travel distance of the received signal between two receiver antennas Δd is,

$$\Delta d = l \ \sin(\theta) \tag{2.30}$$

where l is the spatial location distance between successive receiver antennas, and θ is the AoA. In this antennas configuration, the phase shift between two neighbouring antennas is represented as follows,

$$\Delta\Phi = \frac{2\pi l \sin(\theta)}{\lambda} \tag{2.31}$$

Rearranging Equation 2.31, the angle of arrival θ is calculated as follows,

$$\theta = \sin^{-1}\left(\frac{\lambda\Delta\Phi}{2\pi l}\right) \tag{2.32}$$

The change in phase $\Delta\Phi$ depends on $\sin(\theta)$, which demonstrates a nonlinear relationship. For small angles, $\sin(\theta)$ can be approximated linearly ($\sin(\theta) \sim \theta$). Consequently, the accuracy of

the angle estimation relies on the AoA value and is more accurate when it has small values.

The angle information in extracted by observing the phase change between different antennas, achieved by applying an additional FFT (Angle-FFT) on the phase vector across the receiver antenna array.

Angular Resolution: Considering two objects have angles of θ and $\theta + \Delta\theta$ relative to the radar, the angle resolution determines how small $\Delta\theta$ can be to distinguish between these two objects. Given an object with AoA of θ has a discrete frequency of $\omega = \frac{2\pi l \sin(\theta)}{\lambda}$ in the Angle-FFT, thus, the difference between frequencies corresponding to two objects with $\Delta\theta$ angle apart is,

$$\begin{aligned} \Delta\omega &= \frac{2\pi l}{\lambda}(\sin(\theta + \Delta\theta) - \sin(\theta)) \\ &\simeq \frac{2\pi l}{\lambda}\cos(\theta)\Delta\theta \end{aligned} \tag{2.33}$$

Since the derivative of $\sin(\theta)$ is $\cos(\theta)$ (i.e., $\frac{\sin(\theta+\Delta\theta)-\sin(\theta)}{\Delta\theta} = \cos(\theta)$). As discussed previously, distinguishing two frequencies requires their difference $\Delta\omega > \frac{2\pi}{N}$, where N is the number of samples in the FFT (the number of receivers in this case). Using Equation 2.33,

$$\Delta\theta > \frac{\lambda}{Nl\cos(\theta)} \tag{2.34}$$

Therefore, the angle resolution θ_{res} is,

$$\theta_{res} = \frac{\lambda}{Nl\cos(\theta)} \tag{2.35}$$

The angle resolution variation is dependent on θ, with the optimal angle resolution achievable at $\theta = 0$, where the object is directly in front of the sensor, aligning with the earlier discussion.

Maximum Angular Field of View: As discussed previously, because of the phase periodicity, unambiguous angle measurement requires $|\Delta\Phi|$ to be less than π. From Equation 2.31, this

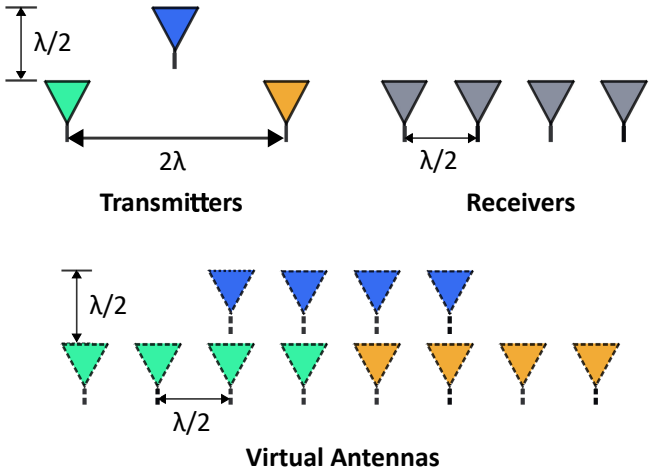


Figure 2.15: MIMO layout of TI AWR2243

corresponds to the following,

$$\pi > \frac{2\pi l \sin(\theta)}{\lambda} \tag{2.36}$$

Thus, the maximum field of view for radar array is,

$$\theta_{max} = \sin^{-1}(\frac{\lambda}{2l}) \tag{2.37}$$

With $l = \lambda/2$, the above equation results in maximum field of view of $[-90^{\circ}, 90^{\circ}]$.

As previously discussed, MIMO technology which refers to an antenna array with multiple transmitters and multiple receivers, is commonly used with the mmWave radar [116]. By arranging antennas in proper locations, each transmitter-receiver pair works as a virtual antenna for better AoA estimation resolution. The mmWave radar used in this thesis is the Texas Instruments TI AWR2243[1] which integrates 3Tx-4Rx MIMO directional antenna array (7 on-board antennas) and typically has a maximum transmit power of 13dBm per transmitter. The configuration of the 2D array is shown in Figure 2.15, which is able to estimate the Azimuth (with 8 virtual antennas) and elevation (with 2 virtual antennas) angles.

[1] www.ti.com/product/AWR2243

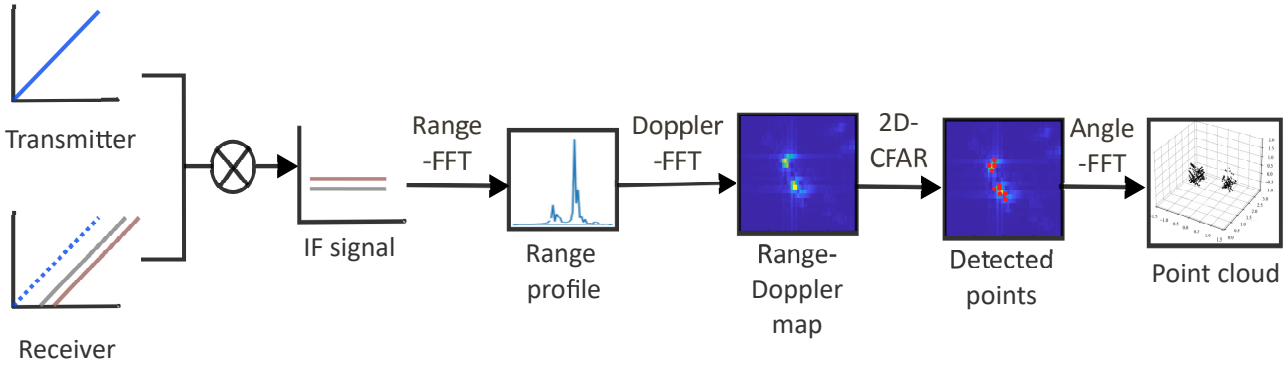


Figure 2.16: Point cloud pipeline

2.3.5 Conventional Point Cloud Generation

FMCW radar array is able to produce 3D point cloud (x, y, z) of the target objects using the range, velocity, and angle measurements [27, 117]. Figure 2.16 presents a conventional pipeline for 3D point cloud generation. The input raw radar data is the radar cube of the 3D signal that is produced at each time frame with dimensions of the chirp data sample (fast time samples), chirp number (slow time samples), and antenna number (spatial dimension). The sampled raw IF signal is first transformed into the frequency domain by applying Range-FFT along the fast time dimension to construct the range profile, followed by applying Doppler-FFT along the slow time dimension to construct the Range-Doppler map. Each peak in this map corresponds to a potential detected object in the environment at a specific range with a particular speed. The peaks can be identified using a peak detection algorithm such as the 2D constant false-alarm rate detector (2D-CFAR) algorithm [118]. In the 2D-CFAR algorithm, the Range-Doppler map is fed into the detector to extract dominant points, i.e., removing background clutter and reducing noise, making it less dependent on the environment's characteristics. Azimuth and elevation AoA are then calculated by applying Angle-FFT along the spatial dimension to observe the phase change between different antennas. Another way is to calculate AoA directly using the range profile across the virtual antennas to construct the Range-Angle map which provides position information for targets without the velocity information.

However, conventional low-cost single-chip mmWave radar systems are limited to producing sparse point clouds due to hardware constraints [26, 27]. Additionally, the noise and limited resolution of certain information, such as AoA measurements, can lead to a performance decline when employing traditional signal processing methods, particularly at longer distances. To address these challenges, this thesis implements additional signal processing approaches that leverage effective noise and interference reduction methods, including wavelet denoising, wavelet transformation, autocorrelation analysis, and Kalman filter. Additionally, the developed localisation technique relies on more robust mmWave measurements (micro-Doppler information) which expand the reliable localisation coverage area.

2.3.6 mmWaves Sensing Applications

The emergence of single-chip mmWave radar technology has expanded the design possibilities for various applications in diverse fields, acquiring significant research attention in recent years. This section introduces an overview of the relevant literature, presenting background information on conventional mmWave sensing methods along with recent advancements. Initially, this section provides an overview of recent developments in FMCW mmWave radar across various domains. Then, it delves into the specifics of techniques relevant to micro-motion sensing, detection and localisation tasks.

mmWave Sensing Solutions

Compared to other wireless sensing technologies, such as WiFi and acoustic signals, mmWave is highly sensitive to tiny millimeter-level displacements of target, making it suitable for a variety of applications. These applications include human sensing, industrial, and robotics applications. Table 2.2 provides a summary of recent advancements across various mmWave sensing categories.

The description of the main methods involves two parts. The first part is the data representation/signal form used in the proposed system, and the second part is the category of the used algorithms for processing.

Category	Name	Target Task	Hardware Platform	Main Methods
Robotics Sensing	[119]	Localisation and mapping	TI AWR1843	Range-Doppler spectrum / GAN
	mmHawkeye [120]	Outdoor drone detection	TI IWR6843ISKODS	Doppler spectrum / LSTM
	mDrone [121]	Indoor drone localisation	TI IWR6843ISK	Range-Angle spectrum / CNN-LSTM
	RIO [122]	Motion estimation	TI AWR1843BOOST	Point cloud / EKF
Human Sensing	MU-ID [123]	Gait recognition	TI AWR1642BOOST	Range-Doppler spectrum / DNN
	mmFER [124]	Recognise facial expressions	TI IWR1843BOOST	phase waveform / GMM, cross domain transfer, autoencoder
	mmTrack[125]	Multi-person tracking	Qualcomm 802.11ad	CIR / MVDR, k-means clustering
	AmbiEar[126]	Voice recognition	TI IWR1642BOOST	Range-Angle spectrum, IQ and Doppler signals/ DNN
	VED [127]	Heartbeat sensing	TI IWR1843BOOST	IQ and phase signals
Industry Sensing	mRotate[128]	Rotation speed sensing	TI IWR1443BOOST	Range, Doppler spectrum / GSV, Chirp frequency hopping
	mmVib [19]	Vibration measuring	TI IWR1642BOOST	Range-Doppler spectrum/ MSC model

Table 2.2: A brief summary of recent works in mmWave FMCW radar sensing for different application categories. DNN: Deep Neural Network; EKF: Extended Kalman Filter; GSV: Group Sum Value; GAN: Generative Adversarial Network; MSC: Multi-Signal Consolidation; CIR: Channel Impulse Response; MVDR: Minimum Variance Distortionless Response.

mmWave Detection and Micro Motion Sensing

A fundamental challenge in tracking tasks is differentiating the target object from static objects in the surrounding environment. This is because the received signal comprises both the reflected signal of the target body and signals reflected from other objects in the environment. Existing research in radio-based sensing frequently relies on analysing object dynamics, leveraging approaches such as recognising features like signal variance or detecting discriminative signatures such as human breathing rates. As previously mentioned, mmWave FMCW radars have the ability to distinguish between objects by tracking displacements with micro-level precision through phase changes detection in the received signal. Micro movements, such as subtle internal mechanical vibrations, can manifest within the structure of an object whether it re-

mains stationary or is engaged in primary bulk motion, where these minute movements may coincide with the object's primary movement when it is in motion. These micro movements induce phase changes that result in frequency modulation of the reflected signal, leading to the observation of the micro-Doppler phenomenon [129]. This phenomenon is observed in variuos situations, including the individual movements of a person's legs and arms while walking, or the rotations of a drone's propellers while flying. To monitor the phase change caused by these micro motions with mmWave FMCW radar, the initial step involves extracting the phase information of the target object by conducting a Range-FFT on the raw IF signal. The Fourier transform maintains the phase information, allowing for the extraction of the phase variation signal from the corresponding peak in the range profile across chirps.

Micro-movement sensing can be useful in many other areas besides object detection. For example, mmVib [19] is designed for monitoring machine vibrations in industrial settings, where micro displacements can be intentionally manipulated and encoded to convey information that can be sensed using mmWave radar technology. A rotation speed monitoring system is proposed to monitor industrial machine health in [128] using mmWave radar. Another system [130] has been proposed to detect the displacement of water surfaces induced by underwater acoustic signals by utilising FMCW radar to transmit information across the water-air boundary. Furthermore, mmWave radar micro-displacement sensing is important for remote vital sign monitoring applications, including heart rate and breath rate monitoring [20, 131, 132].

The proposed approaches in this thesis leverage the mmWave micro-movement sensing capabilities to detect drones in dynamic environments through extracting their propeller spinning signature and to measure the propeller rotation speeds. More details are presented in Chapters 3 and 4.

mmWave Localisation and Tracking

Traditional FMCW radar target tracking methods mainly depend on point clouds, which typically include reflections from multiple targets as well as noise. Clustering algorithms are employed to partition the point cloud into distinct segments. Density-based spatial clustering of applications with noise DBScan algorithm [133] is frequently chosen as the clustering method due to its ability to cluster based on the distances between point pairs without necessitating the number of clusters as a parameter. Additionally, DBScan can effectively filter out noise by setting a minimum number of points required in a cluster. The tracking process primarily consists of linking clusters across frames. The Hungarian algorithm [134], a known solution for the assignment problem, is commonly employed to link clusters across frames. The Kalman filter [135] is also used for correcting and predicting tracks. In complex situations, including multiple target tracking tasks, algorithms such as the Joint Probabilistic Data Association Filter (JPDAF) [136] and Multi-hypothesis Tracking (MHT) [137] demonstrate robust performance in noisy environments.

In Chapter 4, a localisation system is proposed that leverages the DBScan clustering algorithm and a Kalman filter to 3D track drones indoors.

2.4 Summary

This chapter provides a thorough overview of the existing research, methodologies, and advancements in drone localisation and autopilot control systems, which leverage various sensing technologies. It also delves into the fundamentals, advantages, and applications of radio wave sensing, focusing on 5GHz RF OAM and mmWave FMCW radar technologies, showcasing the great potential of radio sensing to enhance drone localisation and navigation control.

The following three chapters each focus on different approaches to enhance indoor drone detec-

tion and localisation, and autopilot control for reliable navigation. These proposed approaches leverage radio wave sensing technologies to enhance the sensing of drone's macro and micro-movements. In the next chapter, Chapter 3, methods for sensing the propeller rotation speed of flying drones are proposed for enhanced detection and precise tracking of drones which will be further explored in the subsequent chapters.

Chapter 3

Drone Propeller Rotation Speed Measurement Using Radio Wave Sensing

Propeller rotational movement plays a crucial role in determining the motion characteristics of drones, influencing their performance in several key areas. The precise measurement of drone propeller speeds has the potential to enhance drone navigation stability, autopilot control, detection and localisation. This chapter introduces two radio sensing approaches to sense the rotation speeds of drone propellers while in flight. These approaches use two sensors operating at the frequency bands of 5GHz RF OAM waves and 77GHz mmWave radar. Extensive flight arena experiments are conducted to compare the performance of both approaches using a commercial drone and to discuss their respective advantages and disadvantages.

3.1 Motivation and Objectives

Drones have experienced a rapid increase in both capability and accessibility, a trend that continues to grow. Consequently, there is a rising demand for several technologies to enhance their operation, including reliable navigation, precise localisation, drone identification, and intruder detection. The rotational movement of propellers is fundamental in determining the motion characteristics of multirotors, a dominant category of drones, as discussed in Chapter 2. Sensing multirotor propeller speeds during flight can assist a wide range of applications, with a significant impact across various domains. For instance, the measurement of propeller rotation speeds can be incorporated into drone autopilot systems to improve autopilot control and state estimation. This leads to more precise localisation and enhanced flight stability for reliable navigation [138, 139, 140]. Additionally, sensing propeller rotational movement enhances the performance and extends the capabilities of security applications that require drone detection and identification [61, 141, 142, 143, 144]. For example, the performance of distinguishing drones from other flying entities is enhanced [142] and the drone identification is extended to identify the drone's load beside the drone's model [143] with the integration of propeller speed sensing.

The aforementioned studies use vision-based sensing [141, 142, 144], acoustic signals [61, 145], or motor current sensing [139] to detect drone rotor motion. However, these sensing techniques are either limited by weather and light conditions (i.e., vision), audio noise interference (i.e., acoustics), or have limited accuracy due to parameter estimation uncertainties (i.e., motor current sensing [146]). Alternatively, there is an increased use of radio waves more generally to sense rotation movements or spin speeds of motors, and these are demonstrably not affected by noise or illumination conditions [17, 128]. For the most part, these techniques leverage radio waves at the 5GHz frequency band or use 77GHz mmWave radar, and they all assume the object being sensed is in a stationary state, even when these techniques are applied for drones

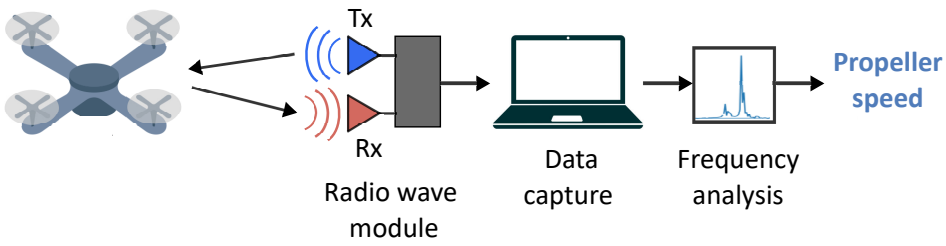


Figure 3.1: Radio sensing-based drone propeller speed measurement system overview.

[138, 147].

To this end, this chapter presents a case study to experimentally evaluate the performance of both the 5GHz RF OAM and FMCW 77GHz mmWave radar sensing approaches for measuring the propeller speed of flying drones, for the first time in literature, to the best of our knowledge. An overview of the radio wave sensing-based propeller speed measurement system is shown in Figure 3.1. Both approaches depend on extracting the micro-Doppler shift that corresponds to the propeller spinning motion, where its frequency band is used to calculate the propeller speed. The advantage of using micro-Doppler shifts to sense propeller speeds during flight lies in their independence of the relative position of the rotating target and transmitter. As a result, their signatures are commonly used for object identification applications, including drones [148, 149, 150]. The experiments are conducted in a flight arena using a commercial drone to primarily assess two metrics: the accuracy of radio waves to measure high rotation speeds within the drone flying speed range, and the sensing distance range.

Theoretically, the shorter wavelengths of mmWave radar, coupled with higher operating frequencies and broader frequency bandwidth, enable finer resolution and improved performance in extracting micro-Doppler of target objects. On the other hand, longer wavelengths of 5GHz RF have the physical advantage of better penetration and less attenuation due to atmospheric absorption and scattering, resulting in better signal propagation over longer distances. To better understand the tradeoff between resolution and sensing distance, the experiments are conducted to compare both the 5GHz RF OAM and 77GHz mmWave radar sensing approaches.

In the experimental setup, the 5GHz RF is paired with OAM to augment spatial resolution performance, particularly for sensing the rotation of flying drone with small propeller blades.

The rest of this chapter is organised as follows: Section 3.2 provides an overview of rotor speed measurement techniques in the literature. Section 3.3 presents the technical details of the 5GHz RF OAM approach and its evaluation results, while Section 3.4 presents the details and evaluation of the mmWave approach. Finally, the chapter is concluded in Section 3.5.

3.2 Rotor Speed Measurement Techniques

In industrial motors, the rotor speed is usually measured and used as a feedback signal to the control system to enhance the motor performance. This approach is also implemented in drones where precise knowledge of actual propeller speeds provides useful information that can enhance drone navigation and task execution [139]. A typical onboard speed tracking technique is available through the drone's electronic speed controllers (ESCs) [139]. However, higher-performance ESCs are often larger and heavier, which can pose challenges for smaller drones where weight and size are critical considerations. Another technique is to estimate the rotor speed based on the motor current sensing approach [151] which estimates the motor speed with the knowledge of motor parameters (e.g., motor constant, resistance, and inductance). Although this approach is common, the estimated speed has limited accuracy due to its dependence on motor parameters, where any variations or inaccuracies in these parameters can affect the precision of the estimated speed. Further, the dynamic response of motor current to changes in speed may not be fast enough with the rapidly changing speed requirements of the drone propellers.

To mitigate these limitations, other techniques directly measure the rotation speed by implementing various types of speed sensors that have been proposed to sense the speed of rotary

parts of stationary objects. One example is the tachometer [152, 153] which is an optical device that provides accurate speed measurement by emitting a laser beam towards the rotating object with attached reflective tape. However, the laser tachometer fails when the target object material is highly reflective, where the laser reflections from the attached tape can not be distinguished from the rotating object surface reflections. Additionally, the effective operating distance of the laser tachometer, approximately $20cm$ [154], is insufficient for many applications that demand a longer measurement distance. The electromagnetic-based speed-sensing approaches detect the change of the electromagnetic field resulting from the object's rotation by employing electrostatic [155, 156] or hall-effect [157] sensors. However, these approaches are constrained in terms of effective working distance, typically limited to a few centimetres (around $10cm$). The vision-based approaches utilise various optical sensors for sensing rotation speed. RGB cameras, for instance, are employed to capture images of a rotating object, extracting features that are analysed to estimate the rotation speed [158, 159]. However, these approaches are limited to sensing a maximum rotation speed of 1500RPM due to the relatively low frame rate of RGB cameras. Other approaches [160, 161] leverage high-speed cameras to enhance the capability of measuring higher rotation speeds. Nevertheless, the high cost of such cameras limits their widespread adoption. Additionally, camera-based systems face constraints in terms of sensitivity to light.

Compared to the previously mentioned technologies, radio waves are resilient to variations in illumination conditions and the light reflectivity of the target object. Although the radio waves sensing approach has demonstrated its effectiveness in sensing the rotation speeds of static objects in the literature [17, 128, 138, 147], its sensing performance has not yet been investigated for moving objects such as drones. The proposed approaches in this chapter investigate the capabilities of radio waves at 5GHz and 77GHz mmWave frequency bands in sensing the rotation speed of drone propellers while flying, for the first time in literature, for the potential of enhancing navigation stability, localisation, intruder detection, and identification.

3.3 Drone Propeller Speed Measurement using 5GHz RF OAM Waves

This section presents a case study on drone propeller speed sensing with 5GHz RF. This is achieved using a custom-built hardware system developed in our research group [17], which was initially developed to sense the rotation speed of stationary objects. First, the methodology is summarised, followed by a discussion of the evaluation results.

3.3.1 Methodology

By exploiting the spatial properties of OAM, 5GHz RF OAM sensing technology has the potential to achieve finer resolution sensing, enabling more precise detection of small rotating blade motion. The rotational Doppler shift phenomenon [100] is leveraged to estimate the rotational speed of the spinning propeller of a drone. With the rotational Doppler effect, the change in received wave frequency reflects the speed of the rotating object, as described in Chapter 2. The RF sensor has a transceiver that operates in the 5GHz band to transmit OAM electromagnetic RF waves. When an OAM wave interacts with the spinning propeller, the Doppler frequency shift Δf on the axis of the scattered wave can be used to measure the RPM of the rotating object as,

$$\omega_{rpm} = \frac{60 \times \Delta f}{l} \tag{3.1}$$

where l is the topological charge (it is the OAM state number that represents the phase front variation in a period of 2π [102]). This relation is used to measure the propeller rotation speeds with the application of signal pre-processing and post-processing procedures.

The process starts by transmitting multiple narrowband signals on several subcarriers. DFT analysis is then applied on the N received subcarriers, followed by localising the frequency peak

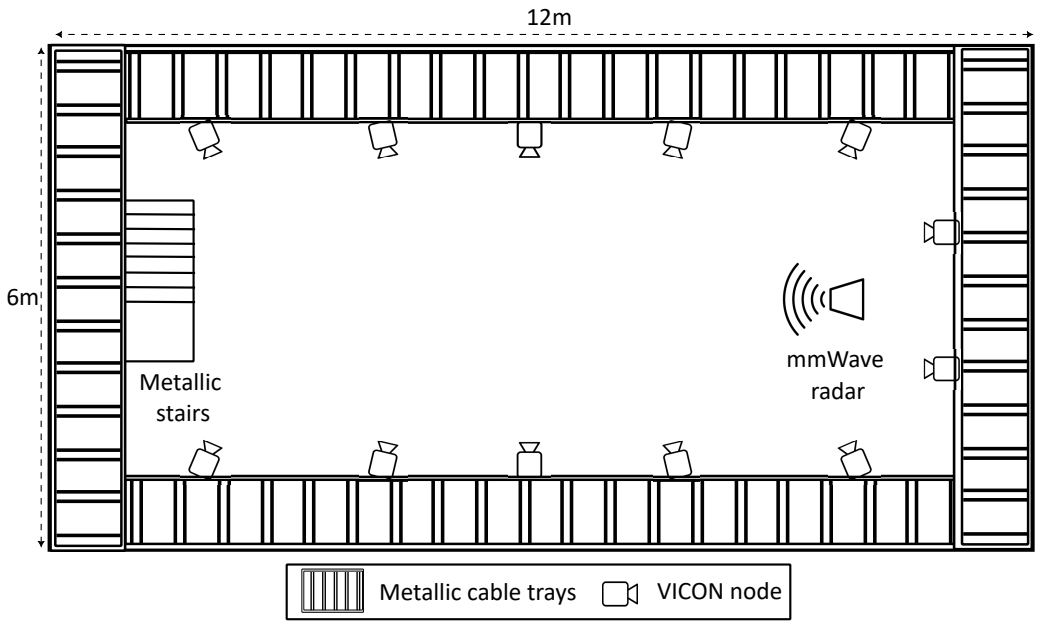


Figure 3.2: Layout of the flight arena.

corresponding to the rotation speed and its harmonics using a thresholding technique. The rotation speed measurement for each subcarrier is then extracted by calculating the greatest common factor of the fundamental frequency and harmonics. Finally, the measurements of the N subcarriers are aggregated after removing outliers. The subcarriers operate at multiple frequency bands to address interference problems caused by dynamic human and object movements.

3.3.2 Evaluation

In a flight arena, physical experiments are conducted to evaluate the accuracy of measuring propeller speeds of a commercial drone using the 5GHz RF OAM sensing technology. The experiments are performed in an indoor flight arena equipped with a VICON motion capture system to trace the drone position ground truth measurements at a sample rate of 100Hz. The flight arena for the experiments includes metallic obstacles, such as stairs, cable trays, and stands (Figure 3.2), which introduce sources of electromagnetic interference (EMI).

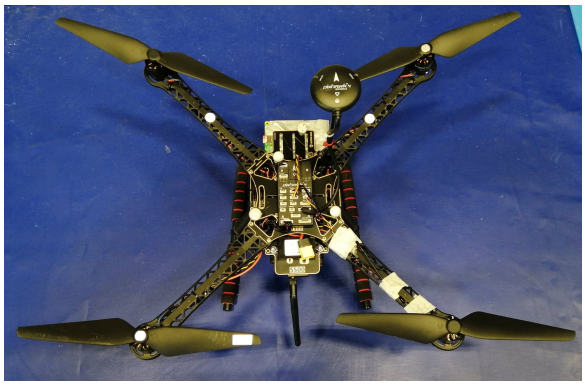
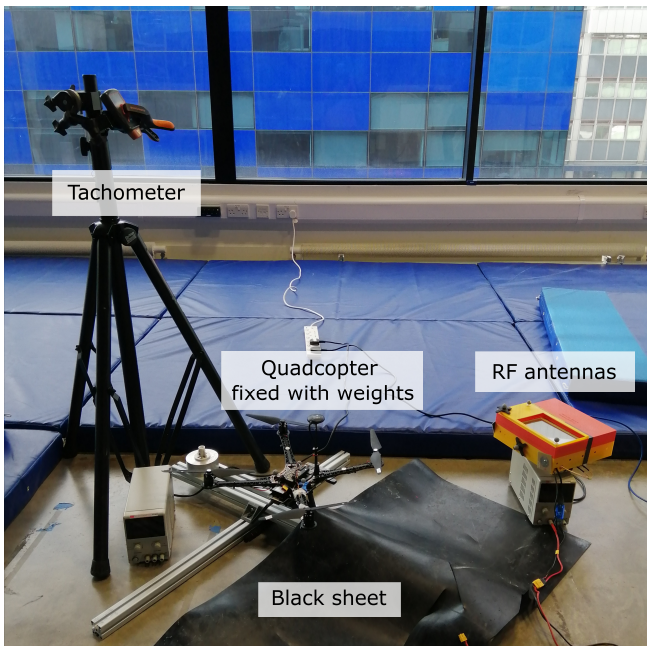
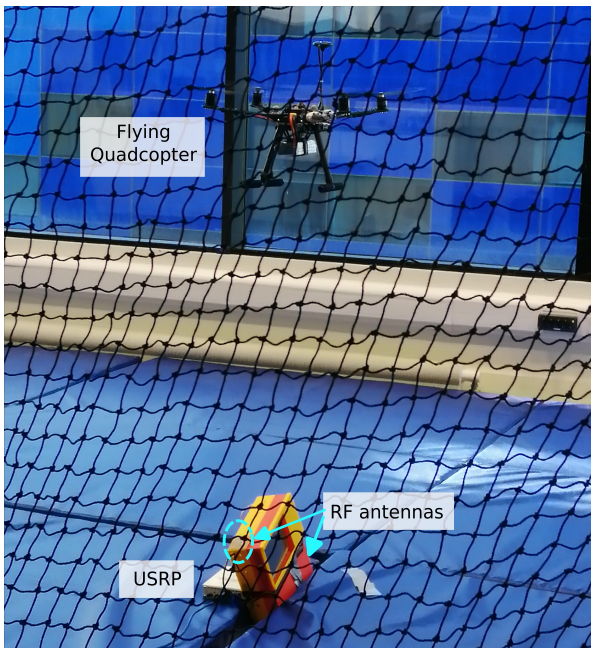


Figure 3.3: Holybro S500 V2 quadcopter, the used drone in the experiments.



(a) Fixed drone scenario setup. The black sheet is used to have accurate measurements of the tachometer.



(b) Flying drone scenario.

Figure 3.4: Experimental setup for RF sensing approach.

The flights are performed using a Holybro S500 V2 quadcopter (Figure 3.3) with Pixhawk 4 autopilot running PX4 firmware[1]. The quadcopter is equipped with four 2216-980KV brushless motors and 9-inch propellers with two blades per propeller. The drone weighs about 782g. Two RF OAM antennas are used as a receiver and transmitter and operate at a frequency band of 5.525GHz with a transmission power of up to 22dBm ($\sim 150mW$). Both antennas are

[1]https://px4.io

connected to USRP B210 Software Defined Radio at a sampling rate of 1MS/s. The USRP is connected to a laptop running GNU Radio 3.7 for processing. The experiments include both fixed and flying drone, as shown in Figure 3.4. The relative error rate of RPM is used to assess the accuracy of the angular speed of the spinning propellers. The RPM relative error rate is calculated as $|\frac{\hat{S}-S}{S}|\%$, where $\hat{S}$ is the RF propeller speed measurement and S is the propeller speed ground truth, where motor commanded speeds are used as the reference (validated with a tachometer). It is assumed that a single drone is present in the flight arena during the experiments.

Capturing Different Rotational Speeds

A fixed-drone scenario is employed to evaluate the system's ability to capture different propeller rotation speeds in the range of arming and flying scenarios. Figure 3.5 shows the commanded pulse width modulation (PWM) received by the flight controller, which represents the magnitude of the commanded RPM, versus the actual RPM measurement using both the RF OAM sensing approach and a tachometer, while the quadcopter is manually controlled. The commanded PWM values are varied by changing the throttle level of a handheld radio remote control. The commanded PWM values in the range of 0 to 100% throttle level on the remote control are from 984 to 2006. Referring to Figure 3.5, each commanded PWM (throttle level) is mapped to a variable propeller speed range. For lower PWM values, the actual RPM linearly changes with the commanded PWM. The actual RPM range then significantly increases with a commanded PWM of 1171 (18% throttle) to be around 11000 RPM and continuously increases until it reaches around 14000 RPM with a commanded PWM of 2006 (100% throttle).

Figure 3.6 shows the relative error rate of estimating the propeller rotational speed using RF sensing (relative to the tachometer). It shows the ability of the RF approach to accurately capture the rotation speed even for the high speeds of $\sim$ 16000 RPM with a relative error rate of 0.63%.

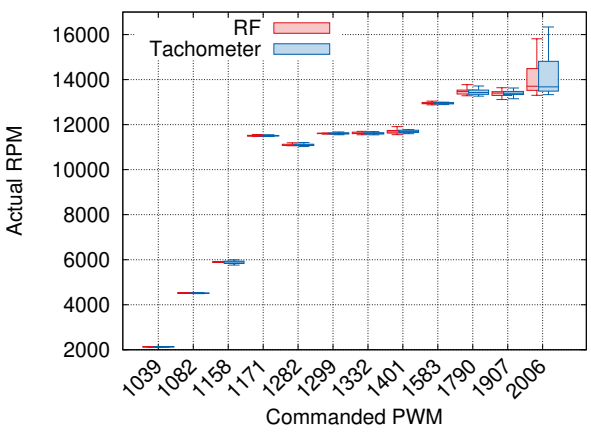


Figure 3.5: Commanded PWM versus actual RPM measured by Tachometer and 5GHz RF OAM approach.

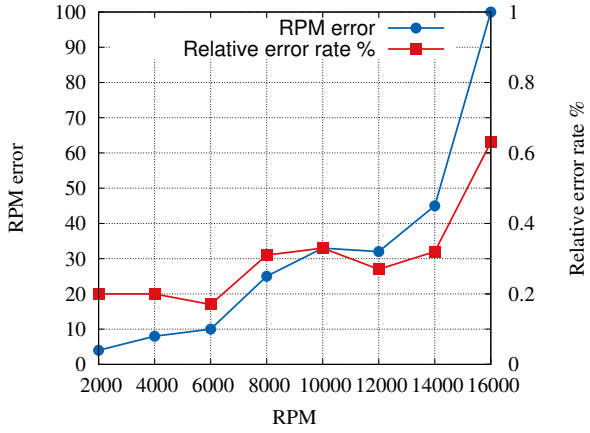
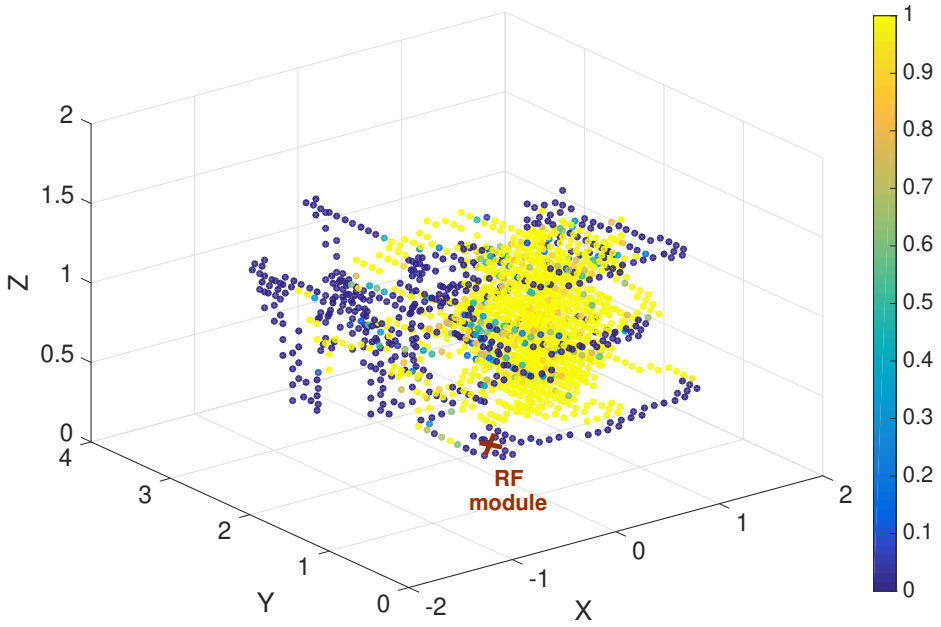


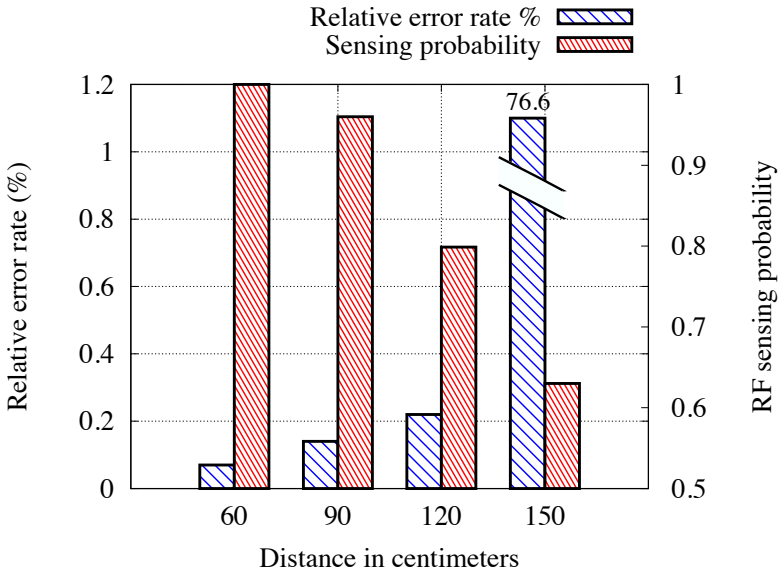
Figure 3.6: RPM estimation error and the relative error rate of RF speed sensing for the different flight speeds.

RF Rotational Speed Sensing Distance Range

In this experiment, the drone hovers randomly in the flight arena while the RF antennas are mounted on the floor to face the ceiling of the flying arena. This setup covers several situations of different distances, motion speeds, and relative angles. Figure 3.7a shows a 3D scatter plot of drone positions during flight. The color of the scattered points indicates the likelihood of the RF sensor capturing the propeller speed at the corresponding 3D points during the flight. This likelihood is depicted using a heatmap color bar, where different colors represent different probabilities. For instance, a probability of 1 for a scatter point denotes that the RF sensor captured a frequency peak within the typical propeller speed range of a flying drone for 100% of the drone's presence at that point. It can be observed that the sensor coverage area for RF speed sensing forms a spheroid with diameter dimensions of 1.5×1 m. Figure 3.7b shows how the distance between the RF module and the drone affects the accuracy of the RF speed measurement. The RF sensor provides an RPM relative error rate of 0.14% with a probability of capturing the propeller speed of 96% at a distance of 0.9m, i.e, RF sensor provides measurements for 96% of the drone presence at 0.9m distance. This sensing range is relatively wide compared with that achieved by a tachometer which can only work when facing in LoS



(a) Scatter plot of captured drone 3D positions while flying in the lab arena. The color of the dots indicates the probability of acquiring a precise RF propeller rotation speed measurement while flying.



(b) The impact of distance between RF module and drone on accuracy and coverage estimation.

Figure 3.7: RF sensing distance range

(the device needs to point at the correct angle to face the reflective tape). This sensing range is sufficient to cover medium-sized drones in case the RF sensor is mounted on the drone's body or using the already mounted sensor for radio communication where 5GHz matches a typical drone's communication band, for enhancing autopilot control or failure detection/diagnosis applications. However, the 0.9m sensing range is not appropriate for applications that require the RF sensor to be separately mounted in the flying environment apart from the drone's body, such as intruder drone detection and identification, and localisation applications.

3.4 Drone Propeller Speed Measurement using FMCW mmWave Radar

This section explores the potential of the second proposed approach (Figure 3.8), utilising 77GHz mmWave radar, a common frequency band employed by off-the-shelf mmWave radars, to sense drone propeller speeds. It starts with an introduction to the fundamentals of FMCW mmWave signal parameters, followed by a discussion of the methodology used to extract the rotation speed from mmWave signals, ending with performance evaluation.

3.4.1 Preliminaries

As described in Chapter 2, FMCW is a modulation technique used in mmWave radar for measuring the range, velocity, and angle of the target object. FMCW radar emits electromagnetic wave chirps whose carrier frequency increases linearly with time. The reflected waves from the target are received by the radar system and mixed with the original transmitted signal to produce an IF signal which provides information about the frequency shift caused by the target object's distance and velocity. mmWave radar systems usually employ MIMO antenna arrays; a configuration that is important for the target object's angle measurement estimation. The

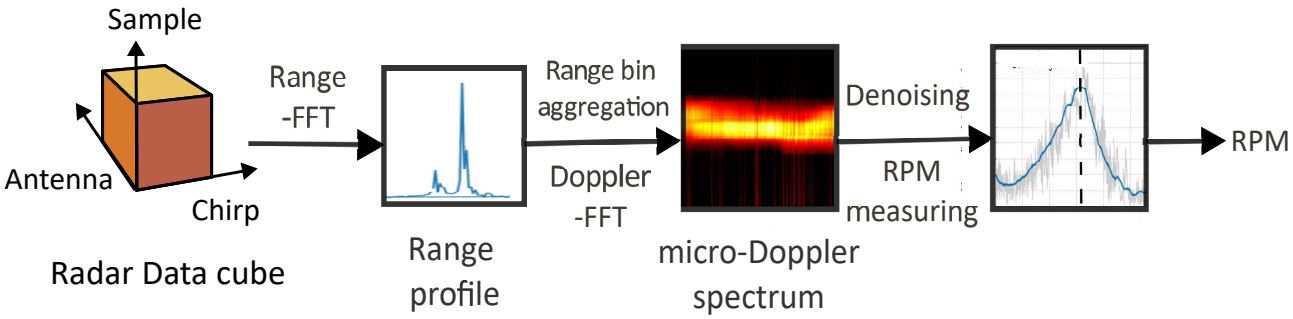


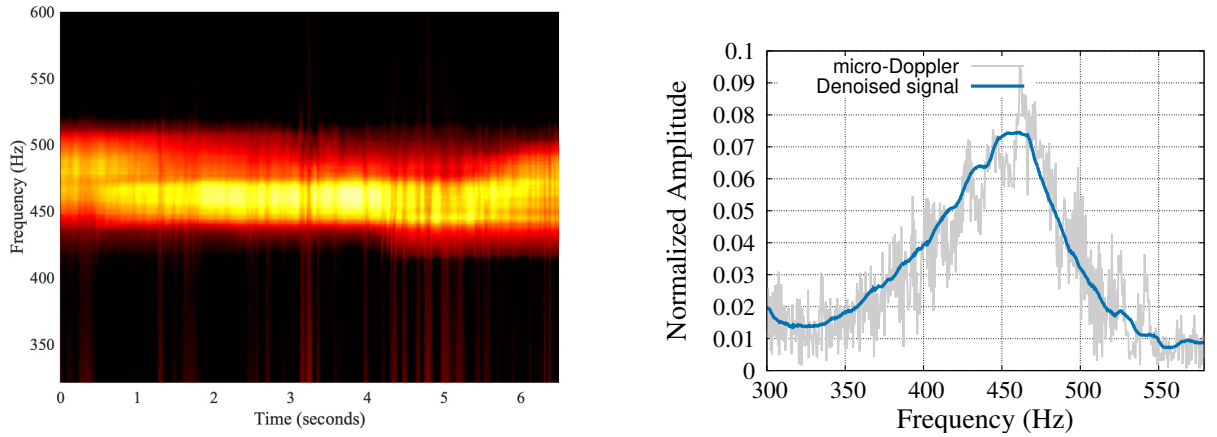
Figure 3.8: RPM extraction workflow.

received data can be arranged into a 3-D tensor of complex numbers, known as a radar data cube, that includes all information provided by the radar device for a given time frame. For one frame that has M chirps where each chirp has N samples and received by K antenna pairs, the radar data cube dimensions are chirp data sample $1..N$ (denoted as fast time samples), chirp number $1..M$ (denoted as slow time samples), and antenna pair $1..K$ (denoted as spatial dimension).

3.4.2 Methodology

After obtaining the raw radar data cube, a Range-FFT operation is conducted. This operation is applied to the fast-time IF signal samples to acquire its frequency spectrum to be mapped to the discrete range bins. As the radar emits continuous chirps, micro-Doppler is then extracted by analysing the rate of chirp phase change. This process is achieved by applying Doppler-FFT on the phase vector corresponding to a range bin across all chirps. Based on the performed analysis, it is observed that the speed of the propeller is highly correlated with the micro-Doppler frequency f_{Dopp} of the range bin corresponding to the propeller location. As the propeller has a number of blades n, two blades for the used drone in the conducted experiments of this study, it is observed that the micro-Doppler frequency represents the blade crossing frequency; thus,

$$\omega_{rpm} = \frac{60 \times f_{Dopp}}{n} \tag{3.2}$$



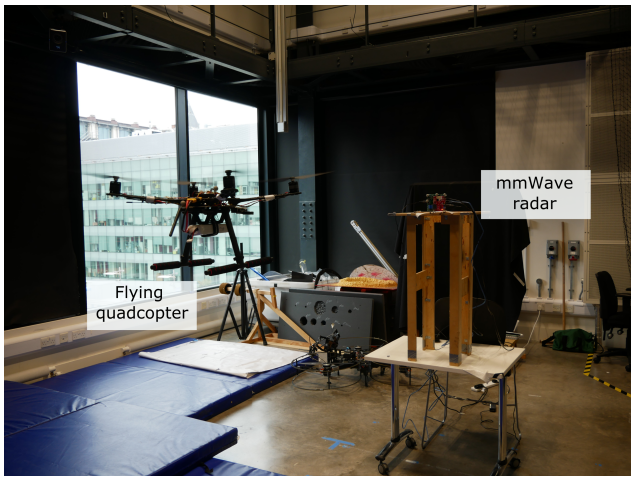
(a) Hovering spectrum (b) Denoising impact

Figure 3.9: Micro-Doppler spectrum of a flying drone.

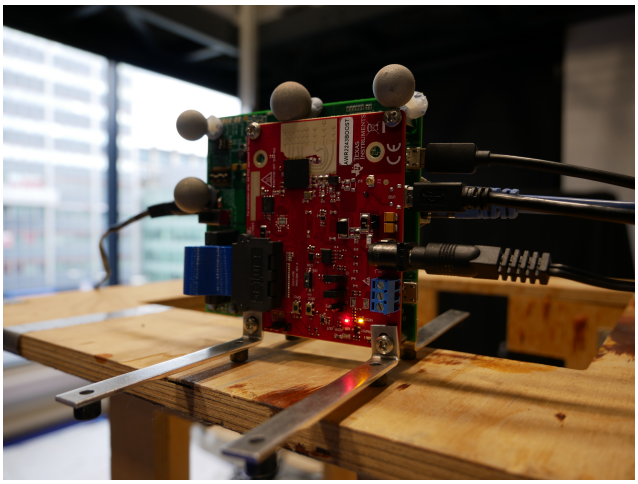
Figure 3.9a shows the micro-Doppler spectrum while the drone is hovering. To filter out noises, wavelet denoising is applied to extract the micro-Doppler frequency corresponding to propeller rotation speed (Figure 3.9b). The micro-Doppler analysis frequency range can be calibrated offline by setting the drone propeller to its minimum and maximum rotation speeds, thereby establishing the limits of the frequency window.

3.4.3 Evaluation

The experiments are conducted with the same setup as described in Section 3.3.2 using the same drone, however with different arrangements as shown in Figure 3.10. The experiments evaluate the performance of the 77GHz mmWave radar in sensing the propeller speeds of the drone in stationary and flying scenarios. The mmWave radar utilised is the Texas Instruments (TI) AWR2243 (Figure 3.10b), operating within the 77-81 GHz mmWave frequency band. It integrates 7 onboard antennas including 3 transmitters and 4 receivers. In experiments implementation, the transmitter antennas transmit FMCW signals starting at 77GHz with 4GHz bandwidth, and all receiver antennas receive the reflected signals. Each frame includes 2 chirps with a single chirp duration of 40μs where the ideal time is 7μs and the ramp end time



(a) Experimental area in flying scenario.



(b) TI AWR2243 77GHz mmWave radar.

Figure 3.10: Experimental setup for the mmWave sensing approach.

is 33μs. The frequency slope of the FMCW signal is 50.018MHz/μs. The raw data is collected through the TI DCA1000EVM data acquisition board with a sample rate of 10MHz. The used metric is the RPM relative error rate to evaluate the performance of the propeller speed sensing accuracy.

mmWave Rotational Speed Sensing Distance Range

This experiment is performed to evaluate the impact of distance on propeller speed sensing performance. Figure 3.11 shows the performance while commanding hovering motion at a relatively low and high speed (at 2000 and 14000 RPM, respectively) to the drone in a fixed situation. The figure illustrates that mmWave can consistently capture propeller speeds with stable accuracy at a distance that reaches up to 8m, maintaining a mean relative error rate of less than 1.5%. After reaching a distance of 8m, errors start to increase, possibly attributed to obstructions present in the flight arena during the experiments.

The performance evaluation demonstrates notable differences between mmWave radar and 5GHz RF in propeller speed sensing at varying distances. The limited coverage of the 5GHz

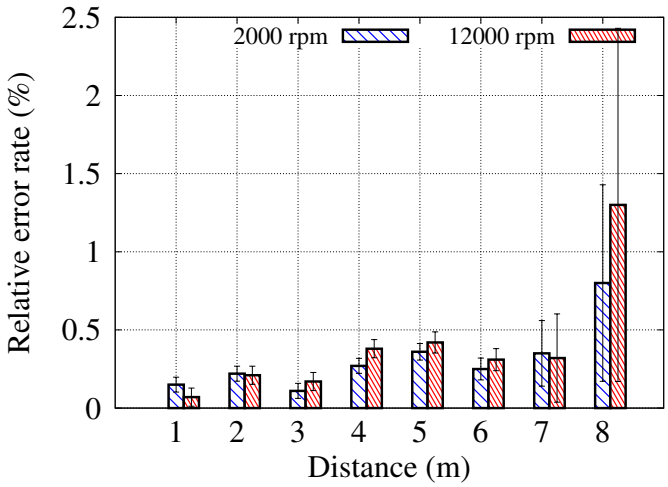


Figure 3.11: The impact of distance between mmWave radar and drone on speed sensing accuracy

RF up to 1m can be attributed to its lower resolution and sensitivity compared to mmWave radar. Despite its ability to propagate signals over longer distances, 5GHz RF may struggle to accurately capture the fine details of propeller speeds beyond short ranges.

Capturing Rotational Speed while Flying

This experiment evaluates the mmWave radar's ability to sense the propeller speeds while the drone is flying. The drone hovers in different locations randomly in an area of 8×4 m. Figure 3.12 shows the RPM relative error rate cumulative distribution function (CDF) of propeller speed during the flight. The median error rate is less than 0.4%, which highlights the capabilities of mmWave propeller speed sensing of a flying drone in a lab area.

3.5 Summary

This chapter explored the effectiveness of radio waves in measuring the propeller speed of a flying drone using two approaches, 5GHz RF OAM waves and 77GHz mmWaves radar. The

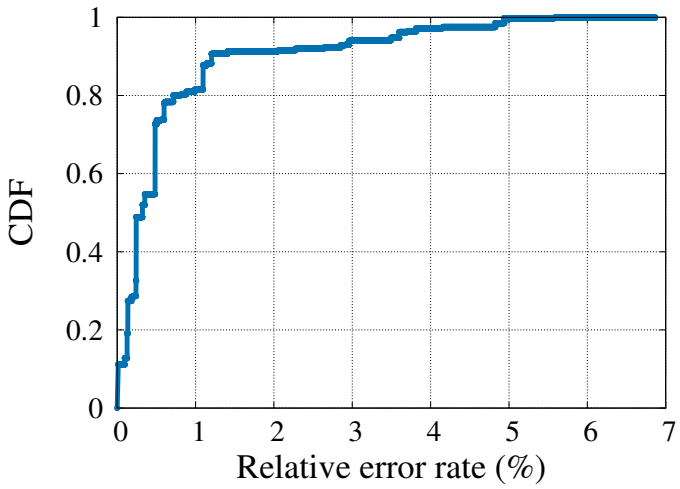


Figure 3.12: Accuracy of propeller speed sensing using mmWave radar when the drone is flying

evaluation results demonstrate the high accuracy of radio waves in sensing drone propeller speeds while rotating within the flying speed range. Additionally, mmWave radar exhibits a superiority over RF OAM waves in terms of sensing range, as mmWave provides accurate measurements at longer distances reaching up to 8m. These results highlight the robust capabilities of radio wave-based sensing methods for propeller speeds during dynamic drone movements. The high accuracy achieved within the flying speed range and the extended sensing distance provided by mmWave radar showcase the potential for enhancing various applications such as failure detection, drone identification, and localisation.

The next chapter introduces an indoor drone localisation system and demonstrates the enhanced impact of integrating sensed drone propeller spinning movement on drone detection in dynamic environments and positioning accuracy.

Chapter 4

Drone Localisation and Tracking using mmWave Radar

This chapter proposes RaDro, a system that leverages mmWave to precisely localise and track drones in an indoor environment. Unlike commonly used alternative technologies, such as optical motion capture systems, RaDro is cost-effective and can penetrate obstacles, a bonus in NLoS scenarios, which enhances its reliability for tracking objects in complex environments. It does this without the need for tags or anchors to be attached to the drone, achieving 3D tracking with just a single radar point, significantly streamlining the deployment process. In order to improve drone localisation accuracy and stability, both micro and macro movements of drones are detected to identify the type of drone motion. Additionally, micro-Doppler information is extracted to measure propeller speeds, which are then integrated into the drone's dynamic model within the tracking module. RaDro is implemented using a commercial mmWave single-chip radar array and an off-the-shelf drone. Extensive experiments in different scenarios are conducted to demonstrate the capabilities of the system in recognising drone motions, extracting fine-grained information, and localising the drone.

4.1 Motivation and Objectives

Drones have various indoor and outdoor applications where they can navigate in locations that are difficult or even inaccessible for humans. The increasing utilisation of drones, especially in urban and densely populated areas such as workplaces, emphasises the growing importance of the safety and accuracy of drone localisation and tracking. A search and rescue application [162] can be considered as an exemplar scenario where a drone acts as a scout for safety staff entering a partially collapsed building, through providing accurate location/mapping information in order to enable them to safely navigate around the space. Another illustrative scenario involves the support of mining operations [163], encompassing exploration, surveying, and mapping. Mining companies can use drones to gather data for topographical surveys and safety inspections, which supports operational optimisation and safety enhancement. For such an application, drone accurate localisation is essential for effective site navigation and data collection.

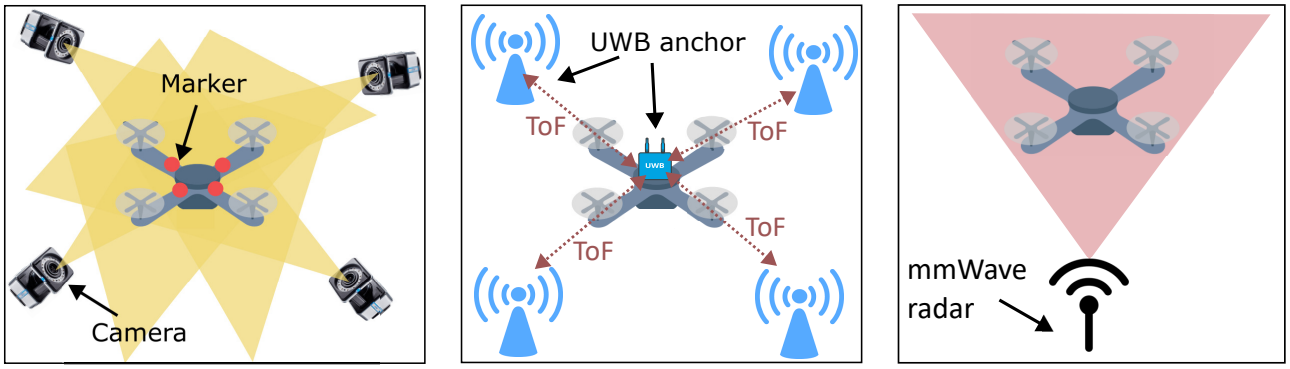
Localisation is required for the drone's own navigation, that is, the autopilot typically relies on real-time tracking of its location during flight. GPS is the main tracking approach in outdoor settings where GPS coordinates are fused with the drone's onboard inertial sensor measurements [164]. However, GPS is rendered unusable if its signal is obscured by an object, this includes flying near tall buildings or moreover, when indoors.

Alternatives to GPS include optical motion capture systems, such as the VICON camera-based tracking solution which is widely used in indoor environments providing accurate tracking over time. However, it is an expensive solution, requiring specialist camera hardware, and more importantly, it requires that the VICON system is pre-installed in the building, which may not always be viable (e.g. the aforementioned search and rescue mission). Camera-based systems, such as VICON, require specialist marker attachments to be added to the drone frame to help the camera identify the drone. The camera's ability to detect this marker is highly dependent on environmental conditions, such as well-lit surroundings and an unobstructed view, i.e., the drone

is within LoS of the camera, which is not guaranteed in many scenarios. In search and rescue missions and mining operations scenarios, drones will navigate behind objects such as furniture, debris, safety workers, equipment, machinery, and structures, where camera-based localisation will fail. Other localisation approaches, such as UWB-based ranging [63, 64] are able to localise the drone in low-light or NLoS. They use transceivers on the drone's body to estimate pair-wise distances based on ToF information. However, these approaches, like VICON cameras, also require careful placement of spatially separated UWB transceiver equipment where the drone will fly; (at least three) positioned around the operational tracking area for trilateration. This introduces significant complexity to their installation and calibration, which is not suitable for the unsafe conditions of our two scenarios.

Eliminating the need for any modifications to the drone's body, *passive* localisation systems based on acoustics have been introduced for drone tracking [61, 165]. However, they exhibit meter-scale inaccuracy and are sensitive to audio noise making them not suitable for precise indoor applications where such large errors can potentially result in poor navigation, drone collisions or crashes involving humans.

This chapter proposes RaDro, a precise drone localisation and tracking system that utilises a single-chip radar array without having to install multiple points in the operational area or requiring any additional hardware or software changes to the drone, which significantly reduces the required effort to setup and deploy in a new environment (Figure 4.1). Radar-based drone detection has a longstanding history, particularly in military contexts with extensive ranges (hundreds of meters) [166, 167], however, they are restricted in spatial resolution; their ability to determine precise location. This limitation is due to the relatively long wavelengths of these radar technologies as they typically operate at lower frequencies, including S-band and X-band. Traditional radar systems tend to be larger in size due to the need for large antenna arrays measuring in meters which consume significant amounts of power. However, recent advancements in microchip manufacturing have resulted in accessibility, cost-effectiveness ($\sim$



(a) Optical motion tracking (b) UWB tracking (c) mmWave radar tracking

Figure 4.1: Drone tracking approaches: compared to the other tracking approaches, the RaDro system utilises only a single-chip mmWave radar array, without requiring to attach any additional hardware to the drone's body.

$300), and reduced power consumption of mmWave radar antennas, operating at millimeter-wave frequencies (typically 30GHz to 300GHz). RaDro leverages the sensitivity of mmWaves to determine precise millimeter-level motion, thanks to its small wavelengths, to detect and track drones. It is also able to work in different levels of LoS and in NLoS scenarios, therefore tolerant to different environmental conditions where other common localisation systems cannot work.

4.1.1 Challenges

While mmWave approaches offer promising prospects for localisation, there are several challenges associated with passively localising drones indoors that need to be addressed, which are introduced below.

Reflections and Interference: In indoor environments, the presence of reflective surfaces and stationary/moving objects leads to complex multipath propagation of radar signals. The mmWave signal received at the sensor antenna is a combination of reflections from the target (flying drone) and signals bouncing off obstacles (causing multipath effects). Indeed, the structure of the drone itself results in multiple signal reflections from its rotating points (blades).

These multipath effects, plus the interference caused by ambient RF noise in the environment, can make signal denoising difficult and localisation identification error prone. To address this challenge, RaDro adopts several signal processing techniques, including wavelet denoising, false rate detectors, and clustering algorithms to filter out the noise and extract the important information reflected from the drone's body to locate it.

Target Detection: Identifying a particular drone and understanding the direction it is taking for tracking purposes is also more difficult for radar due to the lack of identifiers on the drone and the environment in which it is deployed. That is, direction detection is impeded by dynamic environments (e.g., the movement of workers and machinery in mining sites). For instance, camera-based detection relies on identifying reflectors on the drone body for tracking. However, from a radar view, the drone consists of multiple rotating points, which presents extra challenges for drone identification. RaDro addresses this challenge by characterising the drone's multiple rotating point (propeller) reflections and leveraging the unique micro-Doppler signature in the received signal. Leveraging this distinctive signature with autocorrelation analysis allows RaDro to effectively distinguish the flying drone from other moving objects, even when the drone is hovering.

mmWave Information Resolution: Resolution of measurement is another challenge. Typically angle measurements are used to localise the drone and this is prone to error. Therefore, instead of relying on angle measurements, it is observed that the multiple rotating propellers of the drone result in dual channel reflections on the received signal, impacting the signal with distinct fundamental frequencies. These frequencies correspond to the propeller speeds that in turn denote the state of the drone. These rotation speeds are extracted and then fed into the drone's dynamic model, following the recognition of the drone motion type (i.e., hovering, vertical, horizontal, and yaw), and used in the tracking module to maintain robust tracking.

4.1.2 Contributions

This systems's contributions can be summarised as follows:

- This chapter proposes RaDro; an mmWave radar-based system which enhances drone localisation and tracking in indoor environments with minimal hardware requirements. Unlike other existing localisation and tracking alternatives, RaDro utilises a single-chip radar array with no need for multiple point installation in the working environment or any modification requirement to the drone hardware, which significantly reduces the effort required for setup and deployment in new environments. RaDro's capability to operate without additional hardware attachments further extends its application to intruder detection.

- Signal processing techniques are implemented to extract reliable information from received mmWave signals, including the unique micro-Doppler signature of drone propeller speeds, to distinguish the flying drone from moving objects or possible clutter in the working environment and recognise the drone's motion type. The signal processing techniques include wavelet denoising, discrete wavelet transformation (DWT), FFT, 2D-CFAR, and autocorrelation analysis.

- The flying drone propeller speeds are precisely measured based on their sensed mmWave micro-Doppler shift for the first time in literature, to the best of our knowledge. The measured propeller speeds are incorporated into the drone's motion dynamic model to further promote RaDro's tracking accuracy.

- RaDro's performance is evaluated in flying arenas involving complex environments with moving humans and metallic obstacles using commercial drones and off-the-shelf mmWave radar through various operating scenarios to verify its robustness. The experimental evaluation demonstrates RaDro's capability to accurately localise drones in NLoS scenarios

where existing optical-based localisation systems are ineffective. Moreover, it highlights the significant localisation error reduction that RaDro can achieve compared to the baseline mmWave 3D point cloud localisation method.

The rest of this chapter is organised as follows. Section 4.2 provides an overview of the mmWave passive localisation systems in the literature. Sections 4.3 and 4.4 present fundamental concepts and technical details of the RaDro system, respectively. The system is evaluated in Section 4.5. Section 4.6 discusses directions for future work and finally, Section 4.7 concludes the chapter.

4.2 mmWave Radar Passive Localisation and Tracking Solutions

This section briefly reviews the prior localisation and tracking systems that leverage mmWave radar technologies. Recent progress in microchip manufacturing has led to the availability of cost-effective, wideband mmWave radar transceivers operating at millimeter-level wavelengths. These transceivers have been effectively utilised across a range of applications as discussed in Chapter 2.

Several research works have proposed methods for object localisation and tracking using mmWaves [117, 125, 168, 169, 170, 171]. These systems typically extract range, Doppler, and angle measurements from mmWave radar received signals and then apply tracking algorithms, including the KF and JPDAF to estimate the object's trajectory. For instance, a human tracking system [172] uses mmWave radar measurements and adopts the Hungarian algorithm [134] for data association and KF to correct sensor noise for people tracking. To enhance the precision of human detection and tracking, other systems [169, 170] rely on a multi-radar setup, which increases the installation cost. Alternative methods [173, 174] rely on extracting the target's position and speed from the mmWave range-angle and range-Doppler profiles using neural networks.

However, these approaches necessitate extensive data collection for model training, which can be costly and limit their generalisability across different environments. Another system [168] enhances human detection by developing a geometric model to characterise and eliminate multipath of interfering objects from mmWave range-angle profile. However, these localisation systems are tailored for tracking objects such as humans and cannot be extended for drone localisation due to their different structures. Drones are rigid bodies with multiple rotating points, leading to multiple reflections from these rotating points. Former mentioned mmWave localisation systems might interpret these multiple reflections as indicative of distinct objects, potentially failing to specifically detect drones, especially at close ranges from the radar. In contrast, RaDro extracts these multiple reflection signatures to identify drones, effectively distinguishing flying drones from other moving objects. Furthermore, it uniquely correlates these signatures with the drone's propeller speeds, enhancing tracking accuracy by integrating these speeds into the drone's dynamic model.

Recently, a few systems have emerged adopting the mmWave technology for detecting and localising flying drones [121, 175]. Proposed systems leverage neural network and regression methods along with mmWave measurements to discriminate drones from other objects [176, 177]. In outdoor environments, systems have been proposed to detect drones at long distances [120, 178]. The system presented in [178] uses the constant false alarm rate detector on the Range-Doppler spectrum to detect drones in outdoor environments at ranges reaching 40m, while the system in [120] extends the detection range by adopting a neural network with Doppler spectrum. However, the working principle of these systems is to detect the altitude (one dimension) of the drone in outdoor environments which typically have fewer obstacles compared to indoor environments. Additionally, they are designed for relatively heavy drones, typically measuring in the range of $8 \sim 10$ kg drones, that are suitable for outdoor environments. These drones are significantly large compared to the target of RaDro which can detect and localise a 27g drone indoors (more than 300 times smaller compared to [120, 178]). RaDro is

a system proposed for detecting and localising drones indoors in 3D space, which is a more complex problem than only detecting the height in one dimension.

In indoor environments, a passive localisation technique proposed in [121] was to track a drone in a small area of 2.5×2.5 m using FMCW mmWave radar. This technique involved the extraction of range and angle information from the mmWave signal, with a restricted localisation area due to a lack of angle resolution. It also relied on a deep-learning approach, requiring additional time for extensive training that needs to be re-established for new environments. The proposed work leverages mmWave signals to localise drones passively, without requiring any reflectors or any training prior to deployment. It expands the operational tracking area covering up to 8m (more than four times the area compared to [121]) through leveraging micro-Doppler information which is mapped to the propellers' speeds, and integrates the drone's dynamic model in the tracking process. Compared to existing mmWave indoor drone 3D localisation approaches, RaDro achieves the same precision error of less than 10cm at a range of 3m while uniquely extending the working area to 8m with a slight increase in the error to 50cm.

4.3 mmWave Drone Interference

This section highlights the key features of FMCW mmWave technology and explores the impact of drone motion on the mmWave signal.

4.3.1 FMCW mmWave Features

As discussed in Chapter 2, FMCW is a modulation technique used in mmWave radar for measuring the range, velocity and angle of the target object. The received data can be arranged into a 3-D tensor of complex numbers, known as a radar data cube, that contains all the information provided by the radar device for a given time frame with dimensions of chirp data,

chirp number, and antenna number. The 3D point cloud spatial information of the target object, captured using mmWave radar, including range, velocity, and angle data, can be used to track drones [121]. However, conventional point cloud drone tracking is not stable due to the noisy captured frames. The source of the noise is caused by the instability of the radar information accuracy, such as the dependency of AoA estimation accuracy on angle value – i.e., the larger the angle between the radar and the target (reference to the norm of the antenna plane), the lower the accuracy of estimation [28]. Such AoA accuracy restrictions impact the localisation coverage area to obtain reliable angle measurements, particularly for moving targets such as drones. For instance, the system proposed in [121] relies on range and AoA measurements to localise the drone within a limited area of 2.5×2.5 m. To overcome this challenge, RaDro depends on more reliable measurements of micro-Doppler information.

The moving drone introduces a frequency shift in the radar received signal corresponding to the platform movement due to the Doppler effect. However, the structure of the drone's body consists of multiple rotating blades rather than a single point. These small-scale rotations of drone blades produce additional Doppler shifts, referred to as micro-Doppler effects, which cause phase change in the reflected signal. The micro-Doppler shifts work independently of the relative position of the target and radar. The sensitivity of the micro-Doppler effect increases with smaller wavelengths of mmWaves. RaDro system leverages this micro-Doppler information to sense the drone's propeller speeds, as introduced in Chapter 3. The sensed propeller speeds can indicate the drone state by integrating the drone's dynamic model for more robust tracking.

4.3.2 Drone Motion

Drones are mounted with propellers which provide lift and drag forces while spinning. In this work, a quadcopter, a popular type of drone (Figure 4.2), is considered. Quadcopters have four vertically oriented propellers placed symmetrically around the center of the vehicle. The

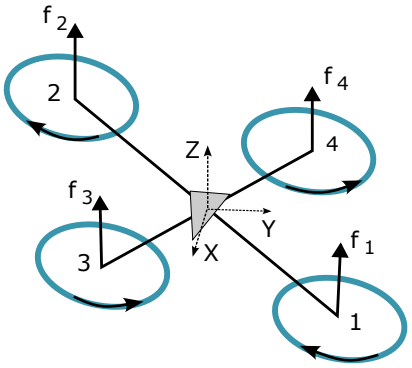


Figure 4.2: Quadcopter model

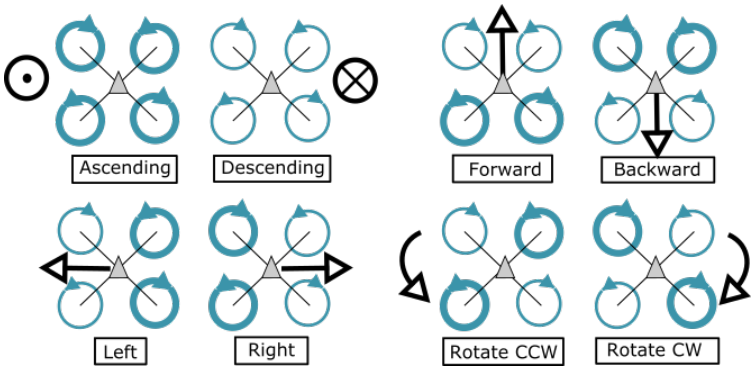


Figure 4.3: Relation between quadcopter different motion types and propellers spinning direction (line thickness denotes high/low propeller speed).

four propellers produce four thrust forces $f_{1..4}$ that pull it upward. f_i is related to the i^{th} propeller spinning speed as $f_i = k\ \omega_i^2$, where ω_i is the spinning speed of the i^{th} propeller and k is the thrust coefficient constant which depends on various factors including the propeller motor specifications and aerodynamic properties. By varying the rotation speed and direction of these propellers, quadcopters can perform different types of movements. The primary quadcopter movements are (Figure 4.3):

- **Hovering**: This maintains stable position for the drone in the air by rotating the propellers in the same speeds (assuming absence of external environmental forces which need compensation). Thus, the relation between the four propeller speeds is: $\omega_1 = \omega_2 = \omega_3 = \omega_4$.
- **Vertical movement**: The drone can move vertically by increasing or decreasing the overall thrust produced with the four propellers. To rise vertically, the rotation speeds of the four propellers are equally and simultaneously increased to generate more lift force. Similarly, equally decreasing the four rotation speeds gradually implements a descend/landing motion. Therefore, the propeller speeds relation is: $\omega_1 = \omega_2 = \omega_3 = \omega_4$.
- **Horizontal movement**: This refers to the forward, backward, rightward or leftward tilt of the quadcopter while maintaining vertical stability. To achieve that, the propellers operate in pairs where each pair rotates at the same speed. For forward/backward tilt,

the rotation speeds are: $\omega_1 = \omega_3$ and $\omega_2 = \omega_4$, which achieve a pitch movement. The same is applied for the rightward and leftward to achieve roll movement.

- **Yaw**: The speeds of each set of diagonal propellers are adjusted to $\omega_1 = \omega_2$ and $\omega_3 = \omega_4$, that achieve yaw movement around the drone's vertical axis. The speed mismatch between the two sets of diagonal propellers generates a torque imbalance steering the drone in the desired direction.

Interestingly, it is found that various drone movements affect the mmWave signal differently as the pattern of propeller angular motion changes. As proposed in Chapter 3, the speed of the propeller is related to the micro-Doppler frequency f_{Dopp} with this relation $f_{Dopp_i} = n\ \omega_i$, where n is the number of blades. This information, in combination with the other mmWave range and angle information, can identify and localise the drone's movement.

It is challenging to differentiate the exact locations of different propellers in the drone's body due to the lack of AoA resolution accuracy. Instead, RaDro leverages the mmWave FMCW ability to differentiate between objects within close range as they move at different speeds. Each object exhibits a distinct chirp phase change rate, extracted using the Doppler-FFT. Thus, the mmWave radar can differentiate micro-Doppler signatures resulting from individual propeller rotations at varying speeds. The extracted rotation speeds are then assigned to different propellers based on the motion type recognition and calibration steps, as discussed next.

4.4 Tracking Pipeline

The proposed approach for drone localisation includes three parts. Firstly, the radar cube data is preprocessed to extract range, AoA, and micro-Doppler mmWave radar information. Secondly, the extracted mmWave information is used to recognise the motion type of the drone,

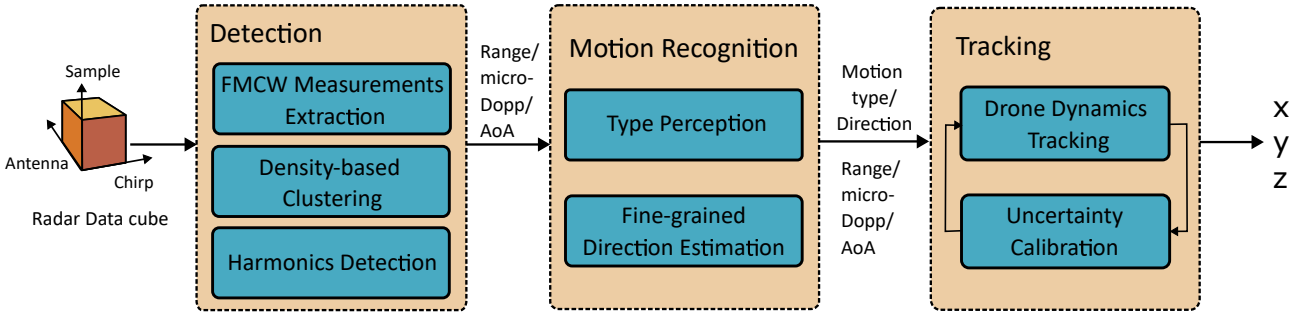


Figure 4.4: Structural overview of RaDro

and finally, the mmWave extracted information with the recognised motion type are combined with the drone's dynamics to achieve accurate drone tracking. Figure 4.4 shows the pipeline of the proposed approach.

4.4.1 Drone Detection

The mmWave signal features are used to detect the presence of the drone and estimate its motion.

Unveiling FMCW Radar Information

The input raw radar data is the radar cube of the 3D signal that is produced at each time frame with dimensions of chirp data sample (fast time samples), chirp number (slow time samples), and antenna number (spatial dimension), as discussed in Section 4.3.1. The radar cube input data is used to build a Range-Doppler-Angle (RDA) map. This is achieved by first applying an FFT along the fast time dimension, followed by a Doppler-FFT along the slow time dimension to construct the Range-Doppler map. This map is then fed into a 2D-CFAR algorithm to extract dominant points, i.e., removing background clutter and reducing noise, making it less dependent on the environment's characteristics. The angle of each dominant point is then estimated by observing the phase change between different antennas, achieved by applying an

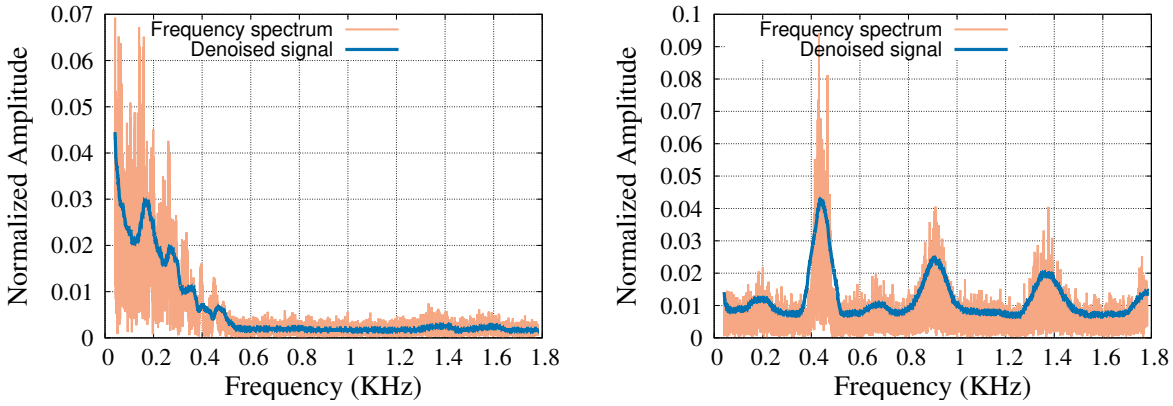
additional FFT on the antenna spatial dimension.

Flying Drone Detection

Then the detection process distinguishes the target drone from other moving objects in the environment through the following steps:

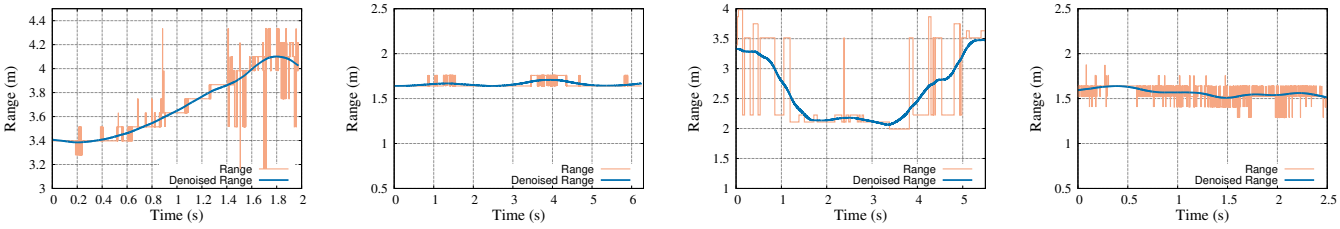
Density-based Clustering DBScan algorithm is applied on the RDA map to separate different clusters, which correspond to potential objects in the operational area. DBScan operates by sequentially scanning all the data points and expanding a cluster until a certain density condition is no longer satisfied.

Harmonics Detection For each cluster, the micro-Doppler information that contains the propellers' motion signature is extracted by applying the short-time Fourier transform (STFT) on the slow-time dimension after integrating along the extracted cluster range bin index. The spinning propeller causes a fundamental frequency component that represents the propeller spinning speed and harmonics which are integer multiples of the fundamental frequency. The other slow-moving objects, relative to drone propeller spinning speed, in the environment (such as human movements) result in low-frequency variations in the received signal. As a result, harmonics of these low frequencies are also in the low-frequencies range. Figure 4.5 demonstrates the difference between human movements and a hovering drone effect on the received mmWave signal spectrum. The distance between the mmWave radar and the drone is set to 2m, with the person standing 1m away along the line perpendicular to the line connecting the radar and the drone. During the experiment, the drone takes off, hovers, and then lands, while the person engages in in-location activities at a normal speed, such as taking out a phone from her pocket, returning it, waving hands, and rotating her body. The experiment lasts for approximately 1 minute. Referring to Figure 4.5, it can be shown that hovering drones produce



(a) Human frequency spectrum (b) Drone frequency spectrum

Figure 4.5: The different effects of humans and drones on the frequency spectrum

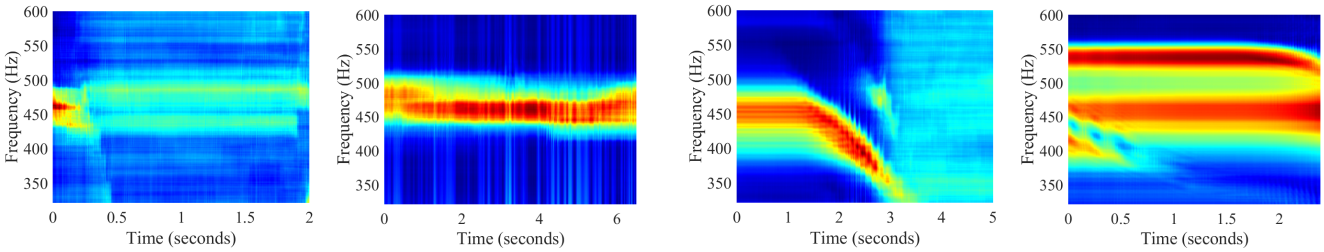


(a) Horizontal (b) Hovering (c) Vertical (d) Yaw

Figure 4.6: Range pattern of the drone while performing different motions

distinct frequency harmonics which are integer multiples of the fundamental frequency. In contrast, human movements do not generate significant harmonics in the received waves, with both the fundamental and harmonic frequencies concentrated at low frequencies. By calculating the autocorrelation of each cluster's micro-Doppler spectrum, the cluster that represents the drone is extracted where its autocorrelation coefficients are much higher than that for spectrums corresponding to other slow moving objects.

The drone cluster range and angle information are used to represent the range and angle of the drone. The unveiled information of range, micro-Doppler and AoA are used to recognise and track the drone as explained next.



(a) Horizontal (b) Hovering (c) Vertical (d) Yaw

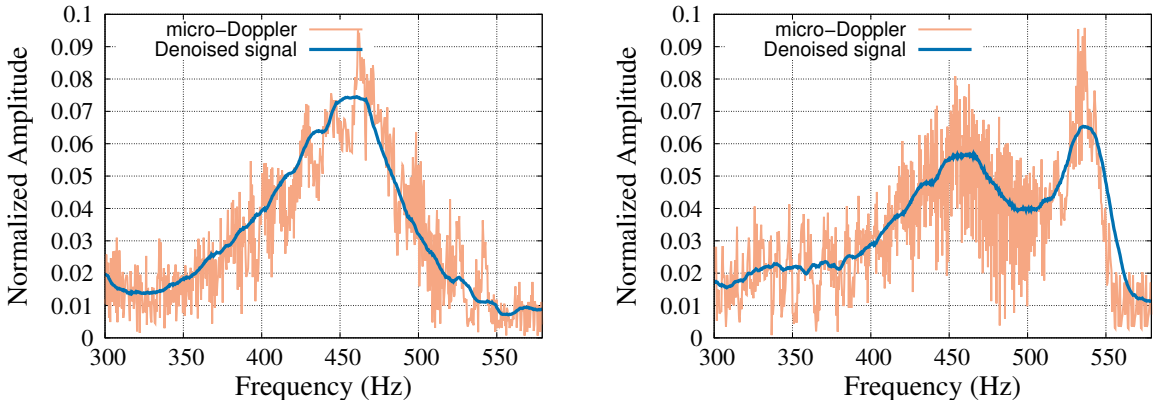
Figure 4.7: Micro-Doppler spectrogram of the drone's different motions

4.4.2 Motion Recognition

FMCW radar information is used to recognise the four main movements discussed in Section 4.3.2 along with further estimated fine-grained motion parameters to distinguish the ambiguity of motion direction.

Coarse-grained Motion Recognition

Different drone motions impact the mmWave signal differently; therefore, the extracted range, AoA, and micro-Doppler patterns are distinct. Figures 4.6 and 4.7 show the range and corresponding micro-Doppler spectrograms of the drone while performing different motions. The drone moves in front of the radar at distances ranging from 1 to 4 meters, executing horizontal, hovering, vertical, and yawing movements, each lasting for a few seconds. During hovering motion, the drone maintains a constant distance from the radar while having a single fundamental frequency band. In vertical motion, the distance from the radar changes while having one frequency peak at a time. Figure 4.7c illustrates a landing vertical motion of the drone, in which the single frequency band decreases with time. In contrast, the frequency band is split when performing horizontal or yaw motions as shown in Figures 4.7a and 4.7d, respectively. During horizontal motion, the drone's distance from the radar changes while in yaw motion, the distance remains stable. Thus, the combination of range and micro-Doppler provides the necessary information to distinguish between different drone movements.



(a) One peak hovering motion

(b) Two peaks yaw motion

Figure 4.8: Wavelet denoising impact on micro-Doppler spectrum

To reduce noise and better extract frequency peaks, a wavelet denoising filtering scheme [179] is used. Wavelet denosing is effective in reducing noise while preserving the important features of the signal. Additionally, it does not make any particular assumptions about the nature of the signal, and permits discontinuities in the signal which makes it compatible in different scenarios. Figure 4.8 shows the impact of applying wavelet denoising on a frequency spectrum of a time frame captured during hovering and yaw motions. Additionally, the AoA is employed as supplementary information to boost recognition accuracy. The AoA remains stable during hovering and varies across horizontal, vertical, and yaw motions.

Fine-grained Motion Recognition

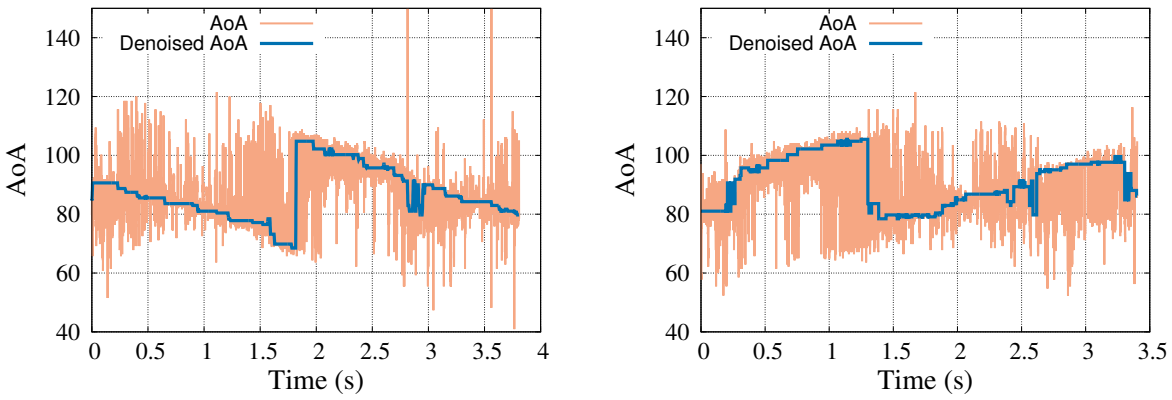
The various potential assignments of the micro-Doppler peaks to propellers can cause ambiguity in determining the direction of motion. To reduce this ambiguity, after recognising the drone basic motion, further processing is applied to recognize the direction of the movement. For yaw motion, the AoA changing pattern over time is processed to distinguish between clockwise (CW) and counterclockwise (CCW) motion. The dominant estimated AoA is the angle of the highest speed propeller facing the radar while yawing. Figure 4.9 shows the angle of the highest speed during full drone rotation (i.e., 360 yawing) in CCW and CW directions. As shown in the

figure, the captured AoA decreases over time for CCW yaw motion and, in contrast, increases for CW yaw motion.

In horizontal motions, the drone motion closer to or farther from the radar is estimated using the range signal. Crucially, it is observed that the estimated range increases with time when the drone moves far away from the radar, as shown in Figure 4.6a, and decreases when moving closer. The fine-grained information is extracted for horizontal motion using the AoA measurements. For example, consider a scenario where the drone is positioned in front of the radar with its front propellers facing the radar, and the detected coarse-grained motion is horizontal. If the range decreases, indicating forward horizontal motion. If the range increases, there are three potential directions. If the AoA is stable, the horizontal motion is in the backward direction. If the AoA decreases, the horizontal motion is to the left, while increasing AoA indicates motion to the right. Due to the susceptibility of AoA's estimation to noise, a weight inversely proportional to the smoothed signal variance is incorporated into the tracking module to represent the confidence level of yaw and horizontal directions estimation, which is used in the uncertainty calibration module as explained in Section 4.4.3.

For vertical motion, the direction of descending (landing) or ascending (take-off) motion is recognised using the micro-Doppler frequency band. The frequency band increases with time during ascending movement. On the other hand, when descending, the frequency band decreases with time (Figure 4.7c).

Such fine-grained information reinforces the estimated location and reduces the motion direction ambiguity. Upon identification of the motion and its corresponding direction, these findings are subsequently fed into the dynamic model of the quadcopter.



(a) CCW yaw motion

(b) CW yaw motion

Figure 4.9: Yaw motion direction

4.4.3 Drone Tracking

This section illustrates the integration of the mmWave information with the drone's dynamics, leading to simplified motion equations to attain precise tracking.

Drone Tracking Model

The dynamic model of the quadcopter is initially derived from its movement, which is subsequently used for tracking. If the recognised motion of the drone is hovering, there will be no change in the drone's state. For the remaining motion types, the following motion equations are applied:

- **Vertical**: The rotation speeds $\omega_{1...4}$ are equal and increase or decrease slightly and simultaneously to produce a vertical force to counteract gravity and downward resistance $b^v\ (v_t^v)^2$ during ascending or descending movements, where b^v is a drag coefficient constant and v_t^v is the vertical velocity at time t. Based on Newton's second law, the vertical

acceleration a^v at time t is captured using the following equation:

$$k \sum_{i=1}^{N} \omega_{i_t}^2 - mg - b^v (v_t^v)^2 = m \; a_t^v \tag{4.1}$$

where ω_i is the angular frequency of propeller i corresponding to the single peak extracted from the micro-Doppler profile.

- **Yaw**: By increasing the speed of one set of diagonally opposite propellers while decreasing the speed of the other set, a torque imbalance is created as $|F_1 + F_2 - F_3 - F_4|$, causing the quadcopter to rotate around its vertical axis. The rotation angular acceleration $\dot{\Omega}$ is acquired using the following equation:

$$k \left| \sum_{i=1}^{N/2} \omega_{2i-1_t}^2 - \sum_{i=1}^{N/2} \omega_{2i_t}^2 \right| = I \; \dot{\Omega}_t \tag{4.2}$$

where I is the moment of inertia constant, while ω_i corresponds to the two extracted peaks from the micro-Doppler spectrum. The direction of orientation is determined from the angle changing pattern as explained in Section 4.4.2.

- **Horizontal**: The rotation speed of two propellers in one side increases while decreasing the rotation speed of the other side, where two frequency peaks can be extracted from the micro-Doppler spectrum. Thus, the quadcopter tilts with angle θ, with respect to the vertical axis of the drone, and the drag force allows the drone to move horizontally. The net force caused by the propeller rotation speeds can be decomposed into two components: vertical and horizontal forces. The vertical force works against the gravity as follows,

$$k \sum_{i=1}^{N} \omega_{i_t}^2 cos(\theta_t) = mg \tag{4.3}$$

With the information of the drone's mass m and gravity acceleration g, the tilt angle θ

can be obtained. The horizontal force works against the resistance force $b^h(v_t^h)^2$ to make the drone move horizontally with an acceleration of a_t^h, where b^h is a drag coefficient constant and v_t^h is horizontal velocity. Based on Newton's law, the motion equation can be represented as follows,

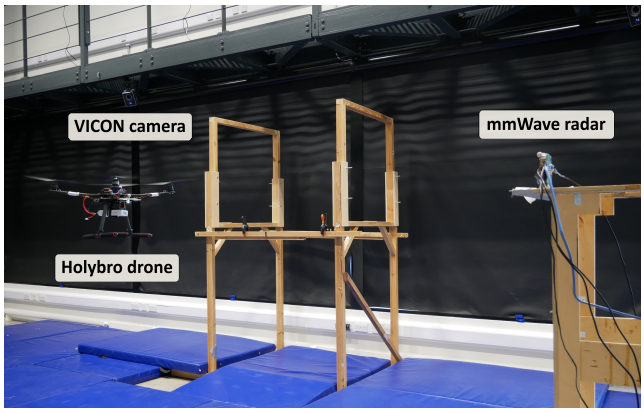
$$k \sum_{i=1}^{N} \omega_{i_t}^2 sin(\theta_t) - b^h \ (v_t^h)^2 = m \ a_t^h \tag{4.4}$$

The angular and linear accelerations and velocities for different motions are used to track the drone using the equations of motion in discrete time [44]. To avoid error drift over time, the estimated coordinates of the drone are calibrated as discussed next.

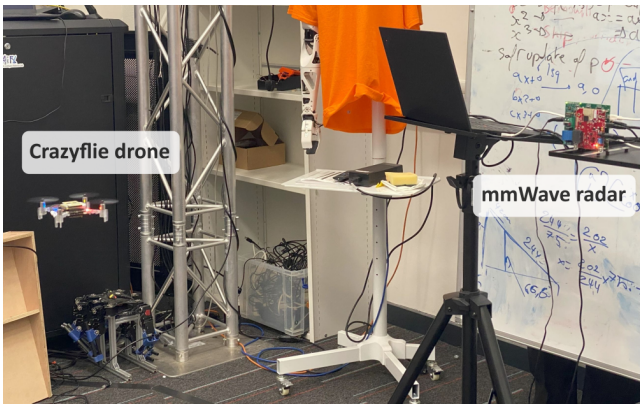
Uncertainty Calibration

An EKF [180] is used to calibrate tracking inaccuracies over time in the estimation of the yaw and horizontal motion direction and in the absolute drone localisation. The drone's state vector represents the position and velocity, denoted as $S_t = [x_t, y_t, z_t, \psi_t, x'_t, y'_t, z'_t, \psi'_t]$ where x_t, y_t, and z_t are the drone position coordinates at time t and ψ_t is the drone yaw orientation angle relative to the radar. The algorithm is outlined through the following steps:

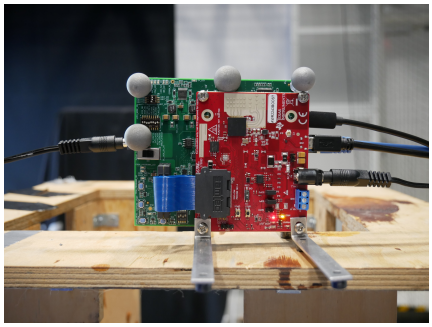
- The state vector is initialised and a prediction step is applied to estimate the a priori state estimate $\hat{S}_t$.
- mmWave parameters are calculated and the drone's motion type with weighted direction estimation is recognised. Then, the drone's location and yaw angle are estimated through the dynamic motion equations.
- The estimated state $\hat{S}_t$ is then corrected with the estimated position of dynamic equations and mmWave range parameters to output the optimal a posteriori state estimate.



(a) Experimental flight arena 1



(b) Experimental flight arena 2



(c) mmWave radar



(d) Holybro S500 drone



(e) Crazyflie 2.1 drone

Figure 4.10: Experiment setup of RaDro.

- All weighted potential trajectories are traced until reliable AoA measurements are obtained. If the variance of the AoA estimations falls below a certain threshold, any ambiguity is resolved by updating the current coordinates through the incorporation of AoA and range information. Consequently, the weights of potential trajectories are updated, taking into account their distance from the current coordinate. The potential trajectories with low weights are then filtered out.

4.5 Evaluation

In this section, RaDro is implemented and experiments are conducted across diverse scenarios. These scenarios include varying LoS and NLoS conditions within dynamic environments,

different flight arenas characterised by varying settings and clutter levels, a range of aerial manoeuvres, and the utilisation of drones of different sizes and models. The experiments are conducted to evaluate the performance of RaDro's modules: coarse- and fine-grained identification of drone movement types, measurement of propeller rotational speeds, and detection and tracking of drones.

4.5.1 Implementation and Settings

Hardware

RaDro is implemented and evaluated using a standard commercial mmWave radar board and drones. An overview of the experimental settings and hardware is shown in Figure 4.10. The mmWave radar utilised is the 77GHz TI AWR2243 (Figure 4.10c) mmWave radar with three transmitters and four receivers. The raw data is collected through the TI DCA1000EVM data acquisition board. The antenna configuration is summarised in Table 4.1. Based on the radar parameters:

- The radar's maximum sensing range can reach $\frac{F_s \ c}{2 \ S} = \frac{3\times10^8 m/s \ \times 10\text{MHz}}{50\text{MHz}/\mu\text{s}\times 2} = 30\text{m}$.
- The Doppler resolution is $\frac{1}{T_f} = \frac{1}{2s} = 0.5\text{Hz}$, where the time frame T_f is the time of the micro-Doppler analysis sliding window. The Doppler resolution of 0.5Hz corresponds to 15rpm. For example, this Doppler resolution can achieve RPM relative error rate of 0.19% for the propeller rotation speed of 8000RPM.

The flights are performed using Holybro S500 quadcopter (Figure 4.10d), weighing 782g and measuring $38.3 \times 38.5 \times 24.0$ cm, equipped with a Pixhawk 4 autopilot running PX4 firmware. Additionally, the Crazyflie 2.1 quadcopter (Figure 4.10e), weighing 27g and measuring $9.2 \times 9.2 \times 2.9$ cm, is utilised with an autopilot control based on an STM32 microcontroller. To

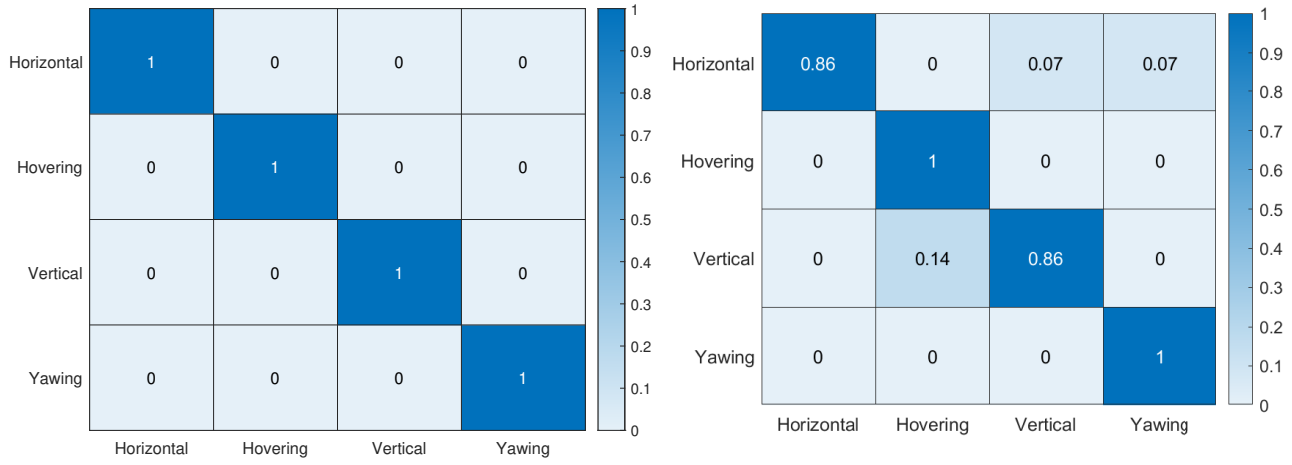
Parameter	Value
Chirp time	40μs
Number of chirps in frame	5
Ramp end time	33μs
Ideal time	7μs
Start frequency	77GHz
Frequency slope	50MHz/μs
Bandwidth	4GHz
ADC sample rate	10MHz
micro-Doppler analysis frame time	2s = (10000 frame $\times$ 5 chirps $\times$ 40μs)

Table 4.1: TI antenna configuration parameters

collect ground truth data, a companion computer, Raspberry Pi4, is installed on the Holybro drone and connected to the autopilot via UART for mavlink communication between the drone and a ground control station PC. The Raspberry Pi4 uses MAVROS to stream time-stamped information of VICON motion tracking to the drone. For Crazyflie drone, the Crazyradio is used for the communication between the drone, the ground control station PC, and VICON information streaming. The time synchronization between different devices is maintained using the Network Time Protocol under the same network subnet. The default drone used to perform the experiments is Holybro, unless the other Crazyflie drone is mentioned.

Experiments Settings

The experiments are conducted in two indoor flight arenas with sizes L $\times$ W $\times$ H = 12$\times$6$\times$7 m (Figure 4.10a) and 5 $\times$ 5 $\times$ 7 m (Figure 4.10b). Throughout the experiments, each flight arena had a minimum of three individuals in motion nearby. The flight arenas have a range of obstacles including metallic stairs, cable trays, and stands, which serve as significant sources of distraction and potential electromagnetic interference. The experiments involving flights covering an 8 $\times$ 4 m area are conducted in the first flight arena, while flights covering 4 $\times$ 4 m area are conducted in the second flight arena. Both arenas are equipped with VICON motion capture system to trace the ground truth of the drone position and attitude at a sample rate



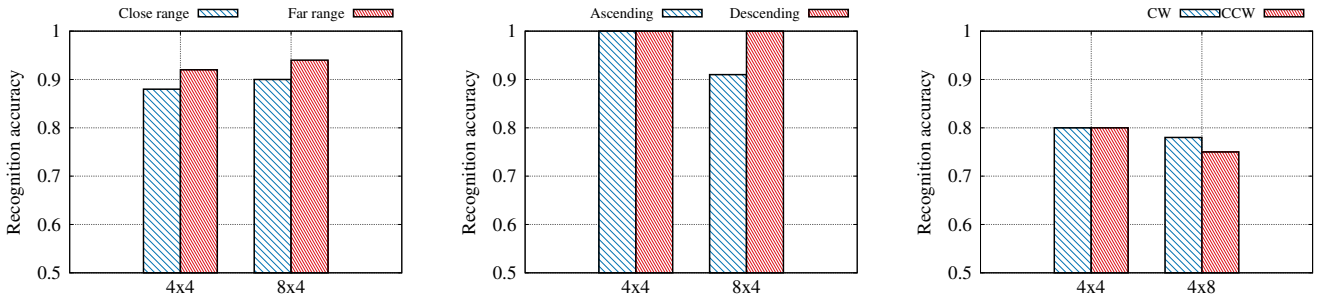
(a) 4×4 m (b) 8×4 m

Figure 4.11: Motion recognition confusion matrix of the four coarse-grained motions.

of 100Hz. A tachometer is used to measure the propeller speed which is considered a reference for the rotation speed ground truth of the system. It is assumed that a single drone, with the same configuration, is present in the flight arena throughout each experiment.

Metrics

The evaluation includes different experimental metrics to assess various parts of the system. These metrics include the true positive and false positive percentages of recognised motion type to evaluate the drone's motion recognition module. RPM error and RPM relative error rate are used to judge the performance of the angular speed of the spinning propellers. The RPM relative error rate is calculated as $|\frac{\hat{C}-C}{C}|\%$, where $\hat{C}$ is the RaDro propeller speed measurement and C is the propeller speed ground truth. Additionally, a localisation error metric is employed to evaluate the overall system performance. The error bars shown in the evaluation figures indicate the 95% confidence interval of the error distribution.



(a) Horizontal motion closer and far away from mmWave antenna.

(b) Vertical motion ascending and descending.

(c) Yawing motion CW and CCW.

Figure 4.12: Fine-grained motion parameters recognition.

4.5.2 Motion Identification Performance

The performance of the system is initially evaluated based on its ability to recognise the drone's motion type. The drone performs the four movement types: horizontal, hover, vertical, and yawing, with each repeated approximately $10 \sim 15$ times at random distances from the radar for each situation. Figure 4.11 shows the performance in two different areas to evaluate the impact of changing distance. In the small area of 4×4 m (Figure 4.11a), RaDro accurately identifies the four basic movements of the drone without any false identifications. In the larger area of 8×4 m, the drone's movements are occasionally misidentified due to the susceptibility of the mmWave signal to noise and interference when the drone moves farther away from the radar (Figure 4.11b).

In the context of fine-grained motion direction identification, which includes distinguishing between closer and far away horizontal directions, ascending and descending vertical directions, and CW and CCW yawing directions, Figure 4.12 illustrates the system performance using true positive accuracy to recognise different motion directions within the 4×4 m and 8×4 m areas. The precise identification performance of the vertical motion direction shown in Figure 4.12b, is a result of the robustness of the micro-Doppler shift information (additional evaluation results are presented in Section 4.5.3). The horizontal motion direction is also be recognised with a high accuracy of around 90% (Figure 4.12a). Conversely, the slightly reduced performance in

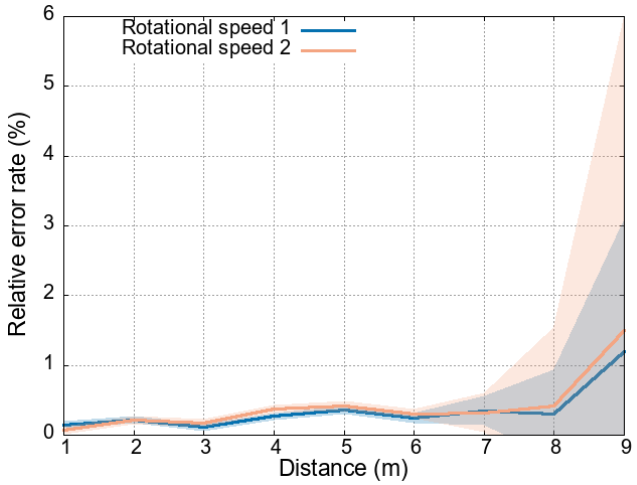


Figure 4.13: RPM relative error rate at different distances from the mmWave antenna. Shadows represent the 95% confidence interval of the error distribution.

identifying the yaw motion direction can be attributed to the sensitivity of the estimated angle information (yet this is still acceptable as the accuracy ranges from 75% to 80% which is then calibrated in the tracking module).

4.5.3 Rotational Speed Measuring Performance

Beyond movement detection, propeller speed detection plays a fundamental role in tracking drones. As a result, an extensive evaluation of the propeller speed estimation performance using mmWaves is provided.

Chapter 3 evaluates the performance of capturing single propeller rotation speed. This section, however, concentrates on evaluating the performance of capturing all rotational speeds of drone propellers in various scenarios, including fixed-drone situations, as well as flying drones with different movement types and trajectories.

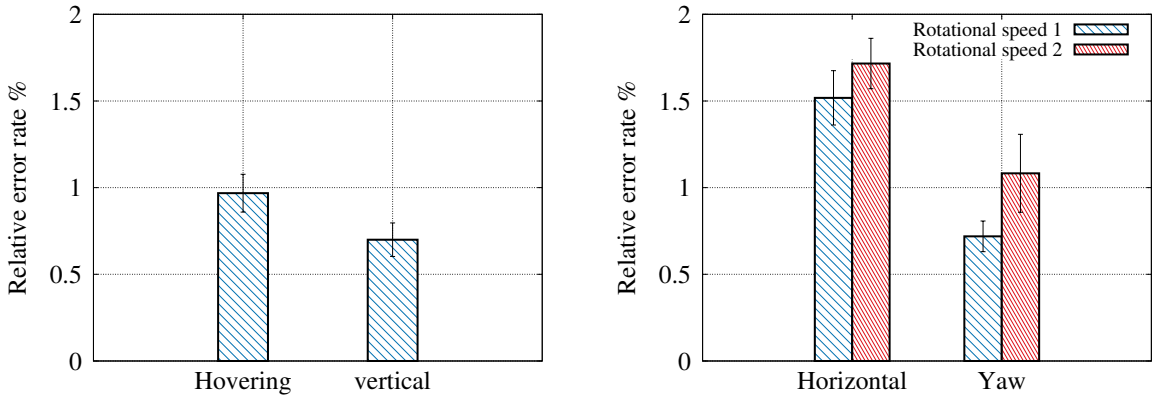
Capturing Different Rotational Speeds at Different Distances

A fixed-drone scenario is employed to evaluate the impact of distance between the drone and the radar on the propeller speeds sensing performance. Figure 4.13 illustrates the performance while the drone is positioned at varying distances from the radar during the application of a pitch-back horizontal motion command. Consequently, the front pair and rear pair of propellers operate at different speeds. The horizontal motion results in two frequency peaks that map to two rotational speeds. The two speeds can be captured with stable accuracy while the distance is less than 8m where the mean relative error rate is maintained less than 0.5%. Based on these results, the defined operational range of the experiments is up to 8m. However, this range can be expanded using multi-radar arrays.

It is worth noting that, according to theoretical calculations, radar capabilities can detect micro motions at distances of up to 30m. However, in this experiment, errors start to increase noticeably after 8m. This is likely due to obstacles present in the flight arena during the experiments, as the available flight area is limited to $9 \sim 10$m. This limitation impacts the accuracy of the measurements, leading to increased errors beyond the specified distance.

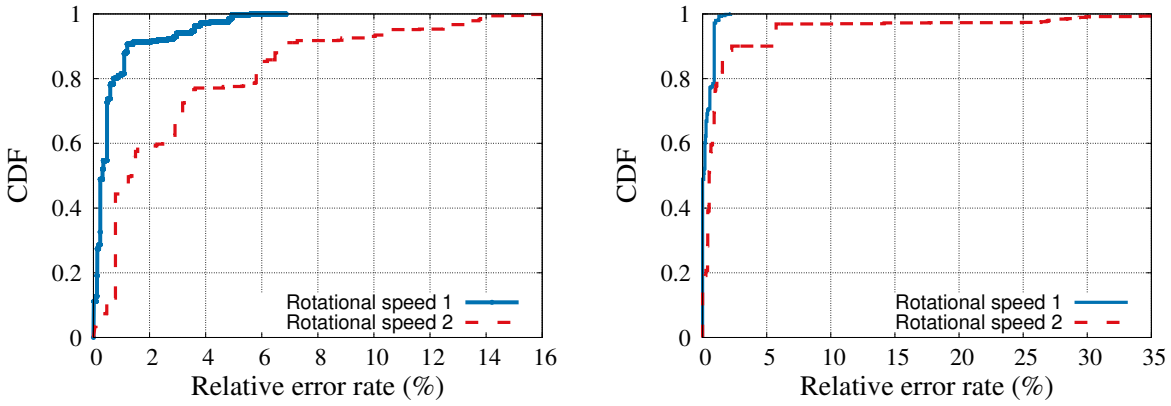
Capturing Rotation Speeds while Flying

This experiment evaluates the system's capability to estimate the propeller speeds during flight across various drone movement types. Because of the complexity of using a tachometer with a flying drone, the relationship between the RPM and PWM is used to obtain the ground truth of the rotational speeds from the commanded PWM. Figure 4.14 shows the impact of different motion types on the accuracy of the propeller rotational speed sensing. The speeds can be accurately captured for all motion types with RPM relative error rate ranges between 0.6% to 1.7%. To further evaluate the impact of changing the distance, experiments are conducted while following flight trajectories in two different areas. The drone flies in both 4×4 m and



(a) One speed motions (b) Two propeller speeds motions

Figure 4.14: RPM relative error rate for the four motions of the quadcopter.



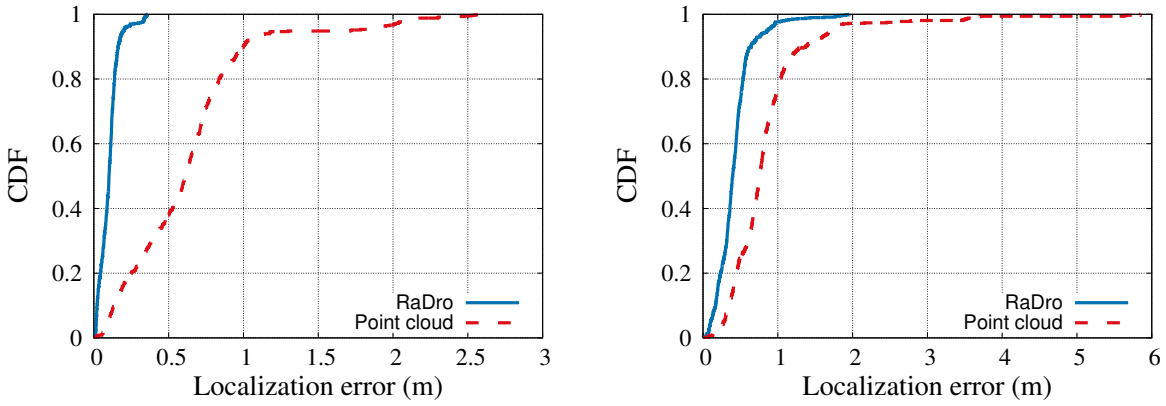
(a) 4 × 4 m trace (b) 8 × 4 m trace

Figure 4.15: RPM relative error rate of propeller speeds during a flight.

8 × 4 m quadrilateral trajectories. As demonstrated in Figure 4.15, the system maintains a maximum median RPM relative error rate of less than 1.3% for both trajectory sizes. On the other hand, the maximum relative error increases when the distance is increased due to the weakening energy of the corresponding frequency peak in far distances.

4.5.4 Drone Tracking

This section presents the system localisation performance in various situations to assess the impact of flight range, drone model size, interference with moving objects, and NLoS situations



(a) Quadrilateral trace of 4×4 m (b) Quadrilateral trace of 8×4 m

Figure 4.16: Drone localisation errors in two different areas.

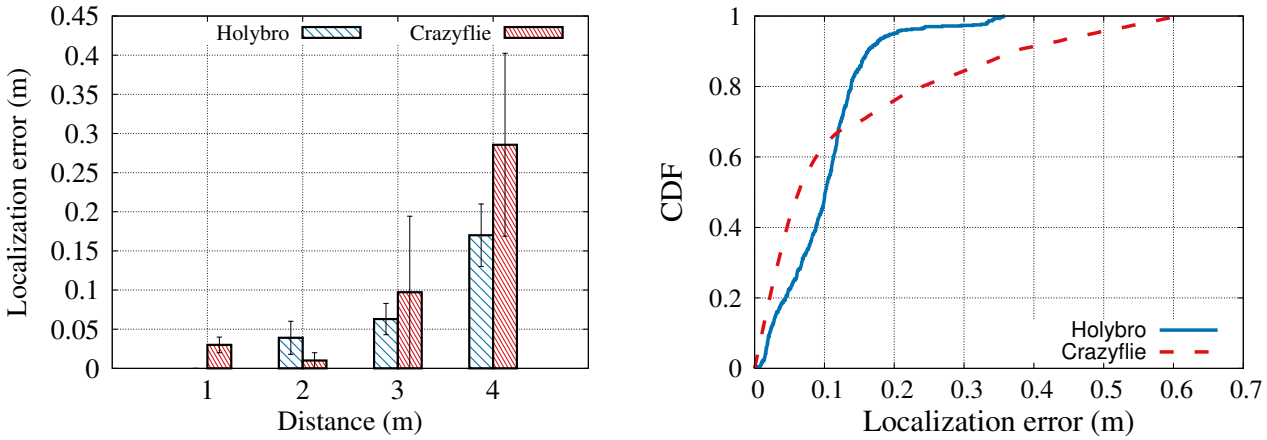
on drone localisation error.

Impact of Flight Range

To evaluate the overall performance of the system, the drone flies in 4×4 m and 8×4 m quadrilateral trajectories. The ground truth is obtained from the VICON system and the localisation error of RaDro is compared with the performance of a Point Cloud based method [121]. Figure 4.16 shows that the median localisation error experiencing more than 50% reduction with RaDro compared to the point cloud based method. For both areas, the maximum estimation error is significantly reduced with RaDro due to the stability of micro-Doppler information used in our system compared to the angle information as explained in Section 4.3.1.

Localisation of Different Drone Models

To evaluate the system's robustness to different drone sizes, the localisation accuracy is compared for two drones, the Holybro S500 V2 with dimensions of $38.3 \times 38.5 \times 24.0$ cm and a much smaller one, the Crazyflie 2.1 with dimensions of $9.2 \times 9.2 \times 2.9$ cm (W x H x D). The experiments are conducted in the $5 \times 5 \times 7$ m flight arena. Figure 4.17a shows the localisation



(a) Drones hover at different distances from the radar.

(b) Localisation error while following the 4×4 m trace.

Figure 4.17: Localisation errors for different drone models.

errors for both drones while hovering at different distances from the radar. The localisation error of the Crazyflie drone slightly increases at 4m distance. Figure 4.17b shows that the median localisation error for both drones during a trace-following flight is less than 10cm with a slight increase in maximum error for Crazyflie. These results can be justified by the fact that the radar cross section depends on the target size, influencing the amount of radar energy reflected back to the source [181], and consequently, affecting the localisation accuracy.

Localisation with Interfering Human

Since RaDro relies on the changes in mmWave signals, humans affecting the LoS between the radar and target drone may severely affect drone detection accuracy. To evaluate RaDro's localisation accuracy, an experiment is performed where the distance between the mmWave radar and the flying Crazyflie drone is set to 2m. An interfering human, performing in-location random activities (moving hands, holding a phone, and rotating body), moves in different positions along the line perpendicular to the line joining the radar and drone. Figure 4.18 reflects the results, indicating that the localisation error remains stable around 3cm, highlighting the robustness of RaDro's detection method as presented in Section 4.4.1.

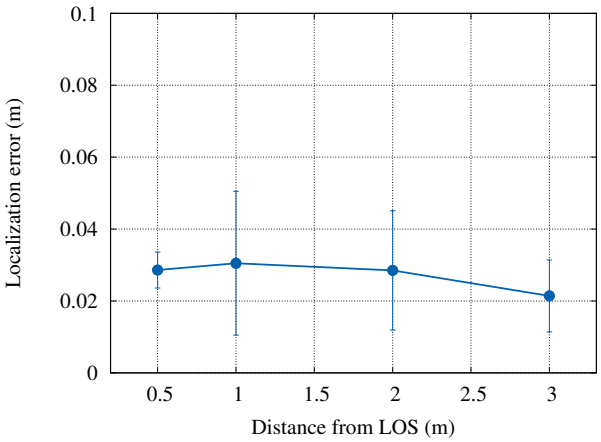


Figure 4.18: Localisation error with interfering human at different distances from the LoS

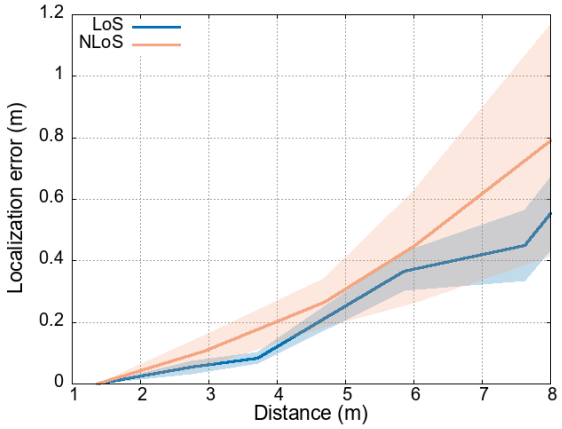


Figure 4.19: Through-the-wall localisation performance. Shadows represent the 95% confidence interval of the error distribution.

NLoS Scenario

The system performance in NLoS scenarios is also evaluated. In an NLoS setup, a vertical block stand is deployed in front of the radar array to block all the LoS paths while hovering the drone at different distances. The results are shown in Figure 4.19. The localisation error slightly increases proportional to the distance between the drone and the radar, while maintaining a maximum mean localisation error of 0.8m in the operational area. These findings highlight RaDro's substantial potential for through-the-wall localisation applications, encompassing intruder detection and security-related purposes across diverse lighting conditions.

4.6 Discussion and Outlook

In the future, RaDro system can be extended in multiple directions including the following.

Drones and Humans Sharing Spaces: RaDro can operate in dynamic environments where the discernible signatures resulting from the propeller rotations are distinguished from those of other moving objects, including humans, as shown in Sections 4.4.1 and 4.5.4. The human

signature (Figure 4.5a) can be further leveraged to detect humans and their activities concurrently with drone localisation. This highlights RaDro's ability to enable secure coexistence of drones and humans in shared spaces for various applications. Further investigation of RaDro's capability for recognising drone and human simultaneously will be considered as interesting future research.

Identifying Drone Structures: While assuming known drone specifications is acceptable for working environments such as warehouses, given their standardisation among well-known companies, it is worth investigating the ability to identify the drone structure for intruder detection applications automatically. RF waves are employed to estimate the drone's model and weight by extracting the drone's body vibration profile [143]. Several studies have demonstrated the capabilities of mmWave radar in extracting vibration characteristics [19, 182]. This highlights the potential of the mmWaves to passively identify the drone structure, thus enabling RaDro to be independent of the drone's parameters identification.

4.7 Summary

In this chapter, RaDro system is presented for passive indoor drone localisation using a single mmWave radar array. RaDro is cost-effective, doesn't require attaching tags or anchors to drones, and works effectively in different LoS and NLoS scenarios independent of lighting conditions. It achieves 3D tracking with a single radar point, resulting in a simpler deployment, indeed the drone can deploy the mmWave sensor itself; useful for several applications such as research and rescue missions. The system captures the micro-Doppler signature corresponding to the drone's propeller speeds which are incorporated into the drone's motion equations to improve the performance of the mmWave tracking technique. Extensive evaluation of RaDro in different scenarios has been conducted using commercial off-the-shelf mmWave radar and drones. The results show that there is a significant reduction in localisation error compared

to the baseline. The results also demonstrate the system's non-vulnerable performance in the presence of interfering objects, including moving people around the experimental space. The system demonstrates that it has the potential to detect humans and some of their behaviours, concurrently while providing drone location. This highlights the further potential of the approach to facilitate the secure coexistence of drones and humans in shared spaces. Additionally, the system exhibits its capability to accurately localise drones through the wall with an average localisation error of less than 0.8m at distances up to 8m without attaching any reflector to the drone body, a task where conventional state-of-the-art optical technologies face limitations. This underscores the effectiveness of RaDro for intruder detection and security applications under varying lighting conditions.

The next chapter introduces approaches that leverage the sensed propeller speeds to enhance the autopilot state estimation and autopilot control, ensuring reliable and stable drone navigation.

Chapter 5

Drone State Estimation and Control Enhancement using Radio Sensing

Propeller rotational speeds play a crucial role in determining the motion characteristics of drones, as discussed in Chapter 2. However, drone autopilots lack the integration of feedback from these speeds in the processes of state estimation and motion control. Following the observed enhancements resulting from integrating micro-movement sensing of propeller rotations into the external detection and tracking system proposed in Chapter 4, this chapter delves into the effects of leveraging propeller rotations internally within the autopilot. This chapter proposes a system that leverages actual propeller speeds, measured with radio sensing, as direct feedback to the autopilot to improve the state estimation and dynamics of the drone. Software-in-the-loop (SITL) simulations informed with real RF sensing data in different scenarios are conducted to demonstrate the impact of combining propeller speeds with typical drone sensors.

5.1 Motivation and Objectives

As previously discussed, in a drone's autopilot, specifically the multirotor category, the adjustment of position and attitude is typically achieved through control inputs that regulate the angular speed of the propellers, a fundamental factor influencing motion properties. However, the autopilot commonly estimates the vehicle state in relation to its surroundings using onboard sensors through the state estimation process, lacking real-time feedback on the behavior of the propellers. State estimation is a fundamental process in drone autopilot to achieve autonomous motion. Drone state estimation typically relies on either GPS for outdoor applications or motion capture systems for indoor applications [183]. However, these techniques encounter several challenges, such as the unavailability of GPS in challenging areas and the complexity and high cost associated with installing motion capture systems. Other technologies have been presented in the literature for utilising IMU sensors [184, 185] and vision sensors [186, 187, 188, 189]. However, these technologies have drawbacks, i.e., IMU sensors suffer from error drifting over time, while vision navigation approaches are sensitive to environmental lighting conditions, are scale ambiguous and not robust enough for high-speed motion.

The proposed approach in this chapter utilises direct feedback of the propeller rotation speed of a drone sensed with an RF module to improve motion stability and safety, especially in challenging conditions including actual propeller speed deviations caused by environmental and mechanical/electrical factors or partial damage to the blades [30]. The radio sensing technology is leveraged which is cost-effective, not sensitive to light, and can achieve a high accuracy for measuring the rotation speed of a spinning object as shown in Chapter 3. The drone's propeller speeds are incorporated into the autopilot's state estimation and motion control processes, aiming to enhance the overall motion performance of the drone. Propeller speeds can be utilised by the motor control as feedback signals to control rotor speeds in a closed-loop fashion [139] to minimise the error between the commanded and actual speeds.

This is typically implemented based on a motor current sensing approach which estimates the motor speed with the knowledge of motor parameters (e.g., motor constant, resistance, and inductance). Although this approach is common, the estimated speed has limited accuracy due to its dependence on motor parameters which are subject to uncertainties.

Measuring propeller speeds has the potential to improve the navigation performance and drone detection and identification applications [61, 139, 140, 141, 142, 143, 144]. However, there is a scarcity of literature studies analysing the impact of incorporating propeller speed feedback in the state estimation or motion control of the drone. In the proposed approach, the actual speeds of drone propellers are provided as feedback to the autopilot's state estimation and motion control processes. In the state estimation phase, the drone's position and orientation are estimated using a dynamic model with the measured propeller speeds as inputs. Subsequently, an EKF [180] is applied to integrate the estimated position and orientation with the measurements from inertial sensors on the drone. Furthermore, the measured propeller speeds are utilised to enhance the control of the autopilot's total torque and thrust. This is achieved by integrating propeller speed errors into the corresponding thrust and/or torque directions within the autopilot's controller stack. Given the challenges associated with the implementation and validation of the system in a real-world environment, an alternative evaluation method is employed. The system is evaluated through SITL simulations, which provide a flexible and efficient way to test and refine the system. These simulations are conducted using Gazebo[1] with modules implemented on the PX4 framework[2]. The RF sensor is implemented in the simulator using real data measurements, where the propeller speeds are measured using the 5GHz RF OAM sensing method proposed in Chapter 3.

The rest of this chapter is organised as follows. Section 5.2 introduces the proposed methods, while Section 5.3 evaluates them. A conclusion and directions for future work are proposed in Section 5.4.

[1] http://gazebosim.org/
[2] https://px4.io

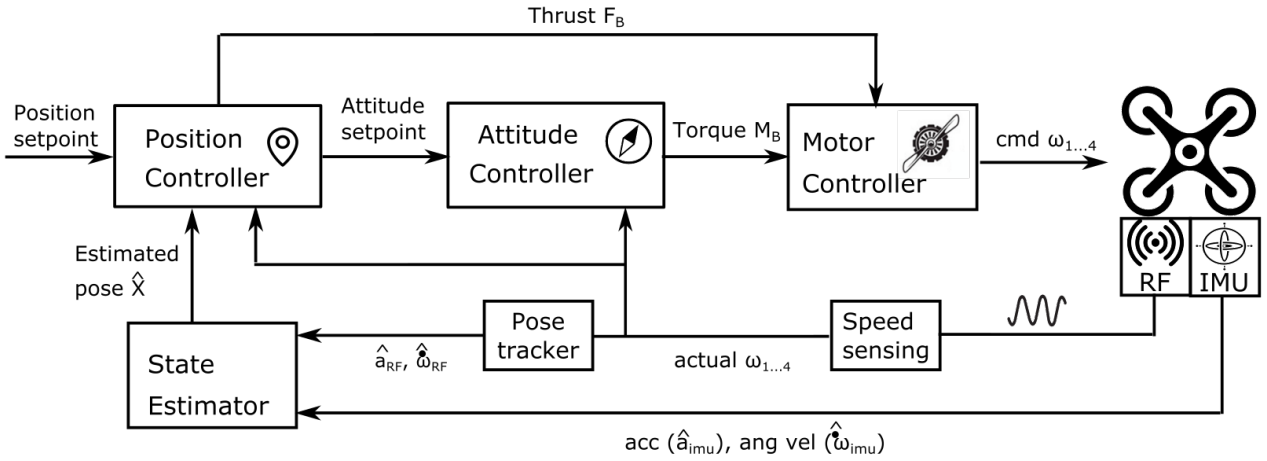


Figure 5.1: The system overview

5.2 System

In this section, the details of the proposed system shown in Figure 5.1 are introduced. Propeller speed sensing is implemented through the signal received from the RF module. The sensed speeds are used to enhance the performance of two modules: the state estimator and the motion controller. For state estimation, the propeller feedback pose tracker module estimates the drone's position and orientation using propeller speed measurements. The state estimator module then combines this pose information, derived from the propeller speeds, with pose estimates from the inertial sensors. This combination is performed using an EKF to provide an accurate estimate of the drone's state. For motion control, the propeller speed feedback is integrated into the drone's motion control system. This integration allows the controller to adjust the propeller speeds to achieve the desired forces and torques for the next motion step, thereby ensuring precise and responsive control of the drone's movements.

5.2.1 Propeller Feedback Pose Tracker

The pose tracker algorithm estimates the drone's position and orientation by utilising the measured speed of the four propellers, employing the dynamic model of the quadcopter, which is detailed in Chapter 2. The actual total thrust and torques are first calculated and then used to obtain the linear and angular acceleration of the drone's body. Using linear and angular acceleration, the drone position and orientation are tracked using drone motion equations in discrete time [190]. As discussed in Chapter 2, the vehicle's four propellers produce four thrust forces $f_{1..4}$ that pull it upward. f_i is related to the i^{th} propeller spinning speed as $f_i = k\ \omega_i^2$ where ω_i is the spinning speed of rotor i and k is a constant related to the propeller motor specifications. The total thrust applied on the body frame is $F_B = [0, 0, -\sum_{i=1}^{4} f_i]^T$.

The actual torque applied on the quadcopter's body can be derived from the four propeller spinning speeds as follows,

$$M_B = \begin{bmatrix} l(-f_1 + f_2 + f_3 - f_4) \\ l(f_1 - f_2 + f_3 - f_4) \\ \tau_1 + \tau_2 - \tau_3 - \tau_4 \end{bmatrix} \tag{5.1}$$

where τ_i is the torque of rotor i and is related to the propeller spinning speed as $\tau_i = b\ \omega_i^2$ and l is the distance between the rotor and the centre of mass of the quadcopter. b is a constant related to the propeller motor specifications.

The estimated thrust F_B and torque M_B are used to track the linear and angular acceleration of the quadcopter using rearranged forms of Equations 2.11 and 2.12 discussed in Section 2.1.4. The drone motion equations in the discrete time form can be described as follows,

$$p_I^{t+1} = p_I^t + v_I^t \Delta t \tag{5.2}$$

$$v_I^{t+1} = v_I^t + (g + \frac{1}{m} R_{IB}(q^t) F_B^t + \frac{1}{m} F_{a,I}^t)\Delta t \tag{5.3}$$

$$q^{t+1} = q^t + \frac{1}{2} q^t \otimes \omega_B^t \Delta t \tag{5.4}$$

$$\omega_B^{t+1} = \omega_B^t + I^{-1}(M_B^t + M_{a,B}^t - \omega_B^t \times I\omega_B^t)\Delta t \tag{5.5}$$

where q is the quaternion that represents the vehicle attitude. $R_{IB}(q^t)$ is the rotation matrix that is derived from q which allows transformation from body to inertial frame. For a comprehensive understanding of term representations, additional details can be found in Chapter 2.

5.2.2 State Estimation Design

The state estimator is a fundamental component that provides real-time information about the position and orientation of the quadcopter to the autopilot. In the proposed system, this information is derived from the fusion of data obtained from the propeller feedback pose tracker and the onboard inertial sensors. To achieve this, an EKF scheme provided by the PX4 autopilot is adopted. The EKF algorithm typically relies on a prediction step based on input signals and a correction step based on observations. In this context, general kinematics equations are preferred for the prediction step due to their robustness against noise. These equations are applicable to any rigid body moving in 3D space and are not dependent on the specific characteristics of the body. These rigid body equations are updated through incorporating measurements from the inertial sensors. The tracked position and orientation obtained from the propeller speed measurements are used as observations for the correction step.

Pose information, consisting of the unit quaternion representing the drone's orientation, velocity, and position, is captured in the first 10 states of the EKF $X = [q_0, q_1, q_2, q_3, v_x, v_y, v_z, p_x, p_y, p_z]^T$. The quaternion defines the angular position of the body frame relative to the navigation frame. The delta quaternion Δ_{quat} that defines the rotation from the quaternion at frame t to t+1 is calculated from the delta angle Δ_{ang} captured using the inertial sensor measurements using a small angle approximation.

$$\Delta_{quat} = \begin{bmatrix} \Delta q_0 \\ \Delta q_1 \\ \Delta q_2 \\ \Delta q_3 \end{bmatrix} = \begin{bmatrix} 1 \\ \frac{\Delta_{ang\_x}}{2} \\ \frac{\Delta_{ang\_y}}{2} \\ \frac{\Delta_{ang\_z}}{2} \end{bmatrix} \tag{5.6}$$

The quaternion product rule is applied to rotate the quaternion state forward by the delta quaternion Δ_{quat} from time frame t to t+1.

$$\begin{bmatrix} q_0 \\ q_1 \\ q_2 \\ q_3 \end{bmatrix}_{t+1} = \begin{bmatrix} q_0 & q_1 & q_2 & q_3 \end{bmatrix}_t \begin{bmatrix} \Delta q_0 & \Delta q_1 & \Delta q_2 & \Delta q_3 \\ -\Delta q_1 & \Delta q_0 & -\Delta q_3 & \Delta q_2 \\ -\Delta q_2 & \Delta q_3 & \Delta q_0 & -\Delta q_1 \\ -\Delta q_3 & -\Delta q_2 & \Delta q_1 & \Delta q_0 \end{bmatrix} \tag{5.7}$$

To calculate the drone velocity v at time $t+1$, the delta velocity Δv, obtained from IMU measurements, is rotated from the body frame to the inertial frame using the rotation matrix $R_{IB}(q^{t+1})$ derived from quaternions at time $t+1$, and the gravitational effect is subtracted.

$$v^{t+1} = v^t + R_{IB}(q^{t+1})\Delta v + \begin{bmatrix} 0 \\ 0 \\ g \end{bmatrix} \Delta t \tag{5.8}$$

The position states are updated using Euler integration.

$$p^{t+1} = p^t + v^t \Delta t \tag{5.9}$$

The tracked position and velocity using propeller speeds in Equations 5.2 and 5.3 involve direct observation of drone states.

5.2.3 Drone Control Enhancement

The sensed propeller speeds are further used in the autopilot motion control. The autopilot motion control is a module designed to adjust the pose of the drone to align with the desired point. Usually, the quadcopter autopilot control is a hierarchical combination of PID controllers with mainly two loops [191]. The outer loop is dedicated to position control, taking estimated and desired positions as inputs. The output comprises the desired attitude and commanded thrust necessary to move the vehicle to the desired position. The inner loop is dedicated to controlling the attitude, taking the estimated and desired attitude as inputs, and producing the desired torques necessary for achieving the desired attitude. In addition to providing estimated pose feedback $\hat{X}$ to the motion controller, the feedback on the actual propeller speed is incorporated. The difference between commanded and actual propeller speeds defines the propeller speed error, represented as follows:

$$\omega_e = \begin{bmatrix} \omega_e^x \\ \omega_e^y \\ \omega_e^z \\ \omega_e^F \end{bmatrix} = \mathbb{M} \begin{bmatrix} \omega_{com_1} - \omega_{act_1} \\ \omega_{com_2} - \omega_{act_2} \\ \omega_{com_3} - \omega_{act_3} \\ \omega_{com_4} - \omega_{act_4} \end{bmatrix} \tag{5.10}$$

where ω_{com_i} is the commanded speed of propeller i and ω_{act_i} is the actual speed of propeller i.

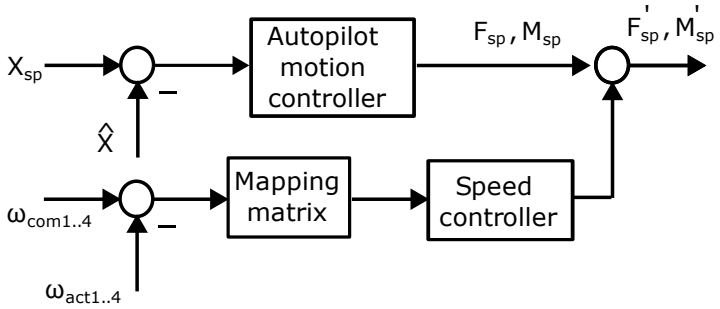
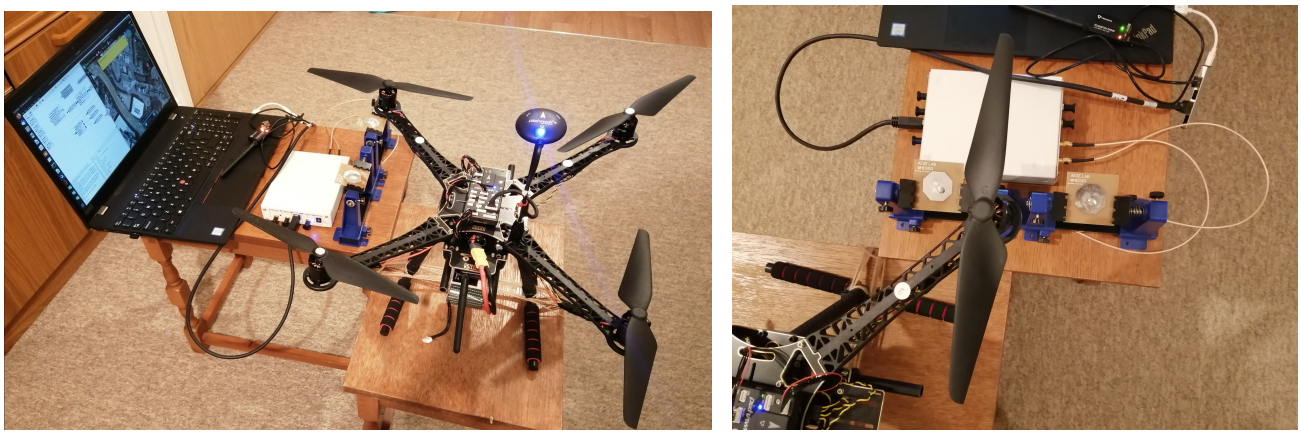


Figure 5.2: Quadcopter enhanced control with feedback of the sensed propeller speeds.

ω_e^x, ω_e^y, ω_e^z and ω_e^F represent the error between the actual and commanded speeds that affect the roll, pitch, and yaw torques, and thrust, respectively. $\mathbb{M}$ is a mapping matrix that maps the propeller speed errors to the torques and thrust forces directions (Figure 4.3 shows the relation between quadcopter propellers movement and the generated torques and force, which can be translated to $\mathbb{M}$) and is defined as follows,

$$\mathbb{M} = \begin{bmatrix} -1 & +1 & +1 & -1 \\ +1 & -1 & +1 & -1 \\ +1 & +1 & -1 & -1 \\ +1 & +1 & +1 & +1 \end{bmatrix} \tag{5.11}$$

With the propeller speed error feedback, the position controller adjusts the total thrust based on the error between the estimated and desired positions, as well as the error between the actual and commanded speeds that affects the total thrust ω_e^F. Meanwhile, the attitude controller compensates for torque based on the error between the estimated and desired speeds, along with the errors between the actual and commanded speeds that impact the roll, pitch, and yaw torques ω_e^x, ω_e^y, and ω_e^z. Figure 5.2 shows the quadcopter control after adding a speed controller for propeller speed error feedback shown in Equation 5.10.



(a) The used quadcopter is Holybro S500 V2 (b) 5GHz RF OAM antennas

Figure 5.3: Quadcopter hardware setup for RF sensor simulation.

5.3 Evaluation

The proposed system is evaluated using SITL simulations incorporating real data from RF sensing measurements across different operating scenarios, including normal flight and rotor failure situations. These simulations are executed on the Gazebo simulator, a powerful tool for simulating complex robotic systems in a realistic 3D environment, which supports both sensor and motor simulation. The adopted autopilot is the PX4 framework, an open-source flight control software stack widely used in drone development, supported by several vendors and voluntary developers worldwide. To emulate real-world quadcopter flying environments, the simulation model in Gazebo includes the addition of wind disturbances to replicate the unpredictable factors that a quadcopter would encounter during actual flight. This simulation approach ensures that the system's performance can be accurately assessed and necessary adjustments can be made before moving to real-world trials.

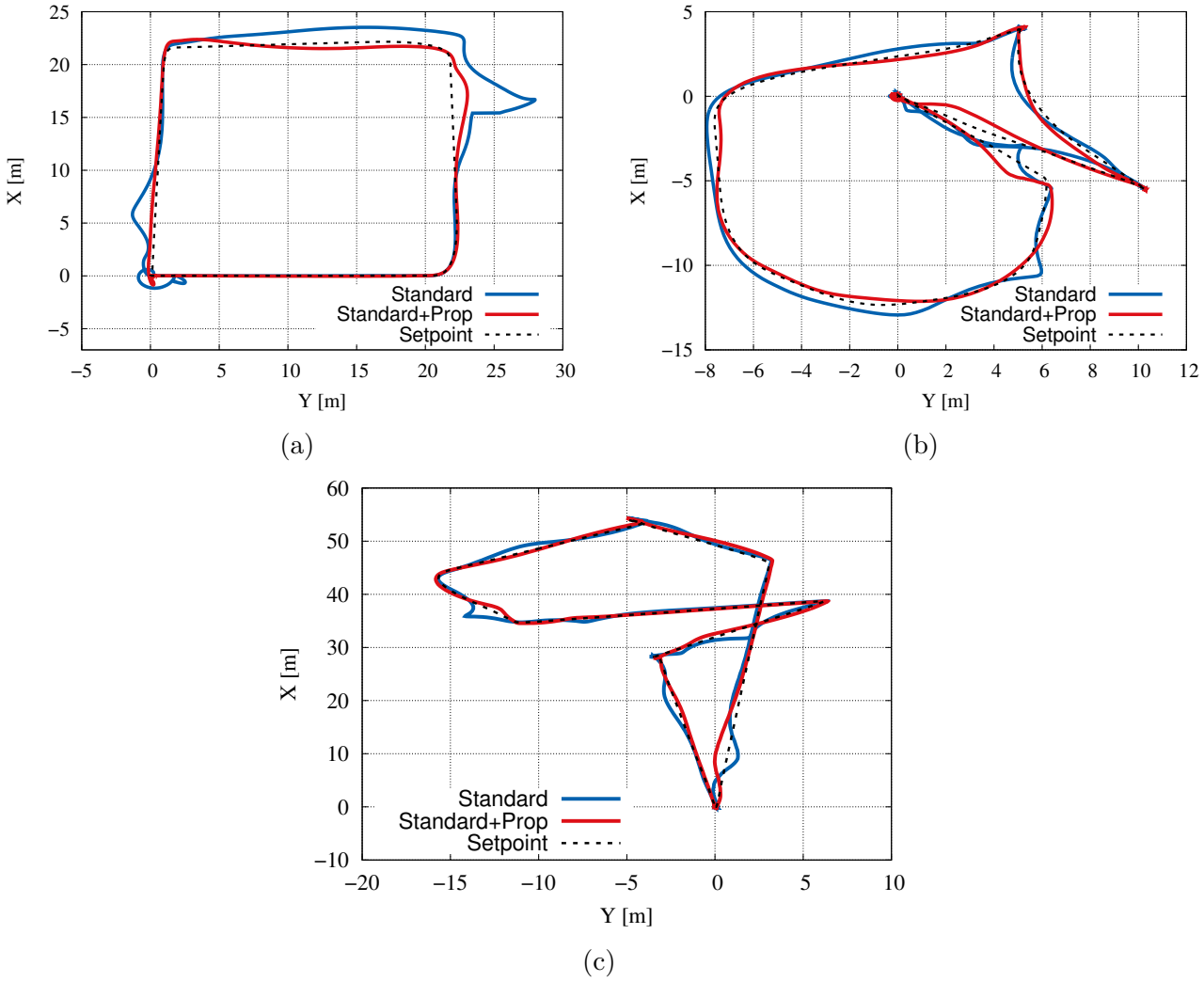


Figure 5.4: Sample trajectories used to test the impact of integrating actual propeller rotation speed to the autopilot. Typical used inertial sensors in PX4 are labelled as 'Standard', while 'Standard+Prop' denotes the case when propeller speeds feedback is added.

5.3.1 RF Sensor Implementation in Simulator

The RF sensor is implemented in Gazebo simulator based on real data from propeller speed measurements. A real quadcopter is used to compare the commanded propeller speeds with the actual speeds. To achieve this, Hardware-in-the-Loop (HITL) simulations (Figure 5.3a) are performed using a Holybro S500 quadcopter equipped with a Pixhawk 4 autopilot running PX4 firmware. The quadcopter is outfitted with four 2216-980KV brushless motors and 9-inch

propellers. HITL is a simulation mode where the PX4 firmware runs on actual flight controller hardware. This approach provides the benefit of testing the actual flight code on real hardware, ensuring that the simulation closely mimics real-world conditions. The HITL setup provided by the PX4 community[3] is adapted to enable the rotation of the quadcopter's hardware propellers during the flight simulation.

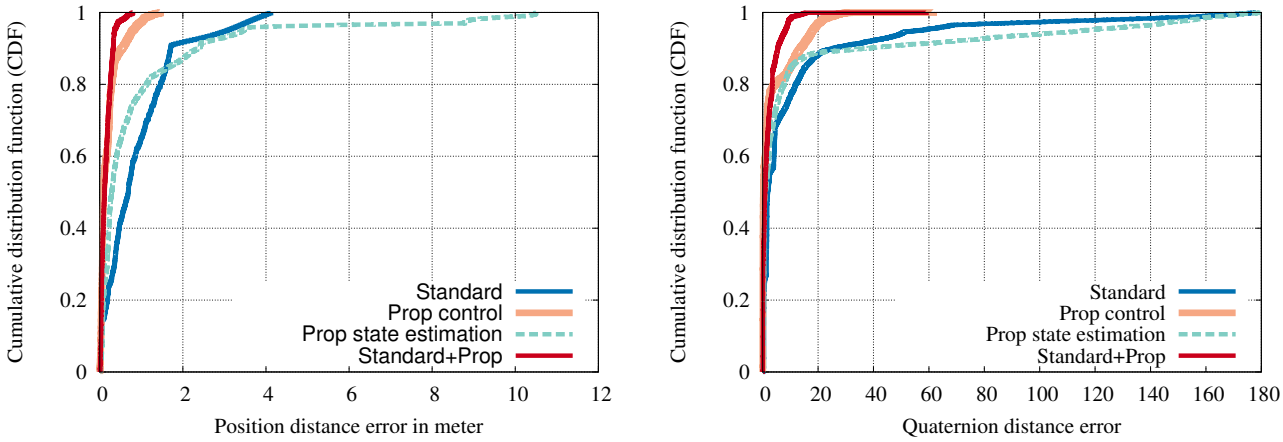
Two RF OAM antennas (Figure 5.3b) are used as a transmitter and receiver, operating at a frequency band of 5.525GHz. This frequency is chosen to match the typical drone communication band, ensuring compatibility and realistic communication scenarios. Both antennas are connected to a USRP B210 Software Defined Radio, which operates at a sampling rate of 1 MS/s. The USRP is connected to a laptop running GNU Radio 3.7, which is used for processing the RF signals.

During the simulation flights, propeller speeds are measured using RF sensing, recorded and compared with the commanded propeller speeds in Gazebo to identify distribution errors, which are then used to simulate the RF sensor. By analysing these errors, the simulation can account for deviations between the commanded and actual propeller speeds, leading to more accurate simulated sensor performance.

5.3.2 Trajectory Tracking Performance

The autopilot performance is evaluated with the two proposed modules as per Section 5.2. Figure 5.4 shows three examples of testing trajectories at fixed altitudes in the simulation that are used to verify the impact of adding the actual propeller speed feedback to the autopilot. It can be noticed that there is a considerable improvement in the quadcopter motion accuracy while following the predefined trajectories. This can be further elucidated in Figure 5.5 showing the CDFs of the quadcopter position and orientation errors after following the trajectories in

[3]https://docs.px4.io/main/en/simulation/hitl.html



(a) Position (b) Attitude

Figure 5.5: The CDF of position and attitude error using typical quadcopter sensors with PX4 autopilot, and after fusing propeller speed feedback in the state estimation (Prop state estimation) and autopilot control stack (Prop control). The impact of adding the combination of two modules is labeled as Standard+Prop.

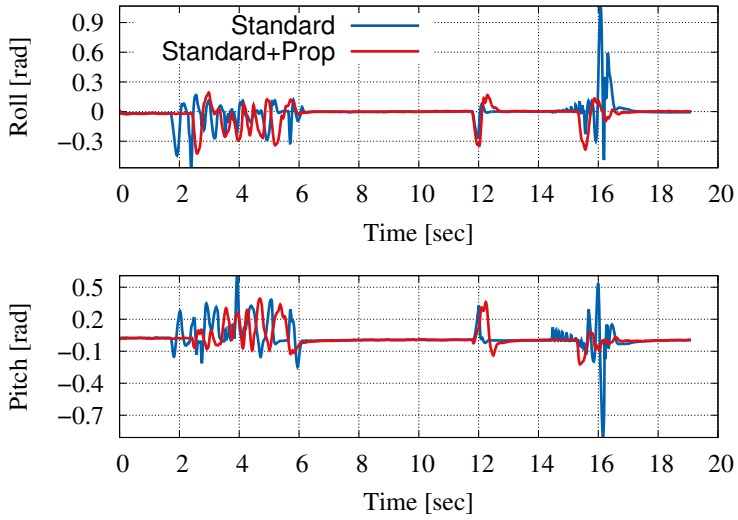
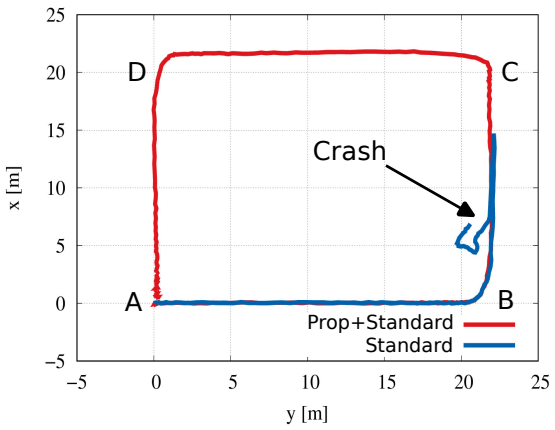
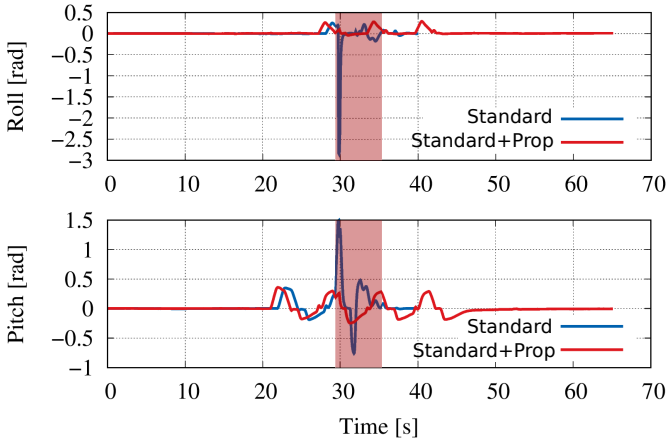


Figure 5.6: Roll and pitch angles estimation over time with standard quadcopter sensors and after combining the speeds feedback.

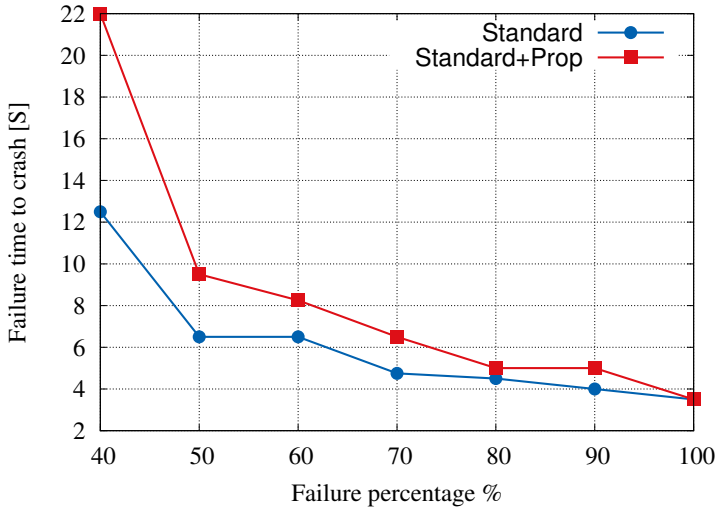
Figure 5.4 successive times. With typical quadcopter autopilot sensors, the median position error is 0.7m with a standard deviation of 0.9m. The median position error decreases to 0.1m with a standard deviation of 0.13m when the propeller speed measurement is integrated to the autopilot state estimation and control stack. The median attitude quaternion distance error using typical quadcopter sensors is 2 with a standard deviation of 26.4 which is significantly



(a) 2D trajectories of the quadcopter with an applied 50% fault in two rotors for 6 seconds between B and C. A to D represent setpoints.



(b) Roll and pitch angle estimates of trajectories in (a). The highlighted area indicates the duration during which the failure is applied.



(c) The relationship between the failure percentage of two rotors and the time taken to crash.

Figure 5.7: The impact of propeller speed feedback fusion on the quadcopter performance with two opposite rotors under failure.

reduced to 0.85 with a standard deviation of 3 after incorporating propeller rotation speed measurements. The reason for this error reduction is that the direct propeller speed feedback improves the quadcopter stability, as explained in Figure 5.6 which shows the impact of the propeller speed fusion on the roll and pitch angles when the quadcopter follows the trajectory presented in Figure 5.4b. It can be noticed that the quadcopter moves with a lower tilt when the propeller speed feedback is incorporated, which enhances its flying stability.

5.3.3 Rotor Failure Time Tolerance

In this evaluation scenario, the quadcopter survival ability is studied in the presence of motor fault [30, 192] to show the impact of the propeller speed feedback fusion, compared to the case where the quadcopter relies only on its other onboard sensors. The longer the quadcopter can maintain control of its attitude under motor fault, the higher the probability it can land safely or regain normal attitude, which is useful when the external disturbances to the motor are temporary. This is examined as shown in Figure 5.7, where in Figure 5.7a, the quadcopter follows a trajectory where a 50% fault is forced on two opposite rotors, to prevent yaw instability, for 6 seconds. The fault percentage represents the reduction in the actual thrust and torque forces generated by the rotating propeller when a fault occurs, such as partial blade damage [30]. This fault is applied at 30 seconds time instance after the quadcopter starts its mission. It can be noted that the integration of propeller speed feedback enables the quadcopter to safely complete its mission, avoiding a possible crash that happens when the quadcopter just relies on its onboard inertial sensor measurements. This is intuitive as the quadcopter control has a faster response to motor failure when it receives immediate feedback about any discrepancies in motor speeds. Figure 5.7b shows the quadcopter's body roll and pitch angles while following the trajectory shown in Figure 5.7a. The quadcopter is more stable during the motor failure time (shaded area in Figure 5.7b) with the incorporated propeller speed feedback. Figure 5.7c shows the relationship between the percentage of applied motor failure and the time duration to crash. Generally, the time duration to crash decreases with increased motor failure percentage. Importantly, for the same percentage of motor failure, the time to crash is longer when the propeller speed feedback is integrated into the autopilot. It is worth mentioning that when applying a total failure to all motors, the quadcopter crashes within the same 3.5 seconds time in both cases. Maintaining balance in such a situation is challenging and requires specialised motion model considerations to handle it, which is addressed in literature [193].

5.4 Summary

In this chapter, a system is proposed that utilises actual propeller speed measurements sensed using radio sensing to improve drone motion accuracy. The propeller speeds are employed to estimate the drone's position and orientation using its dynamic model. The estimated position and orientation are fed into the state estimation module to be fused with other conventional drone sensor measurements. The speed measurements are additionally employed as feedback to the autopilot control system to compensate for torque and thrust errors induced by propeller speed drift. SITL simulations have been conducted to assess the proposed technique in various scenarios. This evaluation will be further extended with experimental validation in future work. The results indicate that incorporating actual propeller speed into the autopilot's state estimation and motion control significantly enhances drone motion accuracy and stability, especially during motor faults.

The next chapter concludes the thesis and summarises its accomplishments.

Chapter 6

Conclusion

This chapter provides a summary of achievements and general conclusions derived from the thesis, along with its primary research contributions. Furthermore, it outlines suggestions for potential future research directions.

6.1 Summary and Contribution

The main objective of this thesis is to investigate different radio wave sensing technologies to sense the micro and macro motions of drones for enhanced detection, localisation, and autonomous control performance. This investigation yields three primary contributions within the thesis, which are as follows: 1. Evaluating the sensing resolution and detection range of two different radio wave technologies to sense micro movements of drone, 2. Introducing a novel passive indoor drone localisation and tracking system based on radio waves, and 3. Developing new state estimation algorithms to enhance drone navigation stability even under failure.

Chapter 3 provides a comparison of the capabilities of two different radio wave technologies (5GHz RF OAM and 77GHz mmWave FMCW radar) in sensing the speeds of drone propellers.

The chapter evaluates how these technologies perform in detecting and measuring the micro-movements of drone propellers, even while the drones are in flight, capturing rotational speeds of up to 16000RPM across various aerial manoeuvres. The results of this comparison show that both radio wave technologies can precisely sense micro propeller motions and measure their speeds with a high degree of accuracy. However, a notable difference between the two technologies is observed in their effective sensing distance ranges. The 77GHz mmWave demonstrates a significant advantage in this aspect, being capable of accurately sensing propeller speeds at distances up to 8m. In contrast, the 5GHz RF is limited to a much shorter range, providing accurate measurements only up to a distance of 1m. The findings in Chapter 3 underscore the superior performance of mmWave radar in terms of sensing range, highlighting its potential for more versatile and wide-ranging applications in drone monitoring and control.

Chapter 4 introduces RaDro: a cost-effective indoor drone localisation and tracking system. It uses a single mmWave radar point, eliminating the need for additional hardware attachments on drones, thereby simplifying deployment and reducing costs. RaDro operates effectively in both LoS and NLoS scenarios, and it performs consistently regardless of lighting conditions. The implementation of RaDro shows a reduction of more than 50% in localisation error compared to the classical baseline. The system demonstrates robust performance even in the presence of interfering objects, such as moving individuals within the experimental area. Moreover, the system excels in NLoS scenarios, where existing state-of-the-art optical technologies cannot work. Additionally, the system showcases the potential capability to detect humans simultaneously while providing drone location information, which underscores the further potential for the safe coexistence of drones and humans in shared spaces. The findings in Chapter 4 demonstrate RaDro's advanced capabilities for enhanced indoor drone tracking and localisation.

Chapter 5 develops approaches that leverage the sensed propeller rotation speeds to improve the stability and autonomous controllability of drones. These approaches enhance autopilot state estimation by integrating the accurately sensed propeller speeds into the dynamic model

of the drone. This integration allows for precise tracking of the drone's position and orientation, which are then fused with measurements from the onboard inertial sensors. Additionally, by incorporating these propeller speed measurements as real-time feedback, the system can effectively compensate for the desired forces/torques applied by the autopilot's motion control by addressing the deviation of the actual sensed propeller speeds from their commanded ones. The verification results show that the drone exhibits increased stability and reduced trajectory errors with a noticeable reduction in the drone position median error while following a predefined trajectory. Furthermore, in scenarios involving motor faults, the system increases the duration the drone can remain airborne before crashing, indicating improved fault tolerance and overall safety. The findings of Chapter 5 underscore the potential of incorporating propeller speed feedback into the drone's control systems to enhance the autonomous navigation stability and safety of the drone.

The thesis contributions illustrate the potential of radio wave sensing as a promising technology for precise drone localisation and reliable navigation. The proposed techniques demonstrate the effectiveness of different radio wave sensing technologies in identifying and tracking drone movements and capturing its micro signatures, including propeller rotation speeds, providing insights into the drones' operational characteristics. These advancements enhance drone detection and localisation while improving the stability and reliability of navigation and autonomous control by refining the autopilot state estimation and motion control mechanisms.

6.2 Discussion and Future Directions

Several advancements can be investigated to further enhance radio wave drone sensing for scalable deployment and widespread adoption. This section outlines potential topics for future research, highlighting areas where further enhancements can be explored.

6.2.1 Deployment Scalability

Advancements in scalability can be categorised into various aspects: working area expansion, multiple drone tracking, different drone categories, and operation in challenging environments including highly cluttered spaces.

Area Expansion This thesis evaluates various radio-sensing technologies based on their sensing range. The experimental findings in Chapters 3 and 4 underscore the effectiveness of macro- and micro-movements drone sensing within 8×4 m flight arena area using a single mmWave radar point. However, there is potential for expanding the sensing space by employing distributed radar arrays to accommodate different layouts and areas of the working environment. Maintaining the optimal distance between each two radar arrays is essential for real-world deployment, particularly for accurate drone tracking with the shortest operational range. This deployment is simpler compared to other technologies; for example, UWB-based systems require precise installation of at least three anchors in the environment, along with attaching a tag to the target body for localisation based on pairwise distance estimation. In contrast, the potential approach to expand the working area of the proposed mmWave-based drone sensing methods simplifies the installation and calibration processes, as each mmWave array chip can independently estimate the target location within its coverage area.

Multiple Drone Detection Multi-target presents another interesting challenge. When multiple drones are concurrently within the radar's field of view, their trajectories are typically distinct enough to ensure flight safety. When employing an external radio wave module, such as the system proposed in Chapter 4 using mmWave radar, differences in range, Doppler and angle dimensions can be utilised to differentiate between multiple drones where each drone would have a different cluster in the mmWave RDA map. Thus, each drone can be individually tracked using the mmWave based tracking approach. In scenarios where drone trajectories intersect, their unique micro-Doppler features can assist in distinguishing their respective paths,

each characterised by a distinct micro-Doppler signature. Algorithms like the JPDAF and MHT can be employed in such intricate scenarios where these algorithms have demonstrated resilient performance in multiple target tracking tasks. Further investigation for multiple drone tracking will be considered as interesting future research.

Drone Category Since the proposed approaches in this thesis leverage the micro-Doppler features of rotary propellers, they can work with all rotary-wing drones. For drone categories that do not have rotors such as fixed-wing drones, studies have shown that they exhibit periodic micro-motions attributed to body vibrations [194], suggesting potential detectability by the externally mounted radio module approaches proposed in Chapter 4. However, it's important to note that the tracking and state estimation enhancements proposed in this thesis in Chapters 4 and 5 primarily rely on the variability in propeller speed, emphasising the significance of movement characteristics influenced by propeller speed variation. This highlights the potential limitations of the proposed methods for drones with distinct propulsion mechanisms. Further exploration and adaptation may be necessary to extend the applicability of these approaches to a broader range of drone types.

Challenging Environments Another issue is the deployment in highly cluttered spaces such as industrial environments for mining tasks. These environments are characterised by numerous obstacles that can significantly impact the radio waves through distraction and interference. Examples of such obstacles include machinery, equipment, and structures, all of which can obstruct or distort the signal, posing challenges for accurate drone localisation and tracking. Moreover, the presence of metallic objects in industrial settings can exacerbate signal interference, further complicating the deployment of the radio-based sensing system in these environments. Addressing these challenges requires careful consideration of signal propagation dynamics and the implementation of robust signal processing techniques tailored to operate effectively in such cluttered spaces, where the proposed methodology for modelling the multipath reflections in [168] can be used. The proposed drone detection approach in Chapter 4 depends on propeller

rotation harmonics detection, demonstrating high accuracy even in dynamic environments with various obstacles, including metallic objects and moving humans. This approach has the potential to operate in highly cluttered industrial spaces, warranting further investigation in future research. The other approach proposed in Chapter 5 relies on utilising either an existing radio module for communication or attaching radio modules to the drone's body. This method is less likely to be affected by various noise sources in the environment because the reflected signal from drone body parts would be at very short ranges with higher strength compared to reflections and interference from other obstacles.

6.2.2 Reducing Complexity and Running Time

mmWave radars often generate vast amounts of data, particularly with the utilisation of MIMO antenna arrays. Each frame produced by such arrays entails a data cube derived from the number of transmitters and receivers, chirps, and samples per chirp. As a result, the raw data size can reach several megabytes per second, posing significant challenges for edge devices with limited computational capabilities. As radar emerges as a promising sensor for integration into future smart devices, addressing the efficient real-time processing of such extensive data becomes essential. The concept of compressed sampling offers a potential solution by enabling sparser sampling of the raw signal while minimising information loss. This approach presents an avenue for further exploration, as it holds the promise of enhancing data processing efficiency in drone localisation systems, particularly when deployed on resource-constrained edge devices.

6.3 Reflections

The field of drone technology continues to advance at a rapid pace, and the integration of radio wave sensing stands out as a reliable and promising direction for future developments. As

the adoption of drones continues to accelerate across various sectors, the demand for reliable and precise localisation and navigation systems will grow. The findings of the research work presented in this thesis underscore the enhancements that radio wave sensing technologies can bring to drone detection, localisation, and autonomous flying stability. These enhancements can pave the way for more reliable and efficient drone operations, supporting the continued growth and evolution of the field, while also address critical safety and regulatory concerns. The advancements presented in this thesis are considered as a foundational framework that can be further refined and adapted to meet the evolving needs of the drone industry. The insights gained from this work can inspire future research and development efforts within the drone community. By demonstrating the effectiveness of radio wave sensing technologies in drone applications, this thesis invites researchers and engineers to explore new approaches and algorithms to achieve higher levels of autonomy and reliability, ultimately expanding the horizons of drone capabilities and their integration into everyday life.

References

[1] Hazim Shakhatreh, Ahmad H Sawalmeh, Ala Al-Fuqaha, Zuochao Dou, Eyad Almaita, Issa Khalil, Noor Shamsiah Othman, Abdallah Khreishah, and Mohsen Guizani. Unmanned aerial vehicles (uavs): A survey on civil applications and key research challenges. *Ieee Access*, 7:48572–48634, 2019.

[2] FAA. Faa aerospace forecasts. `https://www.faa.gov/sites/faa.gov/files/2022-06/Unmanned_Aircraft_Systems.pdf`, 2022.

[3] Aurello Patrik, Gaudi Utama, Alexander Agung Santoso Gunawan, Andry Chowanda, Jarot S Suroso, Rizatus Shofiyanti, and Widodo Budiharto. Gnss-based navigation systems of autonomous drone for delivering items. *Journal of Big Data*, 6:1–14, 2019.

[4] Yuanwei Wu, Yao Sui, and Guanghui Wang. Vision-based real-time aerial object localization and tracking for uav sensing system. *IEEE Access*, 5:23969–23978, 2017.

[5] Andy Couturier and Moulay A Akhloufi. A review on absolute visual localization for uav. *Robotics and Autonomous Systems*, 135:103666, 2021.

[6] Weide You, Fanbiao Li, Liqing Liao, and Meili Huang. Data fusion of uwb and imu based on unscented kalman filter for indoor localization of quadrotor uav. *Ieee Access*, 8:64971–64981, 2020.

[7] Nasser Gyagenda, Jasper V Hatilima, Hubert Roth, and Vadim Zhmud. A review of gnss-independent uav navigation techniques. *Robotics and Autonomous Systems*, 152:104069, 2022.

[8] Heba Abdel-Nasser, Reham Samir, Ibrahim Sabek, and Moustafa Youssef. Monophy: Mono-stream-based device-free wlan localization via physical layer information. In *2013 IEEE wireless communications and networking conference (WCNC)*, pages 4546–4551. IEEE, 2013.

[9] Heba Abdelnasser, Reham Mohamed, Ahmed Elgohary, Moustafa Farid Alzantot, He Wang, Souvik Sen, Romit Roy Choudhury, and Moustafa Youssef. Semanticslam: Using environment landmarks for unsupervised indoor localization. *IEEE Transactions on Mobile Computing*, 15(7):1770–1782, 2015.

[10] Heba Abdelnasser, Khaled A Harras, and Moustafa Youssef. Ubibreathe: A ubiquitous non-invasive wifi-based breathing estimator. In *Proceedings of the 16th ACM International Symposium on Mobile Ad Hoc Networking and Computing*, pages 277–286, 2015.

[11] Youssef N Altherwy and Julie A McCann. Sing: Free-space sensing of grape moisture using rf shadowing. *IEEE Transactions on Instrumentation and Measurement*, 70:1–12, 2020.

[12] Jia Zhang, Rui Xi, Yuan He, Yimiao Sun, Xiuzhen Guo, Weiguo Wang, Xin Na, Yunhao Liu, Zhenguo Shi, and Tao Gu. A survey of mmwave-based human sensing: Technology, platforms and applications. *IEEE Communications Surveys & Tutorials*, 2023.

[13] Rui Chen, Hong Zhou, Marco Moretti, Xiaodong Wang, and Jiandong Li. Orbital angular momentum waves: Generation, detection, and emerging applications. *IEEE Communications Surveys & Tutorials*, 22(2):840–868, 2019.

[14] Chen Chen, Gang Zhou, and Youfang Lin. Cross-domain wifi sensing with channel state information: A survey. *ACM Computing Surveys*, 55(11):1–37, 2023.

[15] Heba Abdelnasser, Moustafa Youssef, and Khaled A Harras. Wigest: A ubiquitous wifi-based gesture recognition system. In *2015 IEEE conference on computer communications (INFOCOM)*, pages 1472–1480. IEEE, 2015.

[16] Chris Xiaoxuan Lu, Stefano Rosa, Peijun Zhao, Bing Wang, Changhao Chen, John A Stankovic, Niki Trigoni, and Andrew Markham. See through smoke: robust indoor mapping with low-cost mmwave radar. In *Proceedings of the 18th International Conference on Mobile Systems, Applications, and Services*, pages 14–27, 2020.

[17] Mohammad Heggo, Laksh Bhatia, and Julie A McCann. Rftacho: Non-intrusive rf monitoring of rotating machines. In *2022 21st ACM/IEEE International Conference on Information Processing in Sensor Networks (IPSN)*, pages 403–414. IEEE, 2022.

[18] Heba Abdelnasser, Khaled Harras, and Moustafa Youssef. A ubiquitous wifi-based fine-grained

gesture recognition system. *IEEE Transactions on Mobile Computing*, 18(11):2474–2487, 2018.

[19] Chengkun Jiang, Junchen Guo, Yuan He, Meng Jin, Shuai Li, and Yunhao Liu. mmvib: micrometer-level vibration measurement with mmwave radar. In *Proceedings of the 26th Annual International Conference on Mobile Computing and Networking*, pages 1–13, 2020.

[20] Peijun Zhao, Chris Xiaoxuan Lu, Bing Wang, Changhao Chen, Linhai Xie, Mengyu Wang, Niki Trigoni, and Andrew Markham. Heart rate sensing with a robot mounted mmwave radar. In *2020 IEEE International Conference on Robotics and Automation (ICRA)*, pages 2812–2818. IEEE, 2020.

[21] Akarsh Prabhakara, Tao Jin, Arnav Das, Gantavya Bhatt, Lilly Kumari, Elahe Soltanaghai, Jeff Bilmes, Swarun Kumar, and Anthony Rowe. High resolution point clouds from mmwave radar. In *2023 IEEE International Conference on Robotics and Automation (ICRA)*, pages 4135–4142. IEEE, 2023.

[22] Moustafa Seifeldin, Ahmed Saeed, Ahmed E Kosba, Amr El-Keyi, and Moustafa Youssef. Nuzzer: A large-scale device-free passive localization system for wireless environments. *IEEE Transactions on Mobile Computing*, 12(7):1321–1334, 2012.

[23] Junchen Guo, Yuan He, Chengkun Jiang, Meng Jin, Shuai Li, Jia Zhang, Rui Xi, and Yunhao Liu. Measuring micrometer-level vibrations with mmwave radar. *IEEE Transactions on Mobile Computing*, 22(4):2248–2261, 2021.

[24] Texas Instruments. mmwave radar sensors. `https://www.ti.com/sensors/mmwave-radar/overview.html`, 2013.

[25] HP Groll and J Detlefsen. History of automotive anticollision radars and final experimental results of a mm-wave car radar developed by the technical university of munich. *IEEE Aerospace and Electronic Systems Magazine*, 12(8):15–19, 1997.

[26] Sameera Palipana, Dariush Salami, Luis A Leiva, and Stephan Sigg. Pantomime: Mid-air gesture recognition with sparse millimeter-wave radar point clouds. *Proceedings of the ACM on interactive, mobile, wearable and ubiquitous technologies*, 5(1):1–27, 2021.

[27] Kun Qian, Zhaoyuan He, and Xinyu Zhang. 3d point cloud generation with millimeter-wave radar. *Proceedings of the ACM on Interactive, Mobile, Wearable and Ubiquitous Technologies*,

4(4):1–23, 2020.

[28] Cesar Iovescu and Sandeep Rao. The fundamentals of millimeter wave sensors. *Texas Instruments*, pages 1–8, 2017.

[29] Hyunsoo Yang, Yongseok Lee, Sang-Yun Jeon, and Dongjun Lee. Multi-rotor drone tutorial: systems, mechanics, control and state estimation. *Intelligent Service Robotics*, 10:79–93, 2017.

[30] Hai Yu, Shizhen Wu, Wei He, Xiao Liang, Jianda Han, and Yongchun Fang. Fault-tolerant control for multirotor aerial transportation systems with blade damage. *IEEE Transactions on Industrial Electronics*, 2024.

[31] Mostafa Hassanalian and Abdessattar Abdelkefi. Classifications, applications, and design challenges of drones: A review. *Progress in Aerospace Sciences*, 91:99–131, 2017.

[32] Alex Zanotti. Retreating blade dynamic stall. 2012.

[33] Get FPV. All about multirotor drone fpv propellers. Retrieved from getfpv.com: `https://www.getfpv.com/learn/new-to-fpv/all-about-multirotor-fpv-drone-propellers/`, 2021.

[34] Fly Dragon. Multi-rotor drone. Retrieved from Fly Dragon: `https://www.dronefromchina.com/product/120-minutes-endurance-quadcopter-drone-fd405-MAX-5-KGS-payload.html`, 2021.

[35] Geo-matching. Delair ux11. Retrieved from Geo-matching: `https://geo-matching.com/products/ux11`, 2021.

[36] Fly Dragon. Fly-380 vtol. Retrieved from Fly Dragon: `http://www.dronefromchina.com/product/FLY-380-VTOL.html`, 2021.

[37] Get FPV. Differences between hexacopters, quadcopters and octocopters. Retrieved from 3D Insider: `https://3dinsider.com/hexacopters-quadcopters-octocopters/`, 2017.

[38] Zoran Benić, Petar Piljek, and Denis Kotarski. Mathematical modelling of unmanned aerial vehicles with four rotors. *Interdisciplinary Description of Complex Systems: INDECS*, 14(1):88–100, 2016.

[39] Dario Brescianini, Markus Hehn, and Raffaello D'Andrea. Nonlinear quadrocopter attitude control: Technical report. Technical report, ETH Zurich, 2013.

[40] Rogelio Lozano. *Unmanned aerial vehicles: Embedded control*. John Wiley & Sons, 2013.

[41] James Diebel et al. Representing attitude: Euler angles, unit quaternions, and rotation vectors. *Matrix*, 58(15-16):1–35, 2006.

[42] Yan-Bin Jia. Quaternions and rotations. *Com S*, 477(577):15, 2008.

[43] Sihao Sun, Giovanni Cioffi, Coen De Visser, and Davide Scaramuzza. Autonomous quadrotor flight despite rotor failure with onboard vision sensors: Frames vs. events. *IEEE Robotics and Automation Letters*, 6(2):580–587, 2021.

[44] Quan Quan. *Introduction to multicopter design and control*. Springer, 2017.

[45] Nathan Michael, Daniel Mellinger, Quentin Lindsey, and Vijay Kumar. The grasp multiple micro-uav testbed. *IEEE Robotics & Automation Magazine*, 17(3):56–65, 2010.

[46] Sergei Lupashin, Markus Hehn, Mark W Mueller, Angela P Schoellig, Michael Sherback, and Raffaello D'Andrea. A platform for aerial robotics research and demonstration: The flying machine arena. *Mechatronics*, 24(1):41–54, 2014.

[47] Guido De Croon and Christophe De Wagter. Challenges of autonomous flight in indoor environments. In *2018 IEEE/RSJ International Conference on Intelligent Robots and Systems (IROS)*, pages 1003–1009. IEEE, 2018.

[48] OptiTrack. Optitrack motion tracking system. Available: `https://optitrack.com/`, 2023. [Online].

[49] Carlos Ruiz, Shijia Pan, Adeola Bannis, Xinlei Chen, Carlee Joe-Wong, Hae Young Noh, and Pei Zhang. Idrone: Robust drone identification through motion actuation feedback. *Proceedings of the ACM on Interactive, Mobile, Wearable and Ubiquitous Technologies*, 2(2):1–22, 2018.

[50] John Wang and Edwin Olson. Apriltag 2: Efficient and robust fiducial detection. In *2016 IEEE/RSJ International Conference on Intelligent Robots and Systems (IROS)*, pages 4193–4198. IEEE, 2016.

[51] Tong Qin, Peiliang Li, and Shaojie Shen. Vins-mono: A robust and versatile monocular visual-inertial state estimator. *IEEE Transactions on Robotics*, 34(4):1004–1020, 2018.

[52] Jeffrey Delmerico and Davide Scaramuzza. A benchmark comparison of monocular visual-inertial odometry algorithms for flying robots. In *2018 IEEE international conference on robotics and automation (ICRA)*, pages 2502–2509. IEEE, 2018.

[53] Todd Lupton and Salah Sukkarieh. Visual-inertial-aided navigation for high-dynamic motion in built environments without initial conditions. *IEEE Transactions on Robotics*, 28(1):61–76, 2011.

[54] Shaojie Shen, Nathan Michael, and Vijay Kumar. Tightly-coupled monocular visual-inertial fusion for autonomous flight of rotorcraft mavs. In *2015 IEEE International Conference on Robotics and Automation (ICRA)*, pages 5303–5310. IEEE, 2015.

[55] Stefan Leutenegger, Paul Furgale, Vincent Rabaud, Margarita Chli, Kurt Konolige, and Roland Siegwart. Keyframe-based visual-inertial slam using nonlinear optimization. *Proceedings of Robotis Science and Systems (RSS) 2013*, 2013.

[56] Mingyang Li and Anastasios I Mourikis. Improving the accuracy of ekf-based visual-inertial odometry. In *2012 IEEE International Conference on Robotics and Automation*, pages 828–835. IEEE, 2012.

[57] Zheng Huai and Guoquan Huang. Robocentric visual–inertial odometry. *The International Journal of Robotics Research*, 41(7):667–689, 2022.

[58] Wenguang Mao, Zaiwei Zhang, Lili Qiu, Jian He, Yuchen Cui, and Sangki Yun. Indoor follow me drone. In *Proceedings of the 15th annual international conference on mobile systems, applications, and services*, pages 345–358, 2017.

[59] Marvelmind robotics. Precise indoor positioning system for autonomous robots, drones, vehicles and humans. `https://marvelmind.com`, 2020.

[60] Alireza Famili, Angelos Stavrou, Haining Wang, and Jung-Min Jerry Park. Pilot: High-precision indoor localization for autonomous drones. *IEEE Transactions on Vehicular Technology*, 2022.

[61] Yimiao Sun, Weiguo Wang, Luca Mottola, Ruijin Wang, and Yuan He. Aim: Acoustic inertial measurement for indoor drone localization and tracking. In *Proceedings of the 20th ACM Conference on Embedded Networked Sensor Systems*, pages 476–488, 2022.

[62] Torea Blanchard, J-H Thomas, and Kosai Raoof. Acoustic localization and tracking of a multirotor unmanned aerial vehicle using an array with few microphones. *The Journal of the Acoustical Society of America*, 148(3):1456–1467, 2020.

[63] AB Bitcraze. Loco positioning system. `https://www.bitcraze.io/documentation/system/`

positioning/loco-positioning-system/, 2022.

[64] Jorge Peña Queralta, Carmen Martínez Almansa, Fabrizio Schiano, Dario Floreano, and Tomi Westerlund. Uwb-based system for uav localization in gnss-denied environments: Characterization and dataset. In *2020 IEEE/RSJ International Conference on Intelligent Robots and Systems (IROS)*, pages 4521–4528. IEEE, 2020.

[65] Janis Tiemann, Andrew Ramsey, and Christian Wietfeld. Enhanced uav indoor navigation through slam-augmented uwb localization. In *2018 IEEE international conference on communications workshops (ICC workshops)*, pages 1–6. IEEE, 2018.

[66] Francisco Javier Perez-Grau, Fernando Caballero, Luis Merino, and Antidio Viguria. Multimodal mapping and localization of unmanned aerial robots based on ultra-wideband and rgb-d sensing. In *2017 IEEE/RSJ international conference on intelligent robots and systems (IROS)*, pages 3495–3502. IEEE, 2017.

[67] Guoxuan Chi, Zheng Yang, Jingao Xu, Chenshu Wu, Jialin Zhang, Jianzhe Liang, and Yunhao Liu. Wi-drone: wi-fi-based 6-dof tracking for indoor drone flight control. In *Proceedings of the 20th Annual International Conference on Mobile Systems, Applications and Services*, pages 56–68, 2022.

[68] Aveek Purohit, Zheng Sun, Frank Mokaya, and Pei Zhang. Sensorfly: Controlled-mobile sensing platform for indoor emergency response applications. In *Proceedings of the 10th ACM/IEEE International Conference on Information Processing in Sensor Networks*, pages 223–234. IEEE, 2011.

[69] Xinlei Chen, Aveek Purohit, Carlos Ruiz Dominguez, Stefano Carpin, and Pei Zhang. Drunkwalk: Collaborative and adaptive planning for navigation of micro-aerial sensor swarms. In *Proceedings of the 13th ACM Conference on Embedded Networked Sensor Systems*, pages 295–308, 2015.

[70] Anežka Chovancová, Tomáš Fico, L'uboš Chovanec, and Peter Hubinsk. Mathematical modelling and parameter identification of quadrotor (a survey). *Procedia Engineering*, 96:172–181, 2014.

[71] Farid Kendoul. Survey of advances in guidance, navigation, and control of unmanned rotorcraft systems. *Journal of Field Robotics*, 29(2):315–378, 2012.

[72] John Brandt and Michael Selig. Propeller performance data at low reynolds numbers. In *49th AIAA Aerospace Sciences Meeting including the New Horizons Forum and Aerospace Exposition*, page 1255, 2011.

[73] Daniel Strash, David Lednicer, and Theodor Rubin. Analysis of propeller-induced aerodynamic effects. In *16th AIAA applied aerodynamics conference*, page 2414, 1998.

[74] Fadri Furrer, Michael Burri, Markus Achtelik, and Roland Siegwart. Rotors—a modular gazebo mav simulator framework. In *Robot operating system (ROS)*, pages 595–625. Springer, 2016.

[75] Shital Shah, Debadeepta Dey, Chris Lovett, and Ashish Kapoor. Airsim: High-fidelity visual and physical simulation for autonomous vehicles. In *Field and service robotics*, pages 621–635. Springer, 2018.

[76] Matthias Faessler, Antonio Franchi, and Davide Scaramuzza. Differential flatness of quadrotor dynamics subject to rotor drag for accurate tracking of high-speed trajectories. *IEEE Robotics and Automation Letters*, 3(2):620–626, 2017.

[77] Sihao Sun, Coen C de Visser, and Qiping Chu. Quadrotor gray-box model identification from high-speed flight data. *Journal of Aircraft*, 56(2):645–661, 2019.

[78] Patricia Ventura Diaz and Steven Yoon. High-fidelity computational aerodynamics of multi-rotor unmanned aerial vehicles. In *2018 AIAA Aerospace Sciences Meeting*, page 1266, 2018.

[79] Somil Bansal, Anayo K Akametalu, Frank J Jiang, Forrest Laine, and Claire J Tomlin. Learning quadrotor dynamics using neural network for flight control. In *2016 IEEE 55th Conference on Decision and Control (CDC)*, pages 4653–4660. IEEE, 2016.

[80] Nima Mohajerin, Melissa Mozifian, and Steven Waslander. Deep learning a quadrotor dynamic model for multi-step prediction. In *2018 IEEE International Conference on Robotics and Automation (ICRA)*, pages 2454–2459. IEEE, 2018.

[81] Leonard Bauersfeld, Elia Kaufmann, Philipp Foehn, Sihao Sun, and Davide Scaramuzza. Neurobem: Hybrid aerodynamic quadrotor model. *arXiv preprint arXiv:2106.08015*, 2021.

[82] Bara J Emran and Homayoun Najjaran. A review of quadrotor: An underactuated mechanical system. *Annual Reviews in Control*, 46:165–180, 2018.

[83] Mark W Mueller and Raffaello D'Andrea. Relaxed hover solutions for multicopters: Application

to algorithmic redundancy and novel vehicles. *The International Journal of Robotics Research*, 35(8):873–889, 2016.

[84] Giulia Michieletto, Markus Ryll, and Antonio Franchi. Control of statically hoverable multirotor aerial vehicles and application to rotor-failure robustness for hexarotors. In *2017 IEEE International Conference on Robotics and Automation (ICRA)*, pages 2747–2752. IEEE, 2017.

[85] João C Monteiro, Fernando Lizarralde, and Liu Hsu. Optimal control allocation of quadrotor uavs subject to actuator constraints. In *2016 American Control Conference (ACC)*, pages 500–505. IEEE, 2016.

[86] Kang Liu, Yongqiang Cheng, Xiang Li, and Yue Gao. Microwave-sensing technology using orbital angular momentum: Overview of its advantages. *IEEE Vehicular Technology Magazine*, 14(2):112–118, 2019.

[87] Jianqiu Wang, Kang Liu, Hongyan Liu, Kaicheng Cao, Yongqiang Cheng, and Hongqiang Wang. 3-d object imaging method with electromagnetic vortex. *IEEE Transactions on Geoscience and Remote Sensing*, 60:1–12, 2021.

[88] Les Allen, Marco W Beijersbergen, RJC Spreeuw, and JP Woerdman. Orbital angular momentum of light and the transformation of laguerre-gaussian laser modes. *Physical review A*, 45(11):8185, 1992.

[89] Bo Thidé, Holger Then, J Sjöholm, Kristoffer Palmer, Jan Bergman, TD Carozzi, Ya N Istomin, NH Ibragimov, and Raisa Khamitova. Utilization of photon orbital angular momentum in the low-frequency radio domain. *Physical review letters*, 99(8):087701, 2007.

[90] Xiaonan Hui, Shilie Zheng, Yiling Chen, Yiping Hu, Xiaofeng Jin, Hao Chi, and Xianmin Zhang. Multiplexed millimeter wave communication with dual orbital angular momentum (oam) mode antennas. *Scientific reports*, 5(1):10148, 2015.

[91] Yan Yan, Guodong Xie, Martin PJ Lavery, Hao Huang, Nisar Ahmed, Changjing Bao, Yongxiong Ren, Yinwen Cao, Long Li, Zhe Zhao, et al. High-capacity millimetre-wave communications with orbital angular momentum multiplexing. *Nature communications*, 5(1):4876, 2014.

[92] Ting Gong, Yongqiang Cheng, Xiang Li, and Dingchang Chen. Micromotion detection of moving and spinning object based on rotational doppler shift. *IEEE Microwave and Wireless Compo-*

nents Letters, 28(9):843–845, 2018.

[93] Kang Liu, Xiang Li, Yue Gao, Hongqiang Wang, and Yongqiang Cheng. Microwave imaging of spinning object using orbital angular momentum. *Journal of Applied Physics*, 122(12):124903, 2017.

[94] Zhenglong Zhou, Yongqiang Cheng, Kang Liu, and Hongyan Liu. Detection of uniformly accelerated spinning target based on oam beams. In *2018 International Conference on Microwave and Millimeter Wave Technology (ICMMT)*, pages 1–3. IEEE, 2018.

[95] Omar A Saraereh. Design and performance evaluation of oam-antennas: A comparative review. *IEEE Access*, 2023.

[96] Masud Mansuripur. Radiation pressure and the linear momentum of the electromagnetic field. *Optics Express*, 12(22):5375–5401, 2004.

[97] Kuang Zhang, Yuxiang Wang, Yueyi Yuan, and Shah Nawaz Burokur. A review of orbital angular momentum vortex beams generation: from traditional methods to metasurfaces. *Applied sciences*, 10(3):1015, 2020.

[98] Nenad Bozinovic, Yang Yue, Yongxiong Ren, Moshe Tur, Poul Kristensen, Hao Huang, Alan E Willner, and Siddharth Ramachandran. Terabit-scale orbital angular momentum mode division multiplexing in fibers. *science*, 340(6140):1545–1548, 2013.

[99] Affan Affan, Shahid Mumtaz, Hafiz M Asif, and Leila Musavian. Performance analysis of orbital angular momentum (oam): A 6g waveform design. *IEEE Communications Letters*, 25(12):3985–3989, 2021.

[100] J Courtial, DA Robertson, K Dholakia, L Allen, and MJ Padgett. Rotational frequency shift of a light beam. *Physical review letters*, 81(22):4828, 1998.

[101] Mingyang Zhao, Xinlu Gao, Mutong Xie, Wensheng Zhai, Wenjing Xu, Shanguo Huang, and Wanyi Gu. Measurement of the rotational doppler frequency shift of a spinning object using a radio frequency orbital angular momentum beam. *Optics letters*, 41(11):2549–2552, 2016.

[102] Olivier Emile, Christian Brousseau, Janine Emile, and Kouroch Mahdjoubi. Energy and angular momentum transfers from an electromagnetic wave to a copper ring in the uhf band. *Comptes Rendus Physique*, 18(2):137–143, 2017.

[103] Jiayu Zheng, Shilie Zheng, Zhenlei Shao, and Xianmin Zhang. Analysis of rotational doppler effect based on radio waves carrying orbital angular momentum. *Journal of Applied Physics*, 124(16), 2018.

[104] DB Phillips, MP Lee, FC Speirits, SM Barnett, SH Simpson, MPJ Lavery, MJ Padgett, and GM Gibson. Rotational doppler velocimetry to probe the angular velocity of spinning microparticles. *Physical Review A*, 90(1):011801, 2014.

[105] Lianlin Li and Fang Li. Beating the rayleigh limit: Orbital-angular-momentum-based superresolution diffraction tomography. *Physical Review E*, 88(3):033205, 2013.

[106] Kang Liu, Yongqiang Cheng, Yue Gao, Xiang Li, Yuliang Qin, and Hongqiang Wang. Superresolution radar imaging based on experimental oam beams. *Applied Physics Letters*, 110(16), 2017.

[107] Kang Liu, Yongqiang Cheng, Zhaocheng Yang, Hongqiang Wang, Yuliang Qin, and Xiang Li. Orbital-angular-momentum-based electromagnetic vortex imaging. *IEEE Antennas and Wireless Propagation Letters*, 14:711–714, 2014.

[108] Guirong Guo, Weidong Hu, Xiaoyong Du, et al. Electromagnetic vortex based radar target imaging. *J. Nat. Univ. Defense Technol*, 35(6):71–76, 2013.

[109] Christian Wolff. Frequency-modulated continuous-wave radar (fmcw radar). `https://www.radartutorial.eu/02.basics/Frequency20Modulated%20Continuous%20Wave%20Radar.en.html`.

[110] Andrzej Wojtkiewicz, Jacek Misiurewicz, M Nalecz, Konrad Jedrzejewski, and Krzysztof Kulpa. Two-dimensional signal processing in fmcw radars. *Proc. XX KKTOiUE*, pages 475–480, 1997.

[111] Texas Instruments. Vision: Possible. `https://news.ti.com/blog/2020/09/29/vision-possible`, 2020.

[112] Texas Instruments. Journey of innovatio. `https://news.ti.com/blog/2020/10/06/journey-innovation`, 2020.

[113] Jaime Lien, Nicholas Gillian, M Emre Karagozler, Patrick Amihood, Carsten Schwesig, Erik Olson, Hakim Raja, and Ivan Poupyrev. Soli: Ubiquitous gesture sensing with millimeter wave radar. *ACM Transactions on Graphics (TOG)*, 35(4):1–19, 2016.

[114] Joe Hindy. Soli on the google pixel 4: Here's why it's a good thing. https://www.androidauthority.com/google-pixel-4-soli-motion-sense-1042448/, 2019.

[115] John G Proakis. *Digital signal processing: principles, algorithms, and applications, 4/E*. Pearson Education India, 2007.

[116] Sandeep Rao. Mimo radar. https://www.ti.com/lit/an/swra554a/swra554a.pdf.

[117] Jacopo Pegoraro, Francesca Meneghello, and Michele Rossi. Multiperson continuous tracking and identification from mm-wave micro-doppler signatures. *IEEE Transactions on Geoscience and Remote Sensing*, 59(4):2994–3009, 2020.

[118] Matthias Kronauge and Hermann Rohling. Fast two-dimensional cfar procedure. *IEEE Transactions on Aerospace and Electronic Systems*, 49(3):1817–1823, 2013.

[119] Yuwei Cheng, Jingran Su, Mengxin Jiang, and Yimin Liu. A novel radar point cloud generation method for robot environment perception. *IEEE Transactions on Robotics*, 38(6):3754–3773, 2022.

[120] Yuan He, Jia Zhang, Rui Xi, Xin Na, Yimiao Sun, and Beibei Li. Detection and identification of non-cooperative uav using a cots mmwave radar. *ACM Transactions on Sensor Networks*, 20(2):1–22, 2024.

[121] Peijun Zhao, Chris Xiaoxuan Lu, Bing Wang, Niki Trigoni, and Andrew Markham. 3d motion capture of an unmodified drone with single-chip millimeter wave radar. In *2021 IEEE International Conference on Robotics and Automation (ICRA)*, pages 5186–5192. IEEE, 2021.

[122] Jan Michalczyk, Roland Jung, and Stephan Weiss. Tightly-coupled ekf-based radar-inertial odometry. In *2022 IEEE/RSJ International Conference on Intelligent Robots and Systems (IROS)*, pages 12336–12343. IEEE, 2022.

[123] Xin Yang, Jian Liu, Yingying Chen, Xiaonan Guo, and Yucheng Xie. Mu-id: Multi-user identification through gaits using millimeter wave radios. In *IEEE INFOCOM 2020-IEEE Conference on Computer Communications*, pages 2589–2598. IEEE, 2020.

[124] Xi Zhang, Yu Zhang, Zhenguo Shi, and Tao Gu. mmfer: Millimetre-wave radar based facial expression recognition for multimedia iot applications. In *Proceedings of the 29th Annual International Conference on Mobile Computing and Networking*, pages 1–15, 2023.

[125] Chenshu Wu, Feng Zhang, Beibei Wang, and KJ Ray Liu. mmtrack: Passive multi-person localization using commodity millimeter wave radio. In *IEEE INFOCOM 2020-IEEE Conference on Computer Communications*, pages 2400–2409. IEEE, 2020.

[126] Jia Zhang, Yinian Zhou, Rui Xi, Shuai Li, Junchen Guo, and Yuan He. Ambiear: mmwave based voice recognition in nlos scenarios. *Proceedings of the ACM on Interactive, Mobile, Wearable and Ubiquitous Technologies*, 6(3):1–25, 2022.

[127] Shujie Zhang, Tianyue Zheng, Zhe Chen, and Jun Luo. Can we obtain fine-grained heartbeat waveform via contact-free rf-sensing? In *IEEE INFOCOM 2022-IEEE conference on computer communications*, pages 1759–1768. IEEE, 2022.

[128] Rong Ding, Haiming Jin, and Dingman Shen. Rotation speed sensing with mmwave radar. In *IEEE INFOCOM 2023-IEEE Conference on Computer Communications*, pages 1–10. IEEE, 2023.

[129] Victor C Chen, Fayin Li, S-S Ho, and Harry Wechsler. Micro-doppler effect in radar: phenomenon, model, and simulation study. *IEEE Transactions on Aerospace and electronic systems*, 42(1):2–21, 2006.

[130] Francesco Tonolini and Fadel Adib. Networking across boundaries: enabling wireless communication through the water-air interface. In *Proceedings of the 2018 Conference of the ACM Special Interest Group on Data Communication*, pages 117–131, 2018.

[131] Mostafa Alizadeh, George Shaker, João Carlos Martins De Almeida, Plinio Pelegrini Morita, and Safeddin Safavi-Naeini. Remote monitoring of human vital signs using mm-wave fmcw radar. *IEEE Access*, 7:54958–54968, 2019.

[132] Toan K Vo Dai, Kellen Oleksak, Tsotne Kvelashvili, Farnaz Foroughian, Chandler Bauder, Paul Theilmann, Aly E Fathy, and Ozlem Kilic. Enhancement of remote vital sign monitoring detection accuracy using multiple-input multiple-output 77 ghz fmcw radar. *IEEE Journal of Electromagnetics, RF and Microwaves in Medicine and Biology*, 6(1):111–122, 2021.

[133] Martin Ester, Hans-Peter Kriegel, Jörg Sander, Xiaowei Xu, et al. A density-based algorithm for discovering clusters in large spatial databases with noise. In *kdd*, volume 96, pages 226–231, 1996.

[134] Harold W Kuhn. The hungarian method for the assignment problem. *Naval research logistics quarterly*, 2(1-2):83–97, 1955.

[135] Rudolph Emil Kalman. A new approach to linear filtering and prediction problems. 1960.

[136] Yaakov Bar-Shalom, Fred Daum, and Jim Huang. The probabilistic data association filter. *IEEE Control Systems Magazine*, 29(6):82–100, 2009.

[137] Samuel S Blackman. Multiple hypothesis tracking for multiple target tracking. *IEEE Aerospace and Electronic Systems Magazine*, 19(1):5–18, 2004.

[138] Heba Abdelnasser, Mohammad Heggo, Oscar Pang, Mirko Kovac, and Julie A McCann. Multirotor motion enhancement using propeller speed measurements. In *2023 International Conference on Unmanned Aircraft Systems (ICUAS)*, pages 401–406. IEEE, 2023.

[139] Kristen N Mogensen. Motor-control considerations for electronic speed control in drones. *Analog Applications Journal [online]. Texas Instruments*, 2016.

[140] Matija Krznar, Denis Kotarski, Danijel Pavković, and Petar Piljek. Propeller speed estimation for unmanned aerial vehicles using kalman filtering. *International Journal of Automation and Control*, 14(3):284–303, 2020.

[141] Chinthaka Premachandra, Daiki Ueda, and Kiyotaka Kato. Speed-up automatic quadcopter position detection by sensing propeller rotation. *IEEE Sensors Journal*, 19(7):2758–2766, 2018.

[142] Frank Billy Djupkep Dizeu, Michel Picard, Marc-Antoine Drouin, and Guillaume GAGN. Extracting unambiguous drone signature using high-speed camera. *IEEE Access*, 10:45317–45336, 2022.

[143] Phuc Nguyen, Vimal Kakaraparthi, Nam Bui, Nikshep Umamahesh, Nhat Pham, Hoang Truong, Yeswanth Guddeti, Dinesh Bharadia, Richard Han, Eric Frew, et al. Dronescale: drone load estimation via remote passive rf sensing. In *Proceedings of the 18th Conference on Embedded Networked Sensor Systems*, pages 326–339, 2020.

[144] Terrence Stewart, Marc-Antoine Drouin, Michel Picard, Frank Billy Djupkep Dizeu, Anthony Orth, and Guillaume Gagné. A virtual fence for drones: Efficiently detecting propeller blades with a dvxplorer event camera. In *Proceedings of the International Conference on Neuromorphic Systems 2022*, pages 1–7, 2022.

[145] Soundarya Ramesh, Thomas Pathier, and Jun Han. Sounduav: Towards delivery drone authentication via acoustic noise fingerprinting. In *Proceedings of the 5th Workshop on Micro Aerial Vehicle Networks, Systems, and Applications*, pages 27–32, 2019.

[146] Jiahao Chen and Jin Huang. Alternative solution regarding problems of adaptive observer compensating parameters uncertainties for sensorless induction motor drives. *IEEE Transactions on Industrial Electronics*, 67(7):5879–5888, 2019.

[147] Gianluca Ciattaglia, Grazia Iadarola, Linda Senigagliesi, Susanna Spinsante, and Ennio Gambi. Uav propeller rotational speed measurement through fmcw radars. *Remote Sensing*, 15(1):270, 2023.

[148] Luca Pallotta, Carmine Clemente, Alessandro Raddi, and Gaetano Giunta. A feature-based approach for loaded/unloaded drones classification exploiting micro-doppler signatures. In *2020 IEEE Radar Conference (RadarConf20)*, pages 1–6. IEEE, 2020.

[149] Carmine Clemente, Luca Pallotta, Christos Ilioudis, Francesco Fioranelli, Gaetano Giunta, and Alfonso Farina. Chebychev moments based drone classification, recognition and fingerprinting. In *2021 21st International Radar Symposium (IRS)*, pages 1–6. IEEE, 2021.

[150] Cameron Bennett, Stephen Harman, and Ivan Petrunin. Realistic simulation of drone micro-doppler signatures. In *2021 18th European Radar Conference (EuRAD)*, pages 114–117. IEEE, 2022.

[151] Vimlesh Verma, Chandan Chakraborty, Suman Maiti, and Yoichi Hori. Speed sensorless vector controlled induction motor drive using single current sensor. *IEEE Transactions on Energy Conversion*, 28(4):938–950, 2013.

[152] Richard Bonert. Design of a high performance digital tachometer with a microcontroller. *IEEE Transactions on Instrumentation and Measurement*, 38(6):1104–1108, 1989.

[153] Richard C Kavanagh. Improved digital tachometer with reduced sensitivity to sensor nonideality. *IEEE Transactions on industrial electronics*, 47(4):890–897, 2000.

[154] UNI-T. Technology. Laser tachometer operating manual. `https://meters.uni-trend.com/product/ut370-series/#Docs/`.

[155] Lin Li, Hongli Hu, Yong Qin, and Kaihao Tang. Digital approach to rotational speed measure-

ment using an electrostatic sensor. *Sensors*, 19(11):2540, 2019.

[156] Lijuan Wang, Yong Yan, Yonghui Hu, and Xiangchen Qian. Rotational speed measurement through electrostatic sensing and correlation signal processing. *IEEE Transactions on Instrumentation and Measurement*, 63(5):1190–1199, 2013.

[157] J Kathirvelan, Babu Varghese, Ubaid A Ponnary, Fajas Kamar, and Renju Thomas Jacob. Hall effect sensor based portable tachometer for rpm measurement. *Int. J. Comput. Sci. Eng. Commun*, 2:100–105, 2014.

[158] Yunfan Wang, Lijuan Wang, and Yong Yan. Rotational speed measurement through digital imaging and image processing. In *2017 IEEE International Instrumentation and Measurement Technology Conference (I2MTC)*, pages 1–6. IEEE, 2017.

[159] Tianyu Wang, Yong Yan, Lijuan Wang, and Yonghui Hu. Rotational speed measurement through image similarity evaluation and spectral analysis. *IEEE Access*, 6:46718–46730, 2018.

[160] Jianfeng Zhong, Shuncong Zhong, Qiukun Zhang, and Zhike Peng. Measurement of instantaneous rotational speed using double-sine-varying-density fringe pattern. *Mechanical Systems and Signal Processing*, 103:117–130, 2018.

[161] Hyuno Kim, Yuji Yamakawa, Taku Senoo, and Masatoshi Ishikawa. Visual encoder: robust and precise measurement method of rotation angle via high-speed rgb vision. *Optics express*, 24(12):13375–13386, 2016.

[162] Balmukund Mishra, Deepak Garg, Pratik Narang, and Vipul Mishra. Drone-surveillance for search and rescue in natural disaster. *Computer Communications*, 156:1–10, 2020.

[163] Sungjae Lee and Yosoon Choi. Reviews of unmanned aerial vehicle (drone) technology trends and its applications in the mining industry. *Geosystem Engineering*, 19(4):197–204, 2016.

[164] Mahanth Gowda, Justin Manweiler, Ashutosh Dhekne, Romit Roy Choudhury, and Justin D Weisz. Tracking drone orientation with multiple gps receivers. In *Proceedings of the 22nd annual international conference on mobile computing and networking*, pages 280–293, 2016.

[165] Xianyu Chang, Chaoqun Yang, Junfeng Wu, Xiufang Shi, and Zhiguo Shi. A surveillance system for drone localization and tracking using acoustic arrays. In *2018 IEEE 10th Sensor Array and Multichannel Signal Processing Workshop (SAM)*, pages 573–577. IEEE, 2018.

[166] Ismail Güvenç, Ozgur Ozdemir, Yavuz Yapici, Hani Mehrpouyan, and David Matolak. Detection, localization, and tracking of unauthorized uas and jammers. In *2017 IEEE/AIAA 36th Digital Avionics Systems Conference (DASC)*, pages 1–10. IEEE, 2017.

[167] M Caris, W Johannes, S Sieger, V Port, and S Stanko. Detection of small uas with w-band radar. In *2017 18th International Radar Symposium (IRS)*, pages 1–6. IEEE, 2017.

[168] Weiyan Chen, Hongliu Yang, Xiaoyang Bi, Rong Zheng, Fusang Zhang, Peng Bao, Zhaoxin Chang, Xujun Ma, and Daqing Zhang. Environment-aware multi-person tracking in indoor environments with mmwave radars. *Proceedings of the ACM on Interactive, Mobile, Wearable and Ubiquitous Technologies*, 7(3):1–29, 2023.

[169] Han Cui and Naim Dahnoun. High precision human detection and tracking using millimeter-wave radars. *IEEE Aerospace and Electronic Systems Magazine*, 36(1):22–32, 2021.

[170] Jiacheng Wu, Han Cui, and Naim Dahnoun. A novel high performance human detection, tracking and alarm system based on millimeter-wave radar. In *2021 10th Mediterranean Conference on Embedded Computing (MECO)*, pages 1–4. IEEE, 2021.

[171] Teng Wei and Xinyu Zhang. mtrack: High-precision passive tracking using millimeter wave radios. In *Proceedings of the 21st Annual International Conference on Mobile Computing and Networking*, pages 117–129, 2015.

[172] Peijun Zhao, Chris Xiaoxuan Lu, Jianan Wang, Changhao Chen, Wei Wang, Niki Trigoni, and Andrew Markham. Human tracking and identification through a millimeter wave radar. *Ad Hoc Networks*, 116:102475, 2021.

[173] Jacopo Pegoraro and Michele Rossi. Human tracking with mmwave radars: A deep learning approach with uncertainty estimation. In *2022 IEEE 23rd International Workshop on Signal Processing Advances in Wireless Communication (SPAWC)*, pages 1–5. IEEE, 2022.

[174] Jacopo Pegoraro, Domenico Solimini, Federico Matteo, Enver Bashirov, Francesca Meneghello, and Michele Rossi. Deep learning for accurate indoor human tracking with a mm-wave radar. In *2020 IEEE Radar Conference (RadarConf20)*, pages 1–6. IEEE, 2020.

[175] Prabhat Kumar Rai, Henning Idsøe, Rajesh Reddy Yakkati, Abhinav Kumar, Mohammed Zafar Ali Khan, Phaneendra K Yalavarthy, and Linga Reddy Cenkeramaddi. Localization and

activity classification of unmanned aerial vehicle using mmwave fmcw radars. *IEEE Sensors Journal*, 21(14):16043–16053, 2021.

[176] Jyoti Bhatia, Aveen Dayal, Ajit Jha, Santosh K Vishvakarma, J Soumya, MB Srinivas, Phaneendra K Yalavarthy, Abhinav Kumar, V Lalitha, Sagar Koorapati, et al. Object classification technique for mmwave fmcw radars using range-fft features. In *2021 International Conference on COMmunication Systems & NETworkS (COMSNETS)*, pages 111–115. IEEE, 2021.

[177] Suhare Solaiman, Emad Alsuwat, and Rajwa Alharthi. Simultaneous tracking and recognizing drone targets with millimeter-wave radar and convolutional neural network. *Applied System Innovation*, 6(4):68, 2023.

[178] Peter Joseph Basil Morris and KVS Hari. Detection and localization of unmanned aircraft systems using millimeter-wave automotive radar sensors. *IEEE Sensors Letters*, 5(6):1–4, 2021.

[179] Sylvain Sardy, Paul Tseng, and Andrew Bruce. Robust wavelet denoising. *IEEE Transactions on Signal Processing*, 49(6):1146–1152, 2001.

[180] Maria Isabel Ribeiro. Kalman and extended kalman filters: Concept, derivation and properties. *Institute for Systems and Robotics*, 43(46):3736–3741, 2004.

[181] Eugene F Knott, John F Schaeffer, and Michael T Tulley. *Radar cross section*. SciTech Publishing, 2004.

[182] Lei Ding, Murtaza Ali, Sujeet Patole, and Anand Dabak. Vibration parameter estimation using fmcw radar. In *2016 IEEE International Conference on Acoustics, Speech and Signal Processing (ICASSP)*, pages 2224–2228. IEEE, 2016.

[183] Victor RF Miranda, Adriano Rezende, Thiago L Rocha, Héctor Azpúrua, Luciano CA Pimenta, and Gustavo M Freitas. Autonomous navigation system for a delivery drone. *Journal of Control, Automation and Electrical Systems*, 33(1):141–155, 2022.

[184] David Titterton and John L Weston. *Strapdown inertial navigation technology*, volume 17. IET, 2004.

[185] Averil Burton Chatfield. *Fundamentals of high accuracy inertial navigation*, volume 174. Aiaa, 1997.

[186] Georg Klein and David Murray. Parallel tracking and mapping for small ar workspaces. In *2007*

6th IEEE and ACM international symposium on mixed and augmented reality, pages 225–234. IEEE, 2007.

[187] Christian Forster, Matia Pizzoli, and Davide Scaramuzza. Svo: Fast semi-direct monocular visual odometry. In *2014 IEEE international conference on robotics and automation (ICRA)*, pages 15–22. IEEE, 2014.

[188] Jakob Engel, Thomas Schöps, and Daniel Cremers. Lsd-slam: Large-scale direct monocular slam. In *European conference on computer vision*, pages 834–849. Springer, 2014.

[189] Raul Mur-Artal, Jose Maria Martinez Montiel, and Juan D Tardos. Orb-slam: a versatile and accurate monocular slam system. *IEEE transactions on robotics*, 31(5):1147–1163, 2015.

[190] Romain Chiappinelli. Simulation-in-hardware dynamic model for quadrotor x. March 2019.

[191] Muhammad Maaruf, Magdi Sadek Mahmoud, and Alfian Ma'arif. A survey of control methods for quadrotor uav. *International Journal of Robotics and Control Systems*, 2(4):652–665, 2022.

[192] Hui Wang, Siliang Lu, Gang Qian, Jianming Ding, Yongbin Liu, and Qunjing Wang. A two-step strategy for online fault detection of high-resistance connection in bldc motor. *IEEE Transactions on Power Electronics*, 35(3):3043–3053, 2019.

[193] Mark W Mueller and Raffaello D'Andrea. Stability and control of a quadrocopter despite the complete loss of one, two, or three propellers. In *2014 IEEE international conference on robotics and automation (ICRA)*, pages 45–52. IEEE, 2014.

[194] Ki-Bong Kang, Jae-Ho Choi, Byung-Lae Cho, Jung-Soo Lee, and Kyung-Tae Kim. Analysis of micro-doppler signatures of small uavs based on doppler spectrum. *IEEE Transactions on Aerospace and Electronic Systems*, 57(5):3252–3267, 2021.